

Study of Electrochemical Behavior of Iodide in LiCl-KCl Eutectic and LiCl-KCl-Li₂O
Molten Salts at High Temperatures of 450, 500 and 550 °C

A Dissertation

Presented in Partial Fulfillment of the Requirements for the

Degree of Doctor of Philosophy

with a

Major in Materials Science and Engineering

University of Idaho

By

Nikunja Shrestha

Major Professor: Krishnan S. Raja, Ph.D.

Committee Members: Vivek Utgikar, Ph.D.; Indrajit Charit, Ph.D.;

I.F. Cheng, Ph.D.

Department Head: Indrajit Charit, Ph.D.

August 2021

Authorization to Submit Dissertation

This Dissertation of Nikunja Shrestha, submitted for the degree of Material Science and Engineering with a Major in Chemical and Materials Engineering and titled “Study of Electrochemical Behavior of Iodide in LiCl-KCl Eutectic and LiCl-KCl-Li₂O Molten Salt at High Temperatures of 450, 500 and 550 °C,” has been reviewed in final form. Permission, as indicated by the signatures and dates below, is now granted to submit final copies to the College of Graduate Studies for approval.

Major Professor: _____ Date: _____

Krishnan S. Raja, Ph.D.

Committee Members: _____ Date: _____

Vivek Utgikar, Ph.D.

_____ Date: _____

Indrajit Charit, Ph.D.

_____ Date: _____

I.F. Cheng, Ph.D.

MSE Program Director: _____ Date: _____

Mark F. Roll, Ph.D.

Abstract

Several radioactive iodine isotopes are formed during neutron induced fission of nuclear fuel, and these radionuclides are retained within the fuel matrix and by the containment provided by the fuel cladding and ^{129}I is one of concern. During reprocessing of the used nuclear fuel, a significant fraction of iodine (78.9 mg/g of heavy metal) was reported to be retained in the molten salt as iodide (I^-) such as NaI , CsI , AgI , PdI_2 , UI_3 , ZrI_4 , ^3HI . Accumulation of iodide species could significantly affect the performance of the electro-refiners that are used for electrolytic reduction of actinides during pyro-processing of used nuclear fuels. Therefore, it is important to understand the electrochemical speciation of iodide in the LiCl-KCl eutectic and $\text{LiCl-Li}_2\text{O}$ molten salts. The electrochemistry of iodine/iodide couples has been extensively studied in aqueous and non-aqueous conditions at room temperature because of its application in dye-sensitized solar cells, and synthetic chemistry. However, only very limited work has been reported in high temperature molten salts.

In this research, electrochemical behavior of iodide in LiCl-KCl eutectic, $\text{LiCl-KCl-Li}_2\text{O}$, and $\text{LiCl-KCl}+1-5 \text{ wt}\% \text{CeCl}_3$ molten salts were investigated at temperatures in the range of $450 - 550 \text{ }^\circ\text{C}$ using different electrochemical techniques such as cyclic voltammetry, electrochemical impedance spectroscopy and square wave voltammetry. Iodide was present in the form of potassium iodide and its concentration varied from 1 – 10%. Ce(III) was added as a surrogate of U(III) to evaluate the effect of iodide on the reduction process. The diffusivity of Ce(III) in LiCl-KCl eutectic at $450 \text{ }^\circ\text{C}$ decreased from $0.5 \times 10^{-5} \text{ cm}^2/\text{s}$ to 2.5, 1.5, $1.1 \times 10^{-5} \text{ cm}^2/\text{s}$ with the addition of 1, 5, and 10 wt% KI . The reduction potential of Ce(III) shifted to more negative potentials with the addition of KI . This presentation will discuss the oxidation of iodide species (I^- and I_3^-), and their interaction with chloride by forming interhalide compounds. Formal potentials of reaction steps, number of electrons involved in the reactions, and diffusivities of various ions will be presented, and how these data are helpful for pyroprocessing of the used nuclear fuels are discussed.

Acknowledgements

I would sincerely like to thank my advisor, Dr. Krishnan S. Raja for giving me this opportunity to work under his guidance. I would also like to thank my Co-PI Dr. Vivek Utigkar for his support throughout the process. Without their guidance, patience, and understanding, I would not make it this far, especially with my project and dissertation. Also, I want to thank my committee members, Dr. Indrajit Charit and Dr. I.F. Cheng for taking time to support me with my dissertation. Also, I want to express gratitude to Department of Chemical and Materials Engineering for the Ph.D. opportunity and support throughout my research. I would like to thank Dr. Thomas Williams for helping me with the instrumental analysis part of project.

I would also like to thank Department of Energy for funding this project and made it possible for me to do research on this interesting topic and complete my Ph.D.

Dedication

This dissertation is dedicated to my family, my wife, my friends and all my professors who directly and indirectly played important role in helping me finish my Ph.D.

Table of Contents

Authorization to Submit Dissertation	ii
Abstract.....	iii
Acknowledgements.....	iv
Dedication	v
List of Figures.....	vii
List of Tables	ix
Chapter 1: Introduction	1
1.1 Motivation.....	1
1.2 Objectives.....	3
Chapter 2: Literature Review	5
2.1 Pyroprocessing.....	5
2.2 Isotope of Iodine	11
2.3. Chemla Effect	16
Chapter 3: Experimental Procedure	25
3.1 Experimental Setup.....	25
3.2 Electrochemical Techniques.....	27
3.2.1 Open Circuit Potential (OCP).....	27
3.2.2 Electrochemical Impedance Spectroscopy (EIS).....	27
3.2.3 Cyclic Voltammetry (CV).....	29
3.2.4 Differential Pulse Voltammetry	34
Chapter 4: Understanding Electrochemical Interactions of Iodide and Chloride Species in LiCl-KCl Molten Salt.....	37
Chapter 5: Study of Cerium Deposition with the Increase in Concentration of KI in LiCl-KCl Eutectic.....	59
Chapter 6: Study of Electrochemical Behavior of Iodide in LiCl-KCl with 1 and 2 wt % Li₂O at 550 °C	75
Chapter 7. Conclusions.....	89
Chapter 8. Future Work.....	90

List of Figures

Figure 2.1	5
Figure 2.2	8
Figure 2.3.....	11
Figure 2.4.....	17
Figure 2.5.....	17
Figure 3.1	29
Figure 3.2.....	29
Figure 3.3.....	31
Figure 3.4.....	33
Figure 4.1	35
Figure 4.2.....	41
Figure 4.3.....	42
Figure 4.4.....	43
Figure 4.5.....	47
Figure 4.6.....	47
Figure 4.7.....	48
Figure 4.8.....	50
Figure 4.9.....	51
Figure 4.10.....	52
Figure 5.1	53
Figure 5.2	61
Figure 5.3.....	63
Figure 5.4.....	66
Figure 5.5.....	67
Figure 5.6.....	69
Figure 5.7.....	71
Figure 6.1	72
Figure 6.2.....	74
Figure 6.3.....	81

Figure 6.4.....	81
Figure 6.5.....	82
Figure 6.6.....	85
Figure 6.7.....	85
Figure 6.8.....	86

List of Tables

Table 2.1.....	6
Table 3.1.....	54
Table 3.2.....	54
Table 3.3.....	55
Table 3.4.....	55
Table 3.5.....	56
Table 3.6.....	56
Table 5.1.....	67
Table 6.1.....	86

Chapter 1: Introduction

1.1 Motivation

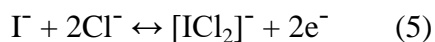
Used nuclear fuel contains a variety of active fission products such as neptunium, plutonium, yttrium, neodymium etc. along with Uranium [1]. Several radioactive isotopes are also formed during neutron induced fission of nuclear fuel and these radionuclides are retained within the fuel matrix and by the containment provided by the fuel cladding. During reprocessing of the used nuclear fuel, a significant fraction of iodine (78.9 mg/g of heavy metal) was reported to be retained in the molten salt as iodide (I) such as NaI, CsI, AgI PdI₂, UI₃, ZrI₄, HI [2]. Accumulation of iodide species could significantly affect the performance of the electro-refiners that are used for electrolytic reduction of actinides during pyroprocessing of used nuclear fuels. The electrochemistry of iodine/iodide couple has been extensively studied in aqueous and non-aqueous conditions because of its application in dye-sensitized solar cells, and synthetic chemistry. However, only very limited work has been reported in high temperature molten salts. Iodide based molten salts have been identified as potential alternatives for thermal batteries because of their low melting point and high conductivities. During reduction of used oxide fuels of light water reactors (LWR), fission products such as Cs, Ba, Sr, and I partition to the salt phase. Reprocessing of mixed oxide (MOX) spent fuels results in elevated concentrations of I and Te in the salt phase [3]. The increase in concentration of I and Te makes the system more complicated and difficult to be understood as it affects in the efficient separation of Uranium from the Used Nuclear Fuel (UNF) during the electrorefining process. Thus, an extensive and in depth study of electrochemical properties of these elements is necessary to improve the efficiency of the UNF processing system. However, only very limited work has been reported in molten salts. Fujiwara et al [4] proposed iodide based molten salt systems such as LiF-LiCl-LiBr-LiI, and LiF-NaBr-LiI for high temperature battery applications because of their higher conductivity (up to 3.5 S/cm) than that of conventional LiCl-KCl (< 2.1 S/cm). Presence of oxygen caused instability of iodide at temperatures higher than 280 °C by following the reactions:



This observation indicates that iodide may not interfere significantly with the reprocessing of oxide fuels. In the absence of oxygen, the iodide may complex with chloride. Even though not much information is available on the interaction of iodide with high temperature molten chloride salts, some work has been reported on iodide- chloride interactions in room temperature ionic liquids. In chloride containing 1-Ethyl-3-methylimidazolium bis-(trifluoromethanesulfonyl)imide ionic liquid, iodide is observed to oxidize to ICl , $[\text{I}_2\text{Cl}]^-$ and $[\text{ICl}_2]^-$. Chloride stabilizes I_2 by complexation and allows I_3^- to oxidize at a less positive potential. Furthermore, Cl^- promotes further oxidation of I^- to I^+ via I_3^- [5]. The electrochemistry of iodide in high temperature molten salts such as LiCl-KCl eutectic or $\text{LiCl-Li}_2\text{O}$ is not documented in detail to the best of our knowledge. In the absence of chloride, the redox reactions of iodide are given as [6]:



With the chloride addition, the redox reactions are given as [4]:



This research will focus on the formation of $[\text{ICl}_x]^{-(x-1)}$ interhalogen compounds, if any, and their effect on reprocessing conditions. This will give better insight to properties of iodide electrochemistry in LiCl-KCl molten salt and the data generated will be useful for optimization of operating parameters and design of a more efficient electro-refiners of UNF processing.

1.2 Objectives

- ❖ Evaluate the electrochemical speciation behavior of iodide in LiCl-KCl eutectic, LiCl-KCl- Li₂O electrolytes at temperatures relevant to reprocessing conditions.
- ❖ Analyze the effect of iodide on reduction of CeCl₃ in LiCl-KCl at temperatures relevant to reprocessing conditions which will help to optimize the recovery of Uranium from UNF during pyroprocessing.
- ❖ Study the thermodynamic properties by carrying out Differential Scanning Calorimetry and Thermo-Gravimetry Analysis.
- ❖ Evaluate the iodide containing LiCl-KCl as a potential catholyte for molten salt battery.

References

1. M.F. Simpson, Development of Spent Nuclear Fuel Pyroprocessing Technology at Idaho National Laboratory, DOI: 10.2172/1044209(2012)
2. Steven M Frank, Summary of Iodine Partitioning in EBR-II Fuel, Internal Report, Idaho National Laboratory, SMF-001-16, Feb 2016
3. P. Masset, Journal of Power Sources 160(2006) 688-697
4. S. Fujiwara et al., J. Power Sources, 194 (2009) 1180-1183 6. C.L. Bentley et al., Analytical Chemistry, 88 (2016) 1915-1921. 7. A.I. Popov, D.H. Geske, J. Am. Chem. Soc., 80 (1958) 5346-5349
5. C.L. Bentley et al., Analytical Chemistry, 88 (2016) 1915-1921.
6. A.I. Popov, D.H. Geske, J. Am. Chem. Soc., 80 (1958) 5346-534

Chapter 2: Literature Review

2.1 Pyroprocessing

Pyroprocessing technology was developed by Argonne national laboratory (ANL) and is currently operated at Idaho National Laboratory (INL) to treat Used Nuclear Fuel (UNF) from Experimental Breeder Reactor- II (EBR-II) [7-9]. It is a high temperature electrochemical fuel processing technology to treat metal and metal oxide form of UNF for nuclear reactor. Recycling the fuel is expected to increase the uranium usage efficiency and decrease both the radiotoxicity and amount of the radioactive waste generated [10-17]. Thus, pyroprocessing technology is one of the major areas of research in present time and is considered a promising way for efficient reprocessing of UNF. A schematic diagram of pyroprocessing of UNF is illustrated in figure 2.1.

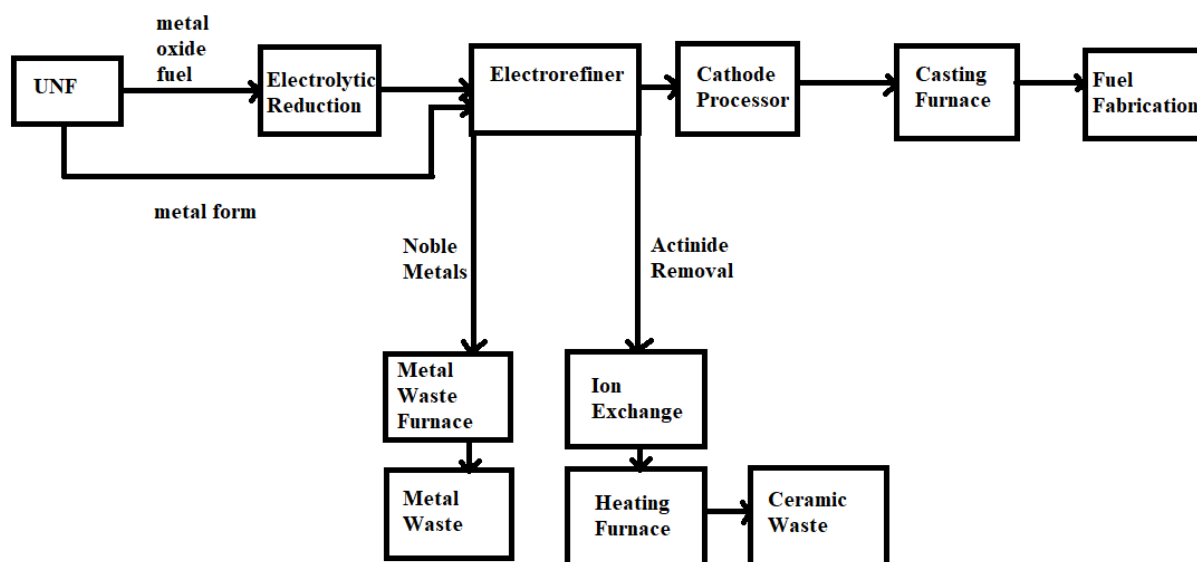


Figure 2.1 Schematic Flowchart of Pyroprocessing of Used Nuclear Fuel

Pyroprocessing uses molten salt electrolytes as medium instead of acid or organic solvents. The advantages of using molten salts include high radiation resistance, low vapor pressure, less secondary waste and high stability [18-23]. Currently, two chloride salt mixtures (LiCl–KCl and NaCl–KCl) and two fluoride salt mixtures (BeF₂–LiF and CaF₂–LiF) have been recognized as good candidates for pyroprocessing [24-26]. But among these salt mixtures, LiCl–KCl molten salt is widely selected as a candidate for electrorefining system because of

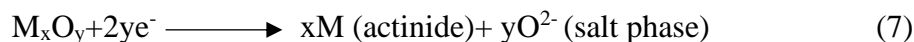
its lower melting eutectic temperature of 623 K compared to 931 K for NaCl-KCl, 733 K for BeF₂-LiF and 1042 K for CaF₂-LiF. The table 2.1 shows the physical properties of LiCl-KCl eutectic salt [27].

Table 2.1: Physical Properties of LiCl-KCl eutectic salt

Parameter	Value and Equation
T _{melt, LiCl}	610 °C
T _{melt, KCl}	770 °C
T _{melt, LiCl-KCl}	355 °C
Density, ρ _{LiCl-KCl}	ρ (T)= 2.0286 - (5.2676x10 ⁻⁴)T

This technology mainly consists of head-end processes, electrochemical process like electrochemical reduction and electro-refining process followed by waste treatment process as shown in figure 2.1[28]. Head-end process consists of decladding, voloxidation and oxide feed preparation. The purpose of this process is to convert a spent fuel assembly into a suitable feed material that can be used in the electrochemical reduction process. In the voloxidation process, the dense oxide pellet discharged from the cladding hull is oxidized and pulverized to the powder form of U₃O₈ at temperature higher than 500 °C under air atmosphere. The oxide feed with proper porosity and shape for the electrochemical processing is prepared with the voloxidized U₃O₈ powder [28-30]. Then, this oxide fuel goes through the electrochemical reduction process which has been used to reduce the spent oxide fuel directly into their parent metals by solid state electrolysis in a molten salt medium LiCl-Li₂O [31,32]. The use of molten LiCl is the most promising option for the electrochemical reduction process for the following reasons due to lower operating temperature can be lowered with LiCl salt because of its melting point, 605 °C compared to CaCl₂ which has melting point of 772 °C. LiCl also has a high current efficiency, high O²⁻ solubility and more compatibility with LiCl-KCl which is employed in next electrochemical process. In the electrochemical reduction process, oxides fuels are loaded at the cathode basket in molten LiCl, and some amount of Li₂O is added to speed up the reduction rate and prevent the anodic dissolution of the platinum anode by providing oxide ions to the salt [33]. The concentration of Li₂O added to LiCl is usually less than 3 wt% because a reaction between the produced uranium metal and Li₂O is not feasible even at such high concentrations. However, a concentration of 1 wt% of Li₂O is usually used

by considering the corrosion resistance and degree of reduction in other oxides such as Pu_2O_3 and most of the rare earth oxides that occur in the spent fuel [34,35]. Based on the strategy of the head-end process, the spent oxide fuel can be loaded in various physical forms such as rod-cut, crushed particles, powder, and porous pellets [36-40], along with different oxidation states of uranium oxide, UO_2 or U_3O_8 [41,42]. The overall cathode reaction for the oxide fuel, mainly actinide oxides, is as follows:



The reduction of UO_2 was caused by two different reduction paths: the direct reduction expressed by equation 2 and an electro-lithiothermic reduction assisted by the lithium metal produced in the fuel basket, represented by equation 3 as follows [43,44]:



Similarly, platinum has been employed as the anode material for the oxide reduction process and the reaction occurring after addition of Li_2O to LiCl melt, the main reaction that takes place is oxygen evolution given by [45]:



However, it can be corroded in two different ways including the formation of Li_2PtO_3 at higher Li_2O concentration or direct dissolution of platinum at lower O^{2-} ion concentration as follows [46]:



During the process of electrolytic reduction, the salt soluble fission products like Cs, Ba, Sr, Rb, Eu, Te and I are dissolved into the molten Li_2O - LiCl salt and get accumulated in the salt bath. Sakamura found out that the reduction rate of UO_2 decreases with the reuse of LiCl salt due to the accumulation of these salt soluble fission products [40]. The metal obtained by electrolytic reduction of metal oxides are then transferred to electrorefining chamber for further process.

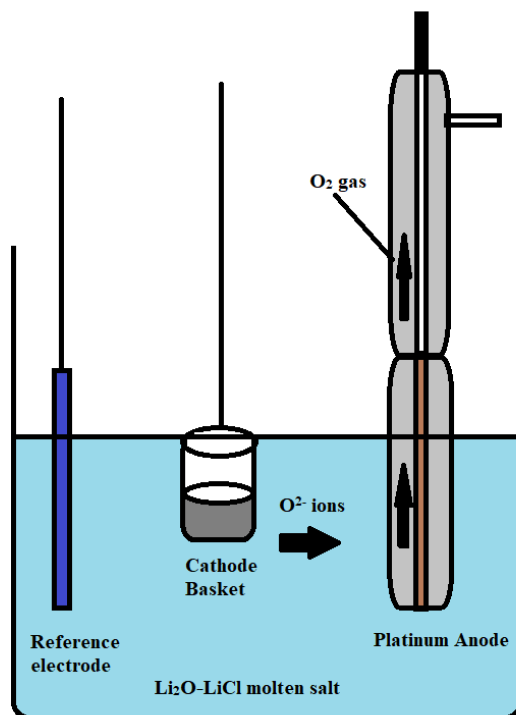
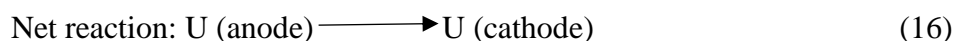
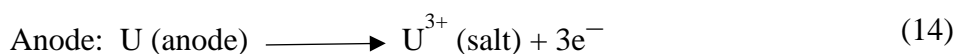


Figure 2.2 Schematic diagram for the electroreduction process

Electrorefining is the major key to the pyroprocessing and can be defined as an electrometallurgical treatment of spent nuclear fuel that uses molten salt to recover the uranium and other actinides for recycling into new fuel [46]. The metallic product from the electrolytic reduction process is transferred to the electrorefining process for recovery of U and a co-deposited U/TRU product. Here, UNFs are loaded in the anode basket and lowered into the LiCl-KCl molten salt. As current is applied through the cell, U metal is oxidized into U^{3+} ions from the anode basket [47]. Fission products, which have more negative redox potential than that of U, are being oxidized together (these products are referred as active products) whereas noble metals which have more positive redox potential than U stay in the anode basket [48]. Therefore, the main goal is to dissolve as much U as possible from the used fuels on the anodic side with minimal oxidation of the noble metals into the salt and collect uranium metal on the cathode side.

For the cathode electrodes, there are two types of electrode: 1) solid electrode (typically stainless steel) and the LCC. By using the solid electrode, selective deposition of pure U is possible by controlling the applied potential. These metal fuels are transferred into the anode basket of an electrorefiner (ER). U, Pu, MAs, and rare earth materials are anodically dissolved into the LiCl-KCl eutectic salt from the anode basket, only U is recovered on the solid cathode

by controlling the voltage applied on the cathode. After that, the residual U, Pu, and MAs are simultaneously collected by using a liquid cadmium cathode (LCC) due to the fact that activity of the elements get very small in liquid metal [49-55]. The deposits (U and U-Pu-MA mixtures) from the cathode electrodes go to the cathode processor. The process is performed in a high temperature vacuum furnace where the salt or cadmium are evaporated, and pure metal product are left. The electrolyte salt is recycled by removing actinides through the ion exchange method. The fission products are collected as ceramic waste forms and noble metal fission products are processed into alloy metal waste for disposal. Overall, the main reaction schemes in an electrorefiner can be described as follows [56]:



The uranium ions are transported through the molten salt to the cathode where they are reduced to produce metallic uranium. The dendritic uranium product collected from the electrorefiner may retain up to 15 wt.% electrolyte salt, which contains transuranic and lanthanide chlorides that must be removed prior to uranium recycle. A distillation process, conducted at approximately 800°C, is used to recover the salt from the dendritic uranium. After salt removal, the uranium is consolidated to an ingot by heating the dendrites to 1200°C [57-59]. The consolidated uranium product can be used in fuel fabrication or stored for future use.

Salt collected during the distillation process is treated in the actinide drawdown process. The (Transuranic) U/TRU product recovered in the electrorefining process has a much lower melting point than pure uranium therefore, separating the adhering electrolyte from the U/TRU metal can be achieved using a lower temperature bottom-pour method. Because the density of the U/TRU product is approximately ten times that of the molten salt, after melting the metal / salt mixture and allowing phase separation to occur, the two phases can easily be separated and poured from the system using a bottom-pour crucible. The U/TRU product is formed into ingots and used in FR fuel fabrication [59-61]. The salt collected during the process is treated in the actinide drawdown process, which is discussed next. The bottom pour process has a number of advantages for treating TRU-bearing materials as compared to the salt distillation process. The salt recovered in the U, U/TRU and metal waste processing

operations is treated by electrolysis to recover the uranium and the transuranic elements. In the electrolysis process, sufficient voltage is applied so that the uranium and transuranic ions present in the electrolyte salt are electrodeposited at a cathode and chlorine gas is evolved at an inert anode (e.g., graphite). The process temperature is 500°C for the LiCl-KCl electrolyte and 650°C in the case of a LiCl electrolyte. The electrolysis process can be operated so that all of the actinides (e.g., >99.9%) and a small amount of the lanthanides (those with reduction potentials near the actinides) are recovered as a metallic deposit on the cathode [60-63]. The salt-coated metallic deposit recovered from the electrochemical cell is transferred to the oxidant production process (along with the lanthanide-free salt after the lanthanide drawdown discussed below) where it is chlorinated and returned to the electrorefiner. After completion of actinide drawdown, the bulk of the now U/TRU-free salt is treated in a subsequent electrolysis process to remove the lanthanide fission products. This process can occur in the same process vessel used for actinide drawdown to minimize salt transfer operations. As in the actinide drawdown process, the lanthanide drawdown process yields a solid metallic lanthanide product at the cathode and chlorine gas at the anode. Operation of the cell is identical to the actinide drawdown process except that different deposition potentials are used. The salt discharged from this process contains only residual fission products (e.g., <0.1 wt%) and is recycled to oxidant production and, subsequently, the electro-refiner [61,63]. The recovered lanthanide metals are converted to oxides and subsequently combined with glass frit to form a lanthanide borosilicate glass, which is discharged as a high-level amount of salt recovered during the metal oxidation process is recycled to the vessels used for electrorefining or electrolytic reduction [63].

Noble metal fission products and cladding recovered from the fuel baskets used in the electrorefiner are treated by distillation to recover the residual salt adhering to the materials. The salt is recycled to the actinide drawdown process for actinide recovery. The noble metals are combined with cladding and assembly hardware and melted at approximately 1700°C to form an ingot, which is discharged as a high-level waste. Cesium and strontium are recovered from the molten salt used in the electrolytic reduction process by zeolite ion exchange. The molten salt is contacted with zeolite to occlude the cesium and strontium chlorides in the zeolite. Iodine present in the molten salt as an alkali iodide is also captured in the zeolite. The zeolite containing the cesium, strontium and iodine is mixed with glass frit and heated to produce a

ceramic waste form [57, 59, 62]. This waste form is held in decay storage to allow for a reduction of decay heat prior to final disposal. The bulk of the LiCl-KCl molten salt remains in the electrolytic reduction cell and is reused indefinitely. The silver impregnated zeolite containing the iodine released during fuel chopping can be combined with the ceramic waste form prior to its disposal.

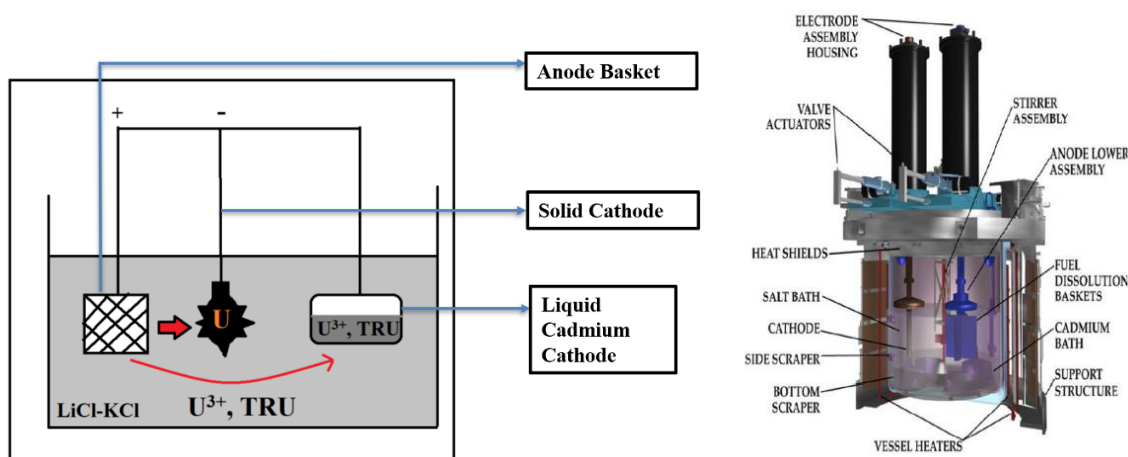


Figure 2.3 (left to right): Schematic of electrorefiner in pyroprocessing and engineering scale electrorefiner at INL Fuel Conditioning Facility [74]

2.2 Isotope of Iodine

Nuclear reactor is source of radioisotope production. Nuclear fission occurs when neutrons interact with uranium or plutonium fuel and this produces various long-lived radioactive isotopes like technetium-99 (^{99}Tc), plutonium-242 (^{242}Pu), neptunium-237 (^{237}Np), iodine-129 (^{129}I) etc. [65-68]. Iodine-129 is one of the long-lived radioactive isotopes found in nuclear waste and is primarily produced from the fission of uranium or plutonium in nuclear reactor. It emits beta particle with average energy of 40 KeV and has a half-life of 1.57×10^7 years. Due to its very long half-life and beta emission, it is considered harmful to the environment as well as hinders the proper processing of Uranium in salt bath [69-71]. Thus, the study of iodide in the eutectic melt has always been a major concern regarding the efficiency of UNF reprocessing. Significant fraction of iodide was reported to be retained in the molten salt during pyro-processing and presence of iodide may affect the reduction behavior of the actinides due to interaction with cations and chloride ions [72,73]. Iodide due to its larger size could affect the diffusivities and shift the redox potentials and deteriorates platinum electrode in the reactors. Thus, the study of electrochemical behavior of iodide is

important at high temperatures. There have been few studies on electrochemical behavior of iodide in the room temperature ionic liquids (RTIL) but not many studies are done in high temperature molten salts. The redox reactions of iodide are given as [74]:



Addition of iodide in the molten chloride will lead to formation of trihalide ions or interhalogen compounds during the pyroprocessing of used nuclear fuel in an electro-refiner. Fujiwara et al [75] proposed iodide based molten salt systems such as LiF-LiCl-LiBr-LiI, and LiF-NaBr-LiI for high temperature battery applications because of their higher conductivity (up to 3.5 S/cm) than that of conventional LiCl-KCl (< 2.1 S/cm). Presence of oxygen caused instability of iodide at temperatures higher than 280 °C by following the reactions:



At high temperatures the reaction (20) is considered to be accelerated which results in large concentration of I_2 through the reaction (21). The molecular iodine evaporates at a faster rate at high temperatures and the iodide is decomposed. This observation suggests that iodide may not interfere significantly with the reprocessing of oxide fuels. In the absence of oxygen, the iodide may complex with chloride. The physical and electrical properties of the molten salt systems depend on the structure and interactions of the constituents. The structural arrangements that are present in molten salts can be viewed as intermediates between discrete chemical bonds and periodic crystalline lattices [76]. The inter-atomic interactions determine the local ordering of the molten salt. The electrochemical properties are significantly influenced by the structural characteristics of the molten salt. The ion size and type in a molten salt system such as KX-LiX would affect the electrochemical stability. The ordering and structure of the melt could be described based on the entropy.

The entropy (ΔS) of the electrolysis of melt can be determined using the relation [77]:

$$\Delta S = nF(\partial E/\partial T)_P \quad (22)$$

Where, n = number of electrons, $\partial E/\partial T$ = change in electrochemical window with temperature. Low entropy values indicate higher order and enhanced attractive interaction of the species in

the molten salt. Generally, an increase in the entropy was observed with increase in the anion size of unary molten salts [78]. The electrolysis potential turns out to be more anodic as the anion size increases due to weaker Coulombic interaction between the anion-cation pairs as well as increased repulsion between the larger anions [79]. When two types of cations are present in molten salt with different sizes and different charge densities, an asymmetric polarization of anions is anticipated which may result in the electrostatic stability of the mixture. When two different types of anions such as chloride and iodide are present along with different cations, the asymmetric polarizations of the ions and their effect on the physical and electrochemical properties are not well documented.

Increase in the temperature shifted the reduction potentials to more positive values. The calculated entropy of KCl-NaCl increased with temperature, whereas KI-LiI do not show significant change in the entropy with temperature. Furthermore, the entropy decreases with increase in the anion size for the KCl-LiCl, KBr-LiBr and KI-LiI mixtures. On the other hand, the entropy increases with increase in the anion size for the pure salts (unmixed) [80].

Even though not much information is available on the interaction of iodide with high temperature molten chloride salts, some work has been reported on iodide-chloride interactions in room temperature ionic liquids. The oxidation behavior of iodide has been investigated by several groups in the room temperature ionic liquids (RTIL) such as 1-butyl-3-methyl imidazolium tetra fluoroborate ([C4mim][BF4]) [81], 1-Ethyl-3-methyl imidazolium bis(trifluoro methane sulfonyl) imide [82], 1-butyl-3-methylimidazolium bis(trifluoro methyl sulfonyl) imide, [C4mim][NTf2] [83]. In solvents like water, methanol, acetic acid etc, iodide yielded a single oxidation peak corresponding to the reaction:



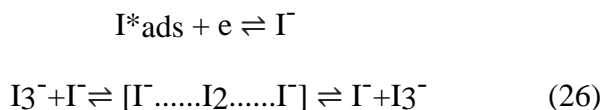
In other solvents such as acetic anhydride, acetone, and acetonitrile, two well defined oxidation peaks are observed. The first anodic peak was assigned to an irreversible reaction that occurred at 0.58 V vs $V_{\text{Ag}/\text{AgCl}}$ in the RTIL [C4mim][BF4] [91] :



The second oxidation peak was reported at about 1.0 V_{Ag} that was associated with a reversible reaction:



The equilibrium constant, K_{eq} , of the reaction $I + I_2 = I_3$ is 10 in aqueous solution and $K_{eq} = 10^7$ in both acetonitrile and RTIL [82]. The higher equilibrium constant is due to a faster diffusion process which is associated with an anomalous charge transfer given by the rapid exchange reaction [84]:



Where I_2 is exchanged between I^- and I_3^- displacing them without physical mass transfer. The reduction of iodine in RTIL occurs at a faster rate [85]. The reduction is a two-electron process occurred in two steps. The first step is the reduction of iodine to triiodide ($3I_2 + 2e^- \leftrightarrow 2I_3^-$), followed by the reduction of I_3^- to iodide (I^-) as the second step ($I_3^- + 2e^- \leftrightarrow 3I^-$). The rate determining step (RDS) for the reduction of iodine is considered to be the adsorption of I^*_{ads} on the electrode surface by following the reaction (27) and further reduced to iodide by the reaction (28):

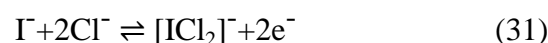


The neutral I_2 and positively charged I^+ are strongly electrophilic. Therefore, the redox process involving $I^-/I_2/I^+$ will be highly sensitive to impurities of Cl^- or Br^- in the nonhaloaluminate ionic liquid [86,87]. Furthermore, during the I^-/I_2 redox process, the product and reactant can form a polyhalogen complex anion based on the reaction:



Such complexation is possible because I^- is a nucleophile (Lewis/Base) and I_2 is an electrophile (Lewis acid) and therefore these species can easily combine to form a complex [86]. Presence of nucleophile halides such as Cl^- can stabilize the electrophilic I_2 and I . Therefore, the oxidation of I is significantly influenced by the Cl . Bentley et al. [87] investigated the sensitiveness of $I^-/I_2/I$ redox processes to the nucleophilic chloride addition in binary IL mixture composed of 1-butyl-3-methylimidazolium chloride ([C4mim]Cl) and 1-ethyl-3-methylimidazolium bis-(trifluoromethanesulfonyl)imide ([C2mim][NTf2]).

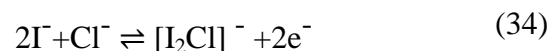
Without chloride addition, the oxidation of iodide to iodine is an overall one electron process with triiodide as an intermediate. When chloride is present additional peaks are observed in the cyclic voltammogram (CV) at less anodic potential than that of I_3^-/I_2 due to the formation of interhalide anion intermediates such as $[I_2Cl]^-$ and $[ICl_2]^-$ depending on the initial ratio of I^-/Cl^- in the electrolyte [87]. Addition of Cl^- makes the iodide oxidation a two-electron process, through stabilization of I^+ by reaction with Cl^- as:



Here $[ICl_2]^-$ is an interhalogen anion formed during oxidation of iodide in the presence of excess chloride. Another interhalogen complex formation could occur when the chloride concentration is low given by the reactions [87]:

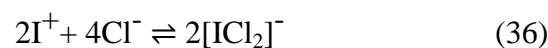
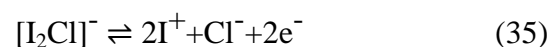


Overall,

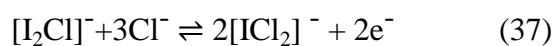


The interhalogen anions can be formed during the anodic sweep by a two-step electrochemical and chemical (EC) reaction steps given by the following reactions [87]:

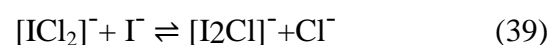
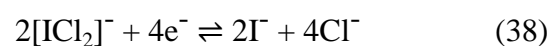
EC mechanism:



Overall:



During the cathodic sweep, $[ICl_2]^-$ is reduced to I^- in a single 2 electron process, which further reacts with I^- to form I_3^- [87]:





2.3. Chemla Effect

The Chemla effect refers to a phenomenon where the internal mobility of a larger cation is higher than that of a smaller cation at high concentrations of the larger cation in a binary salt mixture such as LiCl-KCl that consists of large and small cations with a common anion. This effect could lead to compositional gradient of ions in an electrochemical cell where a local shift in the composition from liquidus range may cause solid precipitation of salt [88]. Chemla effect has been reported for ternary cation systems such as (Na,K,Cs)Cl [89] and also for anions in Li(Cl,NO₃) [80]. Presence of iodide at above a threshold concentration could result in anionic Chemla effect where the internal mobility of iodide could be higher than that of chloride.

Chemla effect is observed in binary molten salt systems consisting of two cations and a common anion or two different anions with a common cation [81, 82]. In case of a binary salt mixture with a common anion, the internal mobilities of the cations vary with the concentration of cations, and the isotherms of the mobilities cross each other at a particular concentration, as seen in Fig. 2.4. The mobility of larger cation is higher than that of the smaller cation beyond this cross-over concentration, which is referred to as the Chemla effect [83]. Two major types of internal mobility isotherms are observed as illustrated in Fig 1(a) and (b). In type-I, internal mobilities of both the smaller (M₁) and larger cations decrease with the increase in the M₂X concentration in the M₁X-M₂X binary mixture. However, the decrease in the mobility occurs at a faster rate in case of the smaller cation than that of the larger cation resulting in a crossing point [93]. Type-I Chemla effect has been observed in the LiCl-KCl binary mixture [84]. In type II Chemla effect, the internal mobility of the smaller cation (M₁) decreases and the mobility of larger cation (M₂) increase with the increase in the concentration of M₂X in the salt mixture, as depicted in Fig. 1(b). Salt mixtures of (Li,K)F, (Ag,Na)I, (Ag,K)I, and (Ag,Cs)I show this type of Chemla effect. The difference in the mobilities can be explained based on a) free space effect, b) tranquilization effect, and c) agitation effect.

When free space is small, large ions cannot move favorably. This effect is the result of restriction in the reorientation motion of the polyatomic anions. Therefore, alkali chlorides do not show free space effect [85]. Tranquilization effect is due to a strong Coulombic interaction of M2 with X that results in the restricted internal mobility of M1.

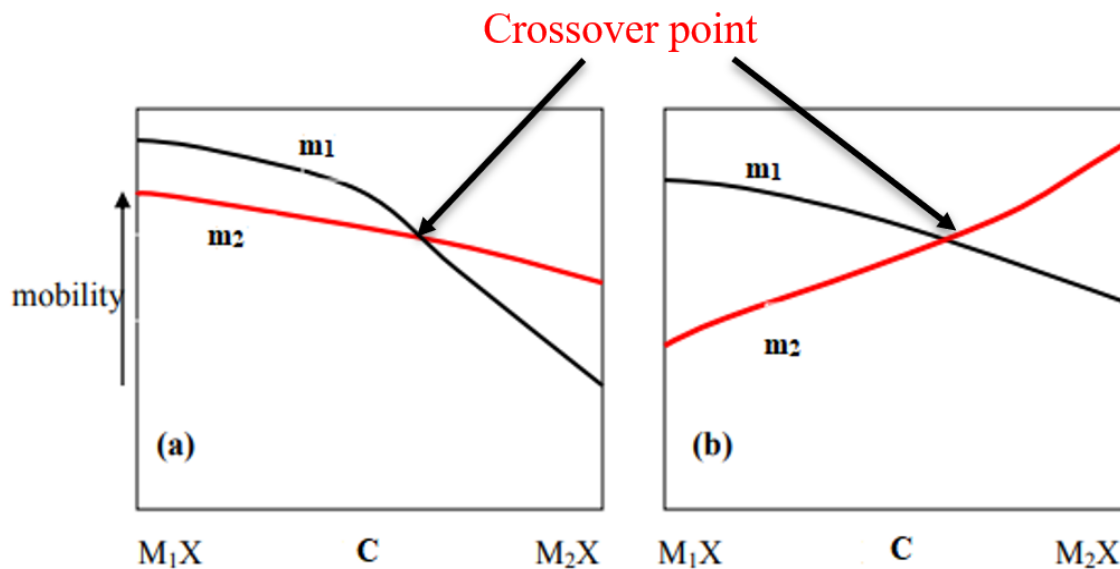


Figure 2.4 Schematic representation of isotherms of internal mobilities of binary salt mixture (M1X+M2X) with smaller cation M1 and larger cation M2 as a function of M2X content (X2). Fig 1(a) depicts type-1 Chemla effect. Type 2 Chemla effect is illustrated in Fig. 1(b).

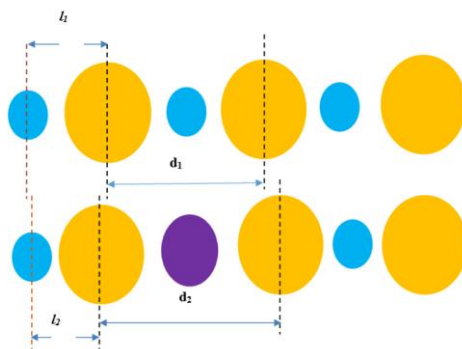


Figure 2.5: Schematic of dynamic dissociation model

Introduction of a larger cation increases the distance between the anions ($d_2 > d_1$). This results in increased association of the smaller cation with the anion ($l_2 < l_1$). The self exchange velocities (SEV) of the cations decrease with increase in the separation of anions. The rate of decrease of SEV is larger for the smaller cation which leads to crossover point in the mobility isotherms. This is referred to as the dynamic dissociation model to explain the Chemla effect.

The tranquilization effect by M2 on the cation M1 is stronger when M2 is divalent or trivalent [83]. The Li^+ has the possible tranquilization effect because Li^+ has a strong interaction with anion. The agitation effect is attributed to the high polarizability of a particular cation in the salt mixture [83]. Dynamic dissociation model proposed by Okada [83] describes the Chemla effect based on the average distance between the anions (d), and the separation distance between the cation-anion pairs (l). According to this model, when a larger cation is introduced in the salt mixture, the anion-anion separation increases which modifies the potential profiles of the neighboring ions. Figure 2.5 schematically illustrates the dynamic association model. Incorporation of a larger cation increase the anion-anion separation from $d1$ and $d2$. This makes the smaller cation to be more associated with the anion by decreasing the initial cation-anion separation from $l1$ to $l2$ as seen in the Fig. 2.5. Internal mobility of an alkali ion is expressed as a function of molar volume (V_m) by the relation:

$$V = \frac{A}{V_m - V_0} \exp\left(\frac{-E}{RT}\right) \quad (42)$$

A, V_0 and E are constants independent of the second cation. Increasing the molar volume decrease the internal mobility. Molecular dynamic simulation studies using rigid ion models indicated that average length between anions become longer due to the strong interaction between Li^+ and Cl^- . Therefore, the self-exchange velocity (SEV) related to the separating motion of neighboring cation and anion will have a crossing point. The diffusion coefficient of Li^+ at 1096 K was considerably smaller than that of K^+ as the KCl addition increased to above 50% and the KCl content for the crossover would shift to lower values as the temperature decreased [82,83]. Li^+ and Cl^- to be four-fold rather than 6 fold. The transport behavior of the cations in LiCl-KCl is related to the cation- anion pair distribution functions along with volume dilation that increased with the KCl content. The Li^+ is ‘trapped’ in the local liquid structure before diffusing out and the time of oscillation within the local liquid structure increased with decreasing temperature of the mole and decreasing average number density [85]. The cross over fraction of KCl (pk) to observe the Chemla effect at 723 K was 0.325 and at 773 K the fraction of KCl decreased to 0.3. The eutectic mixture of LiCl-KCl has a pk of 0.418. Therefore, Chemla effect is expected to occur at eutectic composition and pyroprocessing relevant temperatures. Chemla effect resulted in the increased concentration and precipitation of KCl at the cathode of Lithium-aluminum/iron sulfide batteries that contain LiCl-KCl molten salt electrolyte [85]. Such a high concentration of KCl was reported to result

in the formation of a new phase with the composition of $\text{LiK}_6\text{Fe}_{24}\text{S}_{26}\text{Cl}$ in the iron sulfide electrode [84]. During the pyroprocessing of used nuclear fuels in the LiCl-KCl molten salt electrolyte, Chemla effect could polarize the cathode by excess mobility of the K.

Anion Chemla effect was reported in LiCl-LiNO₃ salt mixture. At chloride fractions greater than 0.15, the mobility of chloride was smaller than that of nitrate [89]. The dynamic dissociation model can be extended to describing the anion Chemla effect. In LiCl-LiI molten salt system, Li are the main charge carriers. The movement of Li^+ was restricted by randomly mixed anions of different size. Furthermore, the diffusion coefficient of Li^+ decreased with mixing of LiCl to LiI [89]. When the common anion was I^- , a negative deviation from the additive law for the electrical conductivity was noted in the LiI-CsI or LiI-TlI due to largely different cation radius. Presence of large and small anions causes asymmetric electric field, especially when the cation is small. Presence of iodide could lead to anion Chemla effect in the molten chloride salt electrolyte during pyroprocessing of the used nuclear fuels.

After literature survey, it is found out that there are few studies on electrochemical behavior of iodide in the room temperature are done but not many studies are done in high temperature molten salt. The iodide plays huge role in affecting the efficiency of the reprocessing of the Uranium from the UNF. So, the focus of the project is to study the electrochemistry of iodide in high temperature molten salts such as LiCl-KCl eutectic or LiCl-KCl in presence of Li_2O . Significant fraction of iodide was reported to be retained in the molten salt during pyroprocessing and presence of iodide may affect the reduction behavior of the actinides due to interaction with cations and chloride ions. Iodide due to its larger size could affect the diffusivities and shift the redox potentials and deteriorates platinum electrode in the reactors. Thus, the study of electrochemical behavior of iodide is important at high temperatures. The project consisted of different tasks which will be covered in following chapters.

Chapter 4: Electrochemical/chemical speciation behavior of iodide in molten chlorides

Chapter 5: Effect of iodide on the reduction of CeCl_3 in LiCl-KCl

Chapter 6: Electrochemical/chemical speciation behavior of iodide in LiCl-KCl- Li_2O melt

References

1. J.P. Ackerman, *Industrial and Engineering Chemistry Research*, 30, 141-145 (1991).
2. C.E. Till and Y.I. Chang, *Plentiful Energy - The Story of the Integral Fast Reactor*, ISBN: 978-1466384606 (2011).
3. J.J. Laidler, J.E. Battles, W.E. Miller, J.P. Ackerman, E.L. Carls, *Prog. Nucl. Energy* 31 131–140(1997).
4. J.P. Ackerman, T.R. Johnson, L.S.H. Chow, E.L. Carls, W.H. Hannum, J.J. Laidler, *Prog. Nucl. Energy* 31 141–154(1997).
5. R.W. Benedict, H.F. McFarlane, *Radwaste Mag.* 5 23 (1998).
6. T. Inoue, L. Koch, *Nucl. Eng. Technol.* 40 183–190 (2008).
7. K.M. Goff, J.C. Wass, K.C. Marsden, G.M. Teske, *Nucl. Eng. Technol.* 43 335–342 (2011).
8. K. Nagarajan, B.P. Reddy, S. Ghosh, G. Ravisankar, K.S. Mohandas, U.K. Mudali, K.V.G. Kutty, K.V.K. Viswanathan, C.A. Babu, P. Kalyanasundaram, P.R.V. Rao, B. Raj, *Energy Procedia* 7 431–436 (2011).
9. T. Koyama, Y. Sakamura, M. Iizuka, T. Kato, T. Murakami, J.-P. Glatz, *Procedia Chem.* 7 772–778 (2012).
10. M. F. Simpson and Jack D. Law, *Nuclear Fuel Reprocessing*, INL/EXT-10-17753, February (2010).
11. T. Todd, *Nuclear regulatory Commission Seminar*, March 25 (2008).
12. S. Phongikaroon, *EGMN 691 – Nuclear Fuel cycle*, Lecture #1, Fall (2015).
13. M. Iizuka, *Journal of The Electrochemical Society*, 145, 84-88 (1998).
14. Y.I. Chang, *Nuclear Technology*, 88, 129-138 (1989).
15. J.P. Ackerman, *Industrial and Engineering Chemistry Research*, 30, 141-145 (1991).
16. G. Janz, *Molten Salt Handbooks*, New York and London: Academic Press (1967).
17. G. J. Janz, G. L. Gardner, U. Krebs, and R. P. T. Tomkins, *Molten Salts: Volume 4, Part 1, Fluorides and Mixtures Electrical Conductance, Density, Viscosity, and Surface Tension Data*, New York (1974).
18. G. J. Janz, R. P. T. Tomkins, C. B. Allen, J. R. Downey, Jr, G. L. Gardner, U. Krebs, and S. K. Singer, *Molten Salts: Volume 4, Part 2, Chlorides and Mixtures—Electrical Conductance, Density, Viscosity, and Surface Tension Data*, New York (1975).

19. G. Janz, Tech. Rep. NSRDS-NBS61-II
20. H. Lee, G.I. Park, J.W. Lee, K.H. Kang, J.M. Hur, J.G. Kim, S. Paek, I. T. Kim, I.J. Cho, *Sci. Technol. Nucl. Install*, 343492 (2013).
21. K.C. Song, H. Lee, J.M. Hur, J.G. Kim, D.H. Ahn, Y.Z. Cho, *Nucl. Eng. Technol.* 42 131–144 (2010).
22. H. Lee, J.M. Hur, J.G. Kim, D.H. Ahn, Y.Z. Cho, S.W. Paek, *Energy Procedia* 7 391–395 (2011).
23. T. Biju Joseph, N. Sanil, K.S. Mohandas, K. Nagarajan, *J. Electrochem. Soc.* 162 E51–E58 (2015).
24. T. Wu, X. Jin, W. Xiao, X. Hu, D. Wang, G.Z. Chen, *Chem. Mater.* 19 153–160 (2007).
25. Y. Sakamura, M. Kurata, T. Inoue, *J. Electrochem. Soc.* 153 D31–D39 (2006).
26. B.H. Park, S.B. Park, S.M. Jeong, C.S. Seo, S.W. Park, *J. Radioanal. Nucl. Chem.* 270 575–583 (2006).
27. K.S. Mohandas, *Trans. Inst. Min. Metall. C* 122 195–212 (2013).
28. S.M. Jeong, J.M. Hur, S.S. Hong, D.S. Kang, M.S. Choung, C.S. Seo J.S. Yoon, S.W. Park, *Nucl. Technol.* 162 184–191 (2008).
29. S.D. Herrmann, S.X. Li, M.F. Simpson, S. Phongikaroon, *Sep. Sci. Technol.* 41 1965–1983 (2006).
30. E.Y. Choi, J.W. Lee, J.J. Park, J.M. Hur, J.K. Kim, K.Y. Jung, S.M. Jeong, *Chem. Eng. J.* 514 207–208 (2012).
31. E.Y. Choi, J.K. Kim, H.S. Im, I.K. Choi, S.H. Na, J.W. Lee, S.M. Jeong, J.M. Hur, *J. Nucl. Mater.* 437 178–187 (2013).
32. J.M. Hur, S.S. Hong, H. Lee, *J. Radioanal. Nucl. Chem.* 295 851–854 (2013).
33. Y. Sakamura, T. Omori, T. Inoue, *Nucl. Technol.* 162 169–178 (2008).
34. S.M. Jeong, H.S. Shin, S.S. Hong, J.M. Hur, J.B. Do, H.S. Lee, *Electrochim. Acta* 55 1749–1755 (2010).
35. J.M. Hur, S.M. Jeong, H. Lee, *Electrochem. Commun.* 12 706–709 (2010).
36. W. Xiao, D. Wang, *Chem. Soc. Rev.* 43 3215–3228 (2014).
37. K.V. Gourishankar, L. Redey, M. Williamson, in: W. Schneider (Ed.), *Light Metals, The Minerals, Metals & Materials Society*, pp. 1075–1082, (2002).

38. S.M. Jeong, H.S. Shin, S.H. Cho, J.M. Hur, H.S. Lee, *Electrochim. Acta* 54 6335–6340 (2009).
39. T. Koyama, M. Iizuka, Y. Shoji, R. Fujita, H. Tanaka, T. Konayashi, and M. Tokiwai, *Journal of Nuclear Science and Technology*, 34, 384 (1997).
40. M. F. Simpson, “Developments of Spent Nuclear Fuel Pyroprocessing Technology at Idaho National Laboratory,” DOI: 10.2172/1044209 (2012).
41. S.X. Li and M.F. Simpson, *Minerals and Metallurgical Processing*, 22, 192-198 (2005).
42. R.O. Hoover, Ph.D. Thesis, University of Idaho, Idaho Falls, ID (2014).
43. O. Shirai, M. Iizuka, T. Iwai, Y. Arai, *Journal of Applied Electrochemistry*, 31, 1055-1060 (2001).
44. G. Cordoba, C. Caravaca, *Journal of Electroanalytical Chemistry*, 572, 145–151, (2004).
45. J.A. Plambeck, *Fused salt systems*. Vol. X., 1976.
46. S. Kim, D. Yoon, Y. You, S. Paek, J. Shim, S. Kwon, K. Kim, H. Chung, D. Ahn, H. Lee, *Journal of Nuclear Materials*, 385, 196–199 (2009).
47. R. Taylor, *Reprocessing and Recycling of Spent Nuclear Fuel*, ISBN-13: 978-1782422129.
48. C.E. Stevenson, American Nuclear Society, LaGrange Park, IL USA (1987).
49. R.K. Steunenbergh, R.D. Pierce and L. Burris, *Progress in Nuclear Energy Series III, Process Chemistry*, 461 (1969).
50. C.E. Till, Y.I. Chang and W.H. Hannum, *Progress in Nuclear Energy*, 31, 1-2, 3 (1997) and references therein.
51. National Research Council, National Academy Press, Washington, DC (2000).
52. K. Gourishankar, L. Redey and M.A. Williamson, *Light Metals 2002*, TMS, 1075 (2002).
53. L.A. Barnes and M.A. Williamson, 2008 International Pyroprocessing Research Conference, Jeju Island, Republic of Korea, August (2008).
54. A.F. LaPlace, J. Lacquement, J.L. Willit, R.A. Finch, G.A. Fletcher and M.A. Williamson, “Electrodeposition of Uranium and Transuranics (Pu) on Solid Cathodes,” *Nuclear Technology*, Vol. 163, 366 (2008).

55. M. F. Simpson, DOI: 10.2172/1044209 (2012).
56. Boustani E, Ranjbar H, Rahimian , Applied Radiation and Isotopes 147 121 (2019)
57. Golabian A, Hosseini MA, Ahmadi M, Soleimani B, Rezvanifard Applied Radiation and Isotopes 131 62 (2018)
58. B. Ponsard, Nuclear Medicine and Biology 41 648 (2014)
59. B Soleimani, MA Hosseini, M Rezvanifard, M Ahmadi, J. Ebadati, Applied Radiation and Isotopes 139 195 (2018).
60. B.G. Hong, Fusion Engineering and Design 89 2493 (2014).
61. B.G. Hong, International Journal of Hydrogen Energy 40 15153 (2015).
62. S.H.,Hong, M.H. Kim, Nuclear Engineering and Technology 50 1060 (2018)
63. S. M. Frank, Summary of Iodine Partitioning in EBR-II Fuel, Internal Report, Idaho National Laboratory, SMF-001-16, (2016).
64. P. Masset, Journal of Power Sources 160 688–697 (2006).
65. C.L. Bentley et al., Analytical Chemistry, 88 1915-1921 (2016).
66. S. Fujiwara et al., J. Power Sources, 194, 1180 (2009).
67. J.D. Martin, S.J. Goettler, N. Fosse, L. Iton, Nature, 419, 381(2002).
68. Y.S. Cohen, Y. Gabay, Y. Cohen, J. Electrochem. Soc., 163, H377 (2016).
69. M. Chemla, I. Okada, Electrochimica Acta 35, 1761 (1990).
70. I.K. Delimarskii, B.F. Markov, Electrochemistry of Fused Salts, The Sigma Press Publishing, Washington, DC, (1961).
71. Y. S. Cohen, Y. Gabay, and Y. Cohen, ECS Electrochem. Lett., 4, H1 (2015).
72. Y. Zhang, J. B. Zheng, Electrochimica Acta 52, 4082 (2007).
73. C. L. Bentley, A. M. Bond, A. F. Hollenkamp, P. J. Mahon, J. Zhang, J. Phys. Chem. C, 118, 22439 (2014).
74. E. I. Rogers, I. Streeter, L. Aldous, C. Hardacre, R. G. Compton, J. Phys. Chem. C 112, 10976 (2008).
75. R. Kawano, Watanabe, Chem. Commun., 330–331 (2003).
76. E. I. Rogers, I. Streeter, L. Aldous, C. Hardacre, R. G. Compton, J. Phys. Chem. C, Vol. 112, (2008).
77. C.L. Bentley, A.M. Bond , A.F. Hollenkamp, P.J. Mahon,J. Zhang, Journal of Physical Chemistry, , 118, 22439 (2014).

78. C. L. Bentley, A.M. Bond , A.F. Hollenkamp, P.J. Mahon,J. Zhang,. Analytical Chemistry, 88,1915 (2016).
79. R. Takagi, H. Shimotake, K. J. Jensen, J. Electrochem. Soc., 131, 1280 (1984).
80. M. Matsumiya, H. Matsuura, R.Takagi, Y. Okamoto, Journal of The Electrochemical Society, 147, 4206 (2000).
81. Endoh, I.Okada, J. Electrochem. Soc., 137, (1990).
82. Okada, H.Horinouchi, F. Lantelme, J. Chem. Eng. Data 55, 1847 (2010).
83. Endoh, I. Okada, J. Electrochem. Soc., 137, 933 (1990).
84. I Okada, J. Molecular Liquid, 83, 5-22 (1999) .
85. R. Takagi, H. Shimotake, K. J. Jensen, J. Electrochem. Soc.131, 1280 (1984).
86. F. Lantelme, P. Turq, J Chem Phys, 72, 3177 (1982).
87. E. Vallet, D. E. Heatherly, R. L. Sherman, and J. Braunstein, J. Electrochem. Soc., 129, 49 (1982).
88. A. Melendres, C. C. Sy, and B. Tani, J. Electrochem. Soc., 124, 1060 (1977).
89. T. Kamiyama, A. Fukase, N. Asahi, Y Nakamura, J Molecular Liquid, 83, 51 (1999).

Chapter 3: Experimental Procedure

3.1 Experimental Setup

All experiments were carried out inside a controlled atmosphere glove box filled with dry ultra- high purity argon where the oxygen and moisture contents were maintained at less than 2 ppm. Molten salt is an important electrolyte for pyroprocessing of used nuclear fuels and part of the electrochemical cell, due to its ability to conduct ionic current easily. The LiCl-KCl salt is hygroscopic and needs to be stored in an inert environment in order to prevent the formation of hydrates/hydroxides/oxy-hydroxides due to interaction with water in the air. In addition, when the salt is in liquid form, the formation of alkali-oxides or rare-earth oxides is possible in the presence of significant oxygen. Glove Box used for this experiment is MBraun MB10 Compact System. Timely purification of gas should be done inside the glove box and this can be done by purging. Gases like nitrogen, argon or helium of commercial purity could be used for purification but in our case, ultra-high purity argon gas was used. The purging procedure for the glove box is given below:

- Setup purge gas sources with pressure reducing valve
- Open “Blind Flange” and feed one end of the reinforced hose through the open flange into the glove box
- Air and excess purge gas escapes through the flange opening until the box O₂ value has reached <100ppm shown in a display meter.
- After reaching an O₂ value reaches the value of <100 ppm , the hose is removed and the flange is immediately closed.
- The purge gas flow is turned off.

Similarly, if the reading of the moisture shows the water content inside the glove box to be very high which is more than 100 ppm then this could be solved by process of regeneration. It should be made sure that enough gas mixture of 10% hydrogen + 90% argon is available before the regeneration program is run. The circulation mode needs to be stopped before the regeneration button is pressed. After the circulation function is activated, circulation RKM1 button should be pressed to switch it off and to release the “Regeneration Purifier” button. The Regeneration button is then pressed to start the regeneration mode. The changing of grey regeneration button to dark grey usually represents the start of regeneration cycle.

Regeneration usually takes 24 hours to 48 hours to complete. This will help to reduce any moisture or water content in the glove box.

The electrodes are a tungsten working electrode, a silver wire (or AgCl coated silver wire by anodizing the silver wire in saturated KCl solution at 5 V for 20 minutes) dipped in a closed-ended pyrex tube filled with a 1wt% AgCl in LiCl-KCl solution as a reference electrode, and a glassy carbon rod connected to the glassy carbon cell crucible as a counter electrode. The electrodes are all immersed in the molten salt electrolyte bath and are then connected to the potentiostat.

The working electrode (WE) was tungsten wire (Alfa Aesar, 99.95%) of 1 mm diameter. Tungsten functions well as an electrode because it is a good conductor and is chemically inert. Tungsten does not react with the molten LiCl-KCl at 500°C. This is important because interaction between the working electrode and rare-earth elements can produce intermetallics which affect the electrochemistry results. In the early stages of this research, platinum was used as a working electrode. However, it was discovered that platinum formed intermetallics with lanthanum or cerium chloride additions to the salt that disrupted the electrochemical measurements. Tungsten has often been reported in literature and was found to be a good replacement since it did not produce any significant intermetallics with the other elements such as Ce, Nd, Dy, and U. Glassy carbon rod (Alfa Aesar, type 1) of 2 mm diameter is used as a counter electrode (CE). Glassy carbon was selected for its good electrical conductivity, high temperature resistance, chemical inertness, and not-wetting characteristics. The main purpose of the counter electrode is to complete the circuit of the electrochemical cell, allowing current to flow. Therefore, it is necessary to ensure that the counter electrode area in contact with the salt is much larger than the WE area, so that the reaction of interest on the working electrode is not limited by the area of the CE. In order to accomplish this, the glassy carbon rod is rested on the bottom of the glassy carbon crucible, effectively making the entire graphite crucible in contact with the salt the counter electrode. A lab fabricated Ag/AgCl electrode was used as reference electrode. Silver wire (Alfa Aesar, 99.999%) of 1 mm diameter was anodized in saturated KCl solution at 5 V for 20 minutes to coat the surface with AgCl and baked in vacuum oven at 120 °C overnight to remove water. The AgCl coated surface will be placed in a 1 mm thick walled 4 mm diameter Pyrex tube whose closed end is polished down to 0.2 mm thick. The thin membrane will be able to conduct the ions but not electrons. The

pyrex tube is filled with a reference solution consisting of LiCl-KCl eutectic + 1 wt% AgCl [1]. The test tube keeps the reference solution physically separated from the bulk salt. However, the thin walls of the test tube allow for ionic conduction between the electrolytes but not electronic conduction.

Anhydrous beads of 99.99% LiCl-KCl eutectic from Sigma Aldrich was used as salt for experiments. Anhydrous 99% KI from Sigma Aldrich was also used to be mixed with the eutectic for the experiment. 15 grams of salt was taken for each experiment with varying concentration of KI ranging from 0 to 5 wt%. All the experiments are performed in glove box to reduce the chances of oxidation of the salt and get reliable results.

3.2 Electrochemical Techniques

3.2.1 Open Circuit Potential (OCP)

The thermodynamic properties in terms of redox reaction can be readily measured by monitoring the OCP. OCP is also known as ‘the zero-current potential’ or ‘the rest potential’ [2,3]. When the redox couple is present at an equilibrium state on the electrode, the OCP indicates a mixed potential between the oxidation and reduction reactions, which is the equilibrium potential. By providing the equilibrium potential, the apparent standard potential (typically referred as a formal potential) of the redox reaction can be calculated by plotting the equilibrium potential vs concentration of species.

3.2.2 Electrochemical Impedance Spectroscopy (EIS)

EIS is used to measure the cell/ electrode impedance as a function of frequency [3]. This technique is useful to understand the electrode process with respect to contributions from diffusion, reaction kinetics, double layer capacitance and adsorption of species on the electrode surface etc. The EIS can be interpreted with equivalent circuit consisting of resistances, capacitances, diffusion related impedances (Warburg components), inductor (contributed by adsorption) etc. The impedance can be measured by applying a perturbation signal which results in a corresponding response like solution resistance, double layer capacitance and charge transfer resistance. The potential input can be expressed as [4]:

$$E(t) = E(0)\sin(\omega t) \quad (43)$$

where $E(t)$ is the potential at time t (V), $E(0)$ is the amplitude of the potential signal (V), and ω is the angular frequency (rad s^{-1}) which is 2π times the conventional frequency in Hz. The current response can be expressed as [5]:

$$i(t)=i(0) \sin (\omega t+\phi) \quad (44)$$

where $i(t)$ is the current at time t (A), $i(0)$ is the amplitude of the current signal (A), and ϕ is the phase angle. This current-voltage relation is analogous to Ohm's law; therefore, the impedance, Z , can be expressed as:

$$Z(t)=E(t)/i(t)=E(0)\sin (\omega t)/i(0)\sin(\omega t+\phi)=Z(0)\sin (\omega t)/\sin(\omega t+\phi) \quad (45)$$

where $Z(t)$ is the impedance (Ω) and $Z(0)$ is the amplitude of the impedance. When the $E(t)$ and $i(t)$ are considered in complex plane, the equations can be described as

$$E(t)=E(0)\exp (j\omega t) \quad (46)$$

$$i(t)=i(0) \exp (j(\omega t-\phi)) \quad (47)$$

where j is the imaginary number, $\sqrt{-1}$. By applying complex function, $\exp(j\phi)=\cos\phi+j\sin\phi$, the impedance, Z , can be expressed in complex plane as

$$Z(t)=Z(0)(\cos\phi+j\sin\phi)=Z(\text{Re})+Z(\text{Im}) \quad (48)$$

where $Z(\text{Re})$ and $Z(\text{Im})$ are the real and imaginary part of the impedance. The $Z(\text{Re})$ and $Z(\text{Im})$ can be plotted on x-axis and y-axis, respectively, which is called the 'Nyquist plot.'

Figure 3.1 shows a simple EIS data in the form of Nyquist plot. The simplest model for the electrode process is called Voigt model containing solution resistance (R_s), charge transfer resistance (R_{ct}), and double layer capacitance (C_{dl}), as shown in Figure 3.2. The impedance of the Voigt model can be expressed by using following equation [6]:

$$Z(t)=R_s+1/(1/R_{ct}+j\omega C_{dl})=R_s+R_{ct}/1+j\tau\omega \quad (49)$$

where τ is the time constant relating with RC circuit. First, it becomes very small and is negligible at high frequency. Second, it approaches R_{ct} at very low frequency. Figure 3.1 shows the ideal Nyquist plot for the Voigt model where R_s and R_s+R_{ct} can be easily found on the x-axis. The R_{ct} is formed when an electrochemical reaction occurs on the electrode at the equilibrium state, $R \leftrightarrow O + ne^-$, and the exchange current density (i_0 , $A \text{ cm}^{-2}$) and rate constant (k_0 , cm s^{-1}) for the charge transfer can be calculated by using [6]:

$$R_{ct}=RT/nFSi_0=RT/n^2F^2Sk^0C_0^{1-\alpha} \quad (50)$$

Since the polarization of the electrochemical system in reality can be non-ideal and more complex according to the interfacial formations, the constant phase element (CPE) is typically being utilized to fit the experimental EIS spectra through the following expression [7]:

$$Z_{CPE}=1T(j\omega)\phi$$

where T is a constant in $F\text{ cm}^{-2}\text{ s}\phi^{-1}$ is the constant, ϕ is the number constant between -1 and 1 , and ω is the frequency. Here, CPE can easily become double-layer capacitance, Warburg resistance, or pure resistance by changing the number of ϕ .

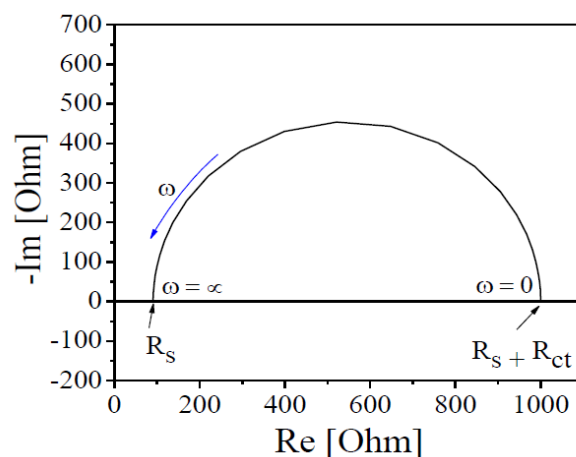


Figure 3.1: Ideal Nyquist curve for the Voigt

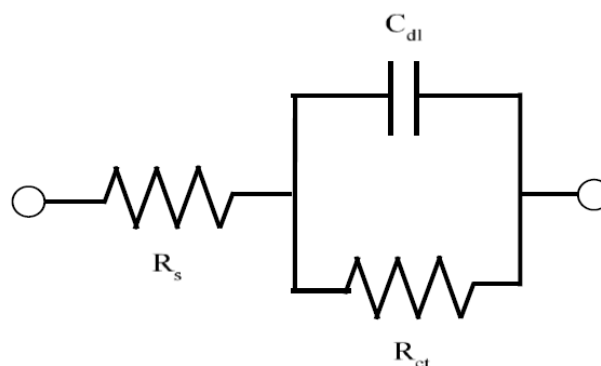


Figure 3.2: An equivalent circuit for Voigt model which is composed with resistance and capacitance

3.2.3 Cyclic Voltammetry (CV)

Cyclic voltammetry (CV) is a common electrochemical analysis technique in which potential is ramped anodically and then reversed in the cathodic direction between two vertex points repeatedly at a constant scan rate, and the analyte both reduces and oxidizes on the WE surface. In general, the more repetitions of the cyclic sweep, the better the resulting voltammograms assuming no adsorption effects at the electrode surface [8]. It is typically applied to study the electrochemistry of electroactive species presents in an electrolyte. Electrodes used in voltametric techniques are generally inert such as glassy carbon or platinum

and do not participate in the electrochemical reaction. There are different types of Voltammetry. The different types of voltammetry techniques can be listed as

- a) Linear sweep voltammetry
- b) Cyclic voltammetry
- c) Potential step voltametric techniques
- d) Differential pulse voltammetry
- e) Square wave voltammetry
- f) Stripping voltammetry.

Typically, linear sweep voltammetry is carried out by scanning the potential between two set points E_1 and E_2 at a desired scan rate and the resultant current is recorded. In case of the cyclic voltammetry, as the name indicates, the potential scan is cycled between two set points. The potential window can range from anodic and cathodic potentials with reference to the open circuit potential of the working electrode in the electrolyte. The extreme potential window will generally be within the stability potentials of the electrolyte. The potential can be scanned only in the anodic or cathodic direction if one wants to study only the oxidation or reduction of the species, respectively. A three-electrode configuration is used for the voltammetry techniques. Inert type solid working and counter electrodes are used. The reference electrode could be silver/ silver chloride or saturated calomel electrode for aqueous electrolytes. At alkaline pH conditions Hg/HgO reference electrode is recommended. For non-aqueous, silver/ silver ion reference electrode is a typically used which contains the same test solution in the reference compartment with silver salt (AgNO_3 , AgClO_4 etc.) dissolved in the non-aqueous solvent. Inert metal wires such as Pt or Au could be used as quasi reference electrode. For high temperature molten salt experiments Ag/Ag⁺ electrode (AgCl coated Ag wire immersed in 1 wt% AgCl containing the test molten salt), Ni/Ni²⁺ ionic electrode (Ni wire immersed in nickel salt containing test molten salt), Pt/Pt²⁺, Li-Al/ Li⁺ and Ni/Ni₃S₂/S₂-electrodes are used [9]. Voltammetry is carried out at different scan rate spanning three decades such as 10mV/s to several volts/s. The recorded voltammograms will be a function of:

- A) The standard electrochemical rate constant (k^0)
- B) Formal potential of the reactant/ product couple
- C) The diffusion coefficients of reactant and product

D) The potential scan rate and the potential window

In addition to the above, the voltammograms depend on the type of electrochemical reactions such as reversible, irreversible and quasi-reversible and reaction mechanisms such as single step electrochemical reaction, multi-step electrochemical reaction, electrochemical-chemical (EC) reaction, electrochemical-chemical-electrochemical (ECE) etc.

The redox reaction, $O + ne^- \rightleftharpoons R$ is considered reversible when the forward and the reverse reaction rate constants are very high and are equal [10]. The rate constant should be higher than the rate of mass transport [7], $k^o \gg m_T$, where $m_T \approx D/\delta \approx \sqrt{D/(RTFv)}$ where v = scan rate. Cyclic voltammograms at different potential scan rates for a reversible reaction are shown in Fig. 3.3.

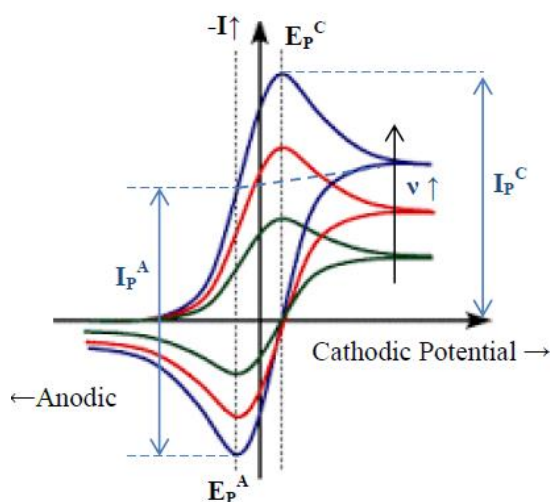


Figure 3.3: Cyclic Voltammograms at different scan rates of a reversible process.

If a very slow linear scan rate is employed, the recorded current will reach a steady value as a function of potential because beyond a certain distance from the electrode the concentration will be uniform due to natural convection. Also, a very slow scan rate leads to a steady state condition where the concentration gradient in the Nernst diffusion layer becomes linear. At very slow scan rates a plateau current profile is observed as function of increased over potentials rather than a peak current profile. This observation is attributed to a decrease in the surface concentration of reactant with increase in the over potential for a reaction which eventually becomes zero. Further increase in the over potential does not change the surface concentration and hence the concentration gradient ($\partial c/\partial x$). Therefore, the current reaches a plateau or limiting the value given by the relation:

$$I_{lim} = nFAC_0\infty / \delta_{eq}$$

Where, δ_{eq} = equilibrium diffusion layer thickness.

When the scan rate is increased, the diffusion layer thickness is altered significantly due to diffusion of reactants from bulk to the electrode surface. The diffusion gradient is not linear. The current varies with potential. Both the change in diffusion layer and electrode potential with time leads to a peak shaped current potential profile. The peak current increases with the scan rate, and given by Randles-Sevcik equation [11]:

$$i_p = 0.4463 (nFRT)^{1/2} C_0^\infty D^{1/2} \nu^{1/2}$$

Where i_p = peak current density (A/cm²), D is in cm²/s, scan rate in ν = V/s, bulk concentration C_0^∞ is in mol/cm³.

When the potential scan is reversed, the current is expected to trace back the forward current profile when the scan rate is slow. During reverse scan, a reduction current is observed until the potential reached the equilibrium redox potential (E_{e^0}). The oxidation current starts to flow when the 'R' present near the electrode starts to be oxidized to 'O'. The potentials of the peak currents of reverse scan (E_p^A) will be different from the potentials of forward peak currents (E_p^C). The difference in the peak potentials ($\Delta E_p = E_p^C - E_p^A$) helps determine the reversibility. The diagnostic tests for reversible processes are listed below [12]:

1. $\Delta E_p = E_p^{\text{anodic}} - E_p^{\text{cathodic}} = 59/n$ mV at 25 °C
2. $|E_p - E_{p/2}| = 59/n$ mV at 25°C or 2.218 RT/F
3. $|I_p^a/I_p^c| = 1$
4. $I_p \propto \nu^{1/2}$
5. E_p is independent of scan rate
6. At potentials beyond E_p , $I^2 \propto t$

Not following one or more of the above criteria indicates that the electrochemical reaction is not reversible within the scan rates employed. The formal potential, $E(O/R)$ can be calculated as the potential between the reduction and oxidation peaks when $D_o = D_R$.

When the electron transfer rate is much slower than the mass transfer rate, irreversible condition exists. At very slow scan rates there is a possibility that the rate of electron transfer is greater than the rate of mass transfer which may lead to reversible condition. When the scan rate is increased, the mass transfer rate becomes comparable to that of electron transfer

rate, that leads to wider separation of reduction and oxidation peak current potentials. The peak current density under the irreversible condition is given by the following relations:

$$i_p = 0.227 n_{\alpha} F C_0^{\infty} k_s \text{Exp} [-\alpha n (E - E^0) / RT]$$

$$i_p = 0.496 n (\alpha n_{\alpha} F / RT)^{1/2} / C_0^{\infty} D^{1/2} \nu^{1/2}$$

Where where n_{α} = number of electrons transferred in the rate determining step. A linear relation will be observed when the peak current density is plotted as a function of $\nu^{1/2}$. The diffusivity can be calculated from the slope of the i_p Vs. $\nu^{0.5}$ plot. The plot will run through the origin for both the reversible and irreversible cases as seen in Fig. 3.4[13].

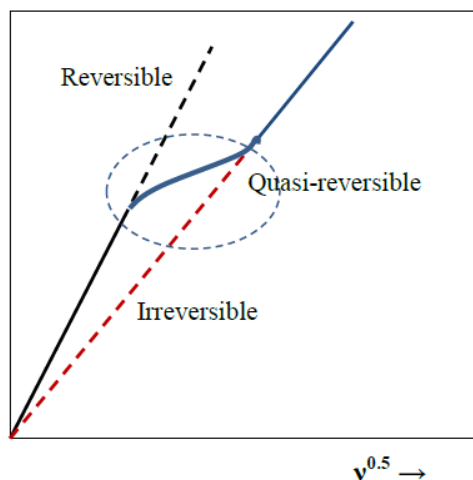


Figure 3.4: Peak current as a function of square root of the scan rate

The cyclic voltammogram of a totally irreversible system will not have a reverse peak current.

The diagnostic tests for a totally irreversible system at 25 oC are listed below [6]:

1. No reverse peak
2. $i_{pc} \propto \nu^{1/2}$
3. For each decade increase in the scan rate the E_{pc} shifts by $-30\alpha c n_{\alpha}$ mV
4. $|E_p - E_p/2| = 48\alpha c n_{\alpha}$ mV

A plot of $\ln(i_p)$ Vs $E_p - E_0$ at different scan rates will be straight line with a slope proportional to αn_0 and the intercept proportional to the rate constant. Therefore, various kinetic parameters such as diffusivity, rate constant, transfer coefficient and number of electrons can be determined from the plots of current density versus scan rate and natural logarithmic of current density versus over potential.

Figure 3.4 schematically depicts i_p vs $\nu^{1/2}$ plots of both reversible and irreversible conditions. As noted, the reversible current is higher than that of irreversible case. These plots follow the

relation of Randles-Sevcik. It is noted that a reversible process at low scan rate changes to irreversible condition at higher scan rates by transitioning through a region called ‘quasi-reversible’ as depicted.

This transition occurs when it is difficult to maintain Nernstian equilibrium at the electrode surface, which is due to the slower rate of electron transfer than that of mass transfer. The transition generally occurs in the region [13]:

$$0.3v^{1/2} \geq k_o \geq 2 \times 10^{-5}v^{1/2} \text{ cm/s}$$

The diagnostic tests for quasi-reversible condition are [6]:

- 1) $|I_p|$ increases with $v^{1/2}$ but not proportional to it.
- 2) $|I_p^a - I_p^c| = 1$ provided $\alpha_c = \alpha_a = 0.5$
- 3) ΔE_p is greater than $59/n$ mV which increases with increasing v
- 4) E_p^c shifts negatively with increasing v

A parameter ‘ Φ ’ is introduced to follow the transition between the reversible and irreversible limits: The parameter Φ is defined as [1,7]:

$$\Phi = k^0 (FD\theta/RT)^{1/2}$$

The following ranges of Φ are assigned to classify the reaction types at stationary macroelectrodes [14] at 298 K and for $\alpha = 0.5$.

$$\text{Reversible: } \Phi \geq 15, \Phi \geq 0.3 v^{1/2} \text{ cm.s}^{-1}$$

$$\text{Quasi-reversible: } 15 > \Phi > 10^{-3} \quad 0.3 v^{1/2} > k_o > 2 \times 10^{-5} v^{1/2} \text{ cm.s}^{-1}$$

$$\text{Irreversible: } \Phi \leq 10^{-3} \quad k_o \leq 2 \times 10^{-5} v^{1/2}$$

3.2.4 Differential Pulse Voltammetry

This technique is used as an electro analytical technique to detect species present in an electrolyte. The detection limit is 10^{-7} M. In this technique the potential is scanned in the form a staircase by super imposing a wave form as depicted in Fig 5. The wave form can be square or sinusoidal. The experiment records the current just before end of each pulse as shown in point 2 and the current just before applying the pulse at point 1. The differential current ΔI is given as $I_2 - I_1$ and plotted as a function of stair case potential. A bell shaped differential current profile is recorded as seen in Fig 3.5. The pulse duration, t_p is at least ten times shorter than the period of the staircase wave form, t_s . The differential pulsing reduces the error introduced by double layer charging and other non-faradaic processes. One of the important variations

in the differential pulse voltammetry is square wave pulse voltammetry. As the name indicates this technique employs a square wave pulse that is superimposed on a staircase potential ramp. The square wave voltammetry parameters are pulse height (ΔE_p), the stair-case height or potential step (ΔE_s), pulse time (t_p) and cycle period or pulse period (t_s). The ΔE_s is much smaller than ΔE_p . The potential shifts by ΔE_s at start of each cycle which is related to scan rate by the relation: $v = \Delta E_s / 2t_p = f \cdot \Delta E_s$, Where $f = \text{frequency} = 1 / 2 t_p$. The half wave potential is given by the relation [15]:

$$E_{1/2} = E_o + RT / nF \ln (D_R / D_o)^{1/2}$$

Where, D_R and D_O are diffusivities of R and O species, respectively. The differential peak current Δi_p is given by the relation [16]:

$$\Delta I_p = (nFA C_o^\infty D_o^{1/2} / \sqrt{\pi t_p}) \Delta \Psi P$$

Where $\Delta \Psi_p$ is a dimensionless parameter that depends on $n\Delta E_p$ and $n\Delta E_s$ and tabulated in reference [16].

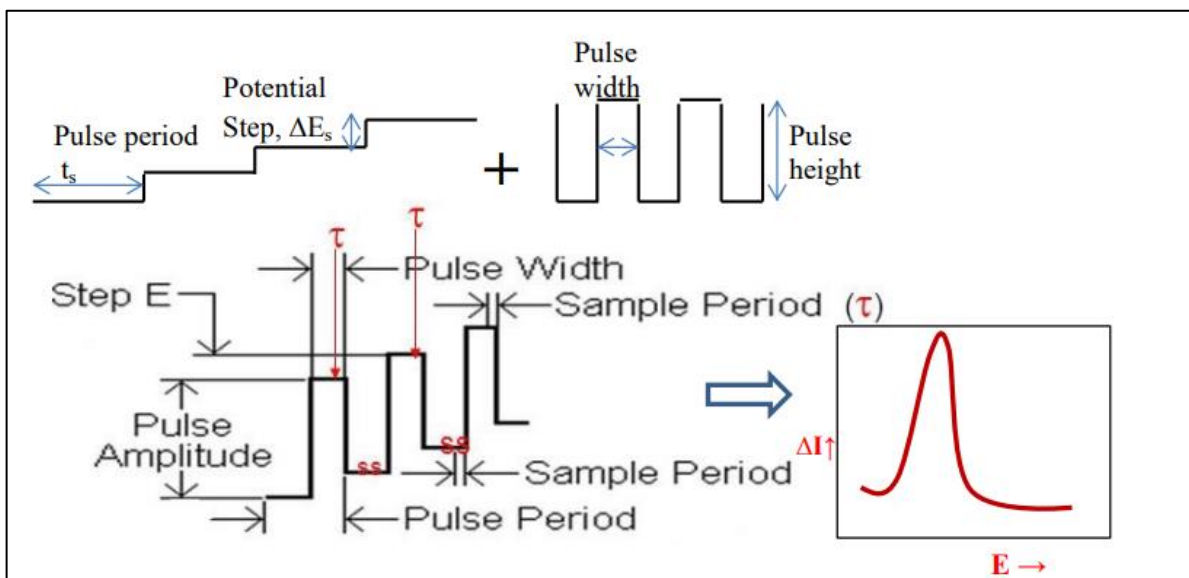


Figure 3.5: Potential wave forms and the recorded differential current versus potential plot of differential pulse voltammetry

References

1. L.R. Morss, N.M. Edelstein, J. Fuger, The chemistry of the actinide and transactinide elements, *The Chemistry of the Actinide and Transactinide Elements*, ISBN 978-94-007-0210-3. Springer Science Business Media BV, 2011. 1 (2011).
2. S. P. Fusselman, J. J. Roy, D. L. Grimmer, L. F. Grantham, C. L. Krueger, C. R. Nabelek, T. S. Storvick, T. Inoue, T. Hijikata, K. Kinoshita, Y. Sakamura, K. Uozumi, T. Kawai and N. Takahashi. *J. Electrochem. Soc.*, vol. 146, pp. 2573-2580, 1999.
3. Barin, *Thermochemical Data of Pure Substances*, Third Edition, Wiley-VCH Verlag GmbH, 1995.
4. W. Zhou and J. Zhang, *Journal of The Electrochemical Society*, **162**, E199-E204 (2015).
5. A. J. Bard, L. R. Faulkner, *Electrochemical Methods, Fundamentals and Applications*, New York: Wiley (2001).
6. A. Lisa, *Electrochemical Impedance Spectroscopy and Its Applications*, New York: Springer (2014).
7. L. Yang and R.G. Hudson, *Journal of the Electrochemical Society*, **106**, 986-990 (1959).
8. P. Delahay, *New Instrumental Methods in Electrochemistry: Theory, Instrumentation and Application to Analytical and Physical Chemistry*, Interscience, New York (1954).
9. T. Berzins and P. Delahay, *Journal of American Chemical Society*, **75**, 555-559 (1953).
10. E. Condon, *Physical Review*. 28: (1926) 1182–1201.
11. L. Redey, D.R. Vissers, Reference Electrode Development for Molten LiCl-KCl Eutectic Electrolyte, *J. Electrochem. Soc.*, 128 (1981) 2705
12. R. Greef, R. Peat, L.M. Peter, D. Pletcher, J. Robinson, *Instrumental Methods in Electrochemistry*, Ellis Horwood, London, (1990) 42 - 228
13. H. Matsuda, Y. Ayabe, *Z. Electrochem* 59 (1955) 494
14. J.E.B. Randles, *Trans Faraday Soc.*, 44 (1948) 327
15. E.J. Laviron, General Expression of the LSP voltammogram in the case of diffusionless electrochemical systems, *J. Electroanal. Chem.* 101 (1979) 19 - 28.
16. J. Osteryoung and J.J. O' Dea *J. Electroanalytical Chemistry* 14(1986) 209.

Chapter 4: Understanding Electrochemical Interactions of Iodide and Chloride Species in LiCl-KCl Molten Salt

The main objective of this task is to determine stable electrochemical potential window, redox potentials of I^-/I_3^- and other reaction intermediates of iodide and chloride in LiCl-KCl molten salt without the presence of Li_2O with different electrochemical measurements like Open Circuit Potential, Cyclic Voltammetry and Square wave voltammetry. In this study the oxidation of iodide will be analyzed by carrying out cyclic voltammetry in LiCl-KCl eutectic molten salt with the addition of 1 – 5 wt% of KI. Addition of iodide in the molten chloride will lead to formation of trihalide ions or interhalogen compounds during the pyroprocessing of used nuclear fuel in an electro-refiner.

Introduction:

Several radioactive iodine isotopes are formed during neutron induced fission of nuclear fuel, and these radionuclides are retained within the fuel matrix and by the containment provided by the fuel cladding. During reprocessing of the used nuclear fuel, a significant fraction of iodine (78.9 mg/g of heavy metal) was reported to be retained in the molten salt as iodide (I^-) such as NaI, CsI, AgI, PdI_2 , UI_3 , ZrI_4 , 3HI [1]. Accumulation of iodide species could significantly affect the performance of the electro-refiners that are used for electrolytic reduction of actinides. The electrochemistry of iodine/iodide couple has been extensively studied in aqueous and non-aqueous conditions because of its application in dye-sensitized solar cells, and synthetic chemistry. However, only very limited work has been reported in high temperature molten salts. Iodide based molten salts have been identified as potential alternatives for thermal batteries because of their low melting point and high conductivities [2].

The redox reactions of iodide are given as:



In this study, the reactions (1) – (3) will be analyzed by carrying out cyclic voltammetry in LiCl-KCl eutectic molten salt with the addition of 1 – 10 wt% of KI. Addition of iodide in the

molten chloride will lead to formation of trihalide ions or interhalogen compounds during the pyroprocessing of used nuclear fuel in an electro-refiner. The electrochemical parameters of following trihalide reactions will be evaluated in this study:



In this reaction, the oxidation state of I⁻ changes from -1 to +1 [1]. The equilibrium constant for the reaction (4) is given as:

$$K_4 = \frac{[\text{ICl}_2^-]}{[\text{I}^-][\text{Cl}_2]} \quad (4 \text{ a})$$

In order to determine K₄, the associated reaction steps need to be considered as detailed below.



$$K_5 = \frac{[\text{I}_2\text{Cl}^-][\text{Cl}^-]}{[\text{I}^-][\text{ICl}_2^-]} \quad (5\text{a})$$



Combining redox reactions (7) and (8) leads to reaction (9) as:



$$K_9 = \frac{[\text{ICl}_2^-]^2}{[\text{Cl}^-][\text{I}_2\text{Cl}^-][\text{Cl}_2]} \quad (9\text{a})$$

$$\frac{RT}{2F} \ln K_9 = E_7^0 - E_8^0 \quad (10)$$

The equilibrium constant K₉ can be evaluated from the redox potentials of reactions (7) and (8).

In order to determine K₅, following two redox reactions are considered



Combining (11) and (12) leads to reaction (13)



Reaction (13) is twice that of reaction (5), that is [K₅²].

$$\frac{RT}{2F} \ln [K_5^2] = E_{11}^0 - E_{12}^0 \quad (14)$$

When the equilibrium constants K_5 and K_9 are determined from reactions (14) and (10) respectively, the equilibrium constant K_4 can be calculated using the relation:

$$K_4 = K_5 \cdot K_9 \quad (15)$$

Other possible reaction could be:



The equilibrium constant for the reaction (16) is given as:

$$K_{16} = \frac{[I_2][Cl^-]^2}{[Cl_2][I^-]^2} \quad (16a)$$

The equilibrium constant K_{16} can be determined by combining the following redox reactions (17) and (18):



$$\frac{RT}{2F} \ln K_{16} = E_{17}^0 - E_{18}^0 \quad (19)$$



$$K_{20} = \frac{[I_2Cl^-]}{[I_2][Cl^-]} \quad (21)$$

The equilibrium constant K_{20} can be calculated using the relation:

$$K_{20} = K_9 K_5^2 / K_{16} \quad (22)$$

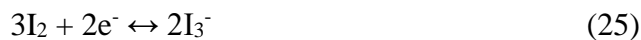
Another trihalide formation reaction is



The equilibrium constant for the reaction (23) is given as:

$$K_{23} = \frac{[I_3^-]}{[I_2][I^-]} \quad (24)$$

Reaction (23) can be obtained by combining the reactions (18) and (25), and given as (26)



This reaction is two times of reaction (23). The equilibrium constant K_{23} can be obtained from the redox reactions of (25) and (18):

$$\frac{RT}{2F} \ln [K_{23}^2] = E_{25}^0 - E_{18}^0 \quad (27)$$

The equilibrium constant K_6 for the trihalide reaction (6) is given as,

$$K_6 = \frac{[I_3^-][Cl^-]}{[I^-][I_2Cl^-]} \quad (28)$$

The K_6 can be calculated using the relation:

$$K_6 = K_{23}/K_{20} \quad (29)$$

The equilibrium constants of different trihalide reactions involving iodide and chloride species were determined based on the cyclic voltametric results and using the relations described in the preceding section. Furthermore, electrochemical reactions of iodide/triiodide species in the molten LiCl-KCl eutectic will be evaluated at 450 – 550 °C. Evaluation of these parameters will be useful for performance optimization of electro-refiners of reprocessing used nuclear fuels. Understanding trihalide interactions will also help optimize the performance of molten salt nuclear reactors as well where accumulation of iodide as fission product is anticipated. These results could also be extended for designing a better molten salt thermal batteries.

Experimental

Cyclic voltammetry (CV) was performed in the LiCl+KCl eutectic melt at 450 - 550 °C with and without addition of 1-10 wt% KI. LiCl-KCl eutectic salt (44 wt% LiCl + 56 wt% KCl) was procured from Sigma Aldrich (SKU: 479330) and used without further purification. Ultra-dry KI (99.998% purity metal basis) was procured from Alfa Aesar (Stock # 13676) and used without further purification. The LiCl-KCl eutectic + KI mixture was melted, held at 450 °C for 30 minutes, solidified and re-melted again in a glassy carbon crucible under inert and dry condition. The pre-melted and solidified salt discs were used in the electrochemical tests. Three-electrode configuration was employed in the electrochemical tests. The working electrode was a 2 mm diameter tungsten rod (99.95%, Alfa Aesar). The counter electrode was a 4 mm diameter glassy carbon rod. The reference electrode was prepared in-house. A silver wire (1 mm diameter) was coated with AgCl layer by anodization in the AgCl saturated KCl solution at 5 V for 20 minutes. The anodized wire was dried at 120 °C for 12 h. The AgCl coated silver wire was immersed in LiCl+KCl eutectic salt containing 1 wt% AgCl in a 4 mm inner diameter pyrex tube. The end of the pyrex tube was thinned down to approximately 0.2 mm by grinding using emery papers. The thinned end of the tube ensured required ionic

conductivity. All the experiments were carried inside a glovebox (mBraun) filled with UHP argon environment, where the oxygen and moisture level were maintained less than 2 ppm. Three cycles were carried out at each condition, and the final cycle is reported. Anodic scans were performed at a narrow potential window between OCP and $0.55 V_{\text{Ag}/\text{AgCl}}$ to better resolve the redox reaction of I/I_3^- couple and at a broader potential window of OCP to $+1.6 V_{\text{Ag}/\text{AgCl}}$ to reveal other oxidation reactions including chlorine evolution. Cathodic CV scans were carried out from OCP to $-2.8 V_{\text{Ag}/\text{AgCl}}$ at different scan rates. Electrochemical impedance spectroscopy (EIS) was carried out at OCP, and at different potentials (where anodic and cathodic current peaks were noted) under potentiostatic conditions by super imposing an ac signal of 10 mV by scanning the frequency from 10 kHz to 0.1 Hz. Square wave voltammetry (SWV) was carried out by scanning the potential from OCP to $1.6 V_{\text{Ag}/\text{AgCl}}$ at a frequency of 25 Hz, pulse size of 25 mV, step size of 1 mV, and pulse time of 0.04 s. All the electrochemical tests were either duplicated or triplicated to ensure reproducibility. The average values are presented.



Figure 4. 1: Experimental Setup

The procedure described by Marsden and Pesic [3] was followed each experiment to clean the working electrode. An anodic potential ($0.0 V_{\text{Ag}/\text{AgCl}}$) was applied for 120 s to strip the material coated on the working electrode during the cathodic cycle. After this anodic polarization, the system was left under the open circuit condition for another 120 s to ensure relaxation of concentration gradients or electrode polarization. Reproducible test behavior was

verified by repeating the full window CV for three cycles before each test series [5]. The immersed surface area of the working electrode was calculated using geometrical relation by measuring the immersed length of the working electrode and the diameter after the electrochemical tests using a micrometer.

Results and Discussion

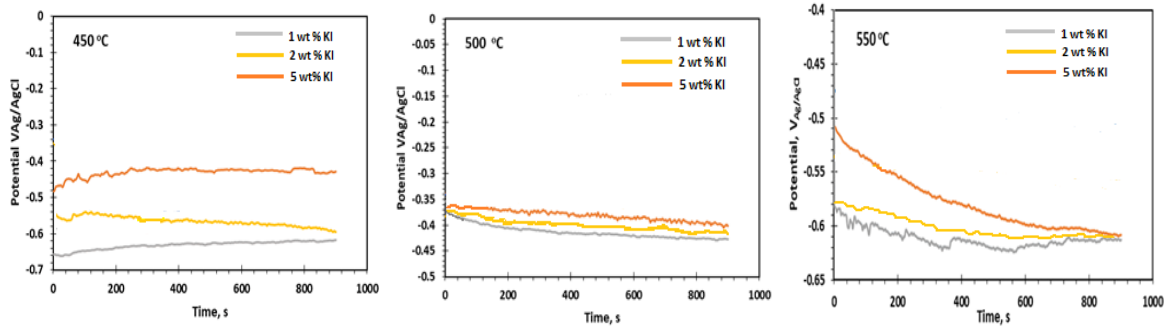
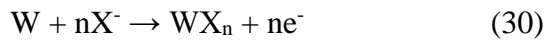
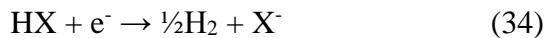
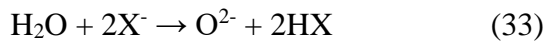


Figure 4.2: Open Circuit Potential at 450, 500 and 550 °C

Figures 4.2 (a), (b) and (c) show the open circuit potentials (OCP) of the tungsten working electrode in 1 – 5 wt% KI containing LiCl-KCl eutectic at 450, 500, and 550 °C, respectively. The OCP of the tungsten electrode shifted in the positive direction with the increase in the KI addition at 450 – 550 °C. Increasing the temperature from 450 °C to 550 °C shifted the OCP to more positive values for a given KI addition. The OCP is a mixed potential of the following anodic and cathodic half-cell reactions given in (30) and (31), respectively.



where X represents halides such as Cl⁻ and I⁻. Impurities such as oxygen and moisture (even though their concentration is less than 2 ppm) could also contribute to the cathodic reactions as given in (32) and (34) [3,4].

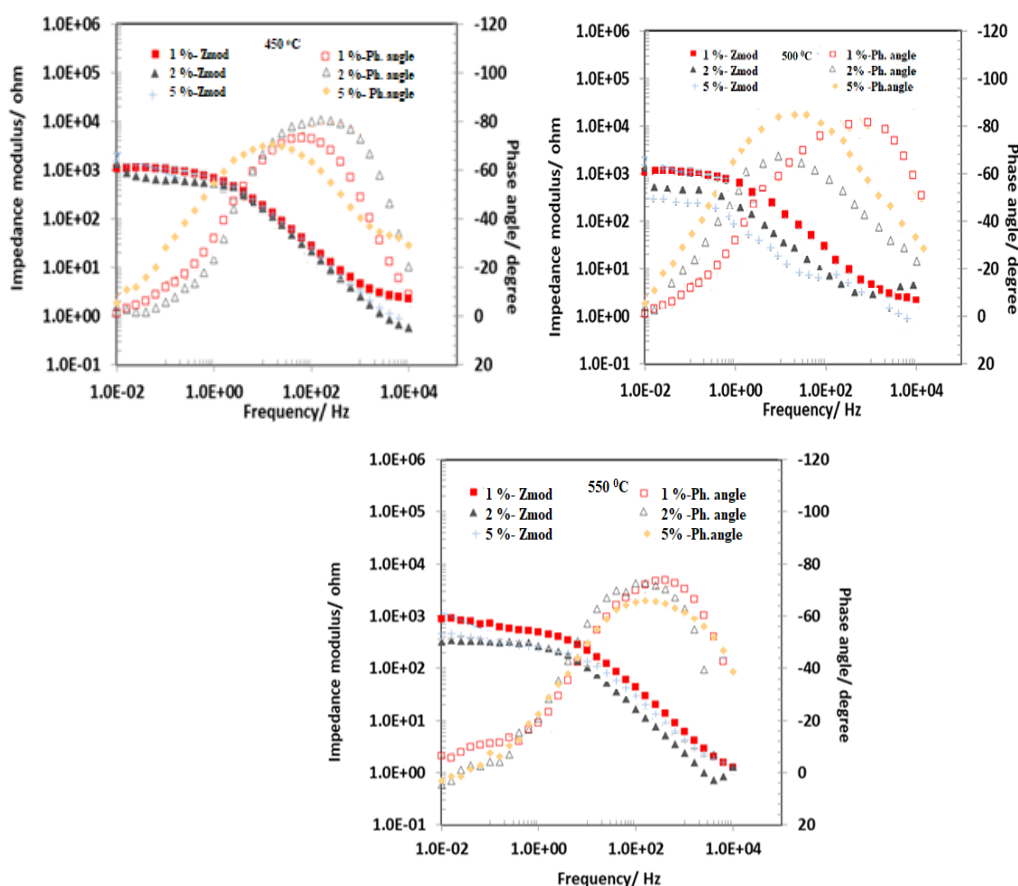


The published reports on the polarization of tungsten in the LiCl molten salt at 650 °C indicated a ‘passivation-like’ behavior where the current density did not change with increase in anodic polarization [3]. A similar behavior could be observed in the LiCl-KCl eutectic at 450 – 550 °C. The OCP will shift to more positive values if the ‘passivation’ current density

decreased for a given cathodic half-cell reaction. Also, the OCP will increase when the Tafel slope of the cathodic reaction becomes smaller or the exchange current density for the cathodic reaction increases. Increase in the KI concentration will increase the exchange current density (i_0) by following the relation [4]:

$$i_0 = nFk_0C_I^- \quad (35)$$

Where, n = number of electrons, F = Faraday's constant, k_0 = rate constant, and C_I^- is bulk concentration of KI in the molten salt. The increase in the i_0 value will shift the Tafel plots of the I_2/I^- redox reactions to the right such that the OCP could increase with the increase in the KI concentration.



Figures 4.3 (a) – (c) EIS results of tungsten electrode at open circuit potentials

Figures 4.3 (a) – (c) show the EIS results of tungsten electrode at open circuit potentials in LiCl-KCl eutectic with and without addition of 1 – 5 wt% KI at 450 – 550 °C. The impedance decreased with the temperature. Fig 4.3 (a) – (c) illustrate the Bode plots at 450, 500, and 550 °C for three KI additions. The increase in KI concentration decreased the impedance values at all temperatures. The effect of temperature between 450 and 550 °C was less pronounced on

the impedance for a given concentration of KI. The impedance profiles showed two time constants, in general. Different electrical equivalent circuits have been proposed for the impedance behavior of molten salts in the literature [5-8]. Vandarkuzhali et al [9] proposed an equivalent electrical circuit (EEC) consisting of parallel RC elements with a Warburg component to describe the impedance behavior of tungsten electrode in LiCl-KCl eutectic containing LaCl₃ at 425-525 °C. Yoon et al [10] proposed an EEC consisting of two parallel RC loops connected in series to describe the impedance behavior of Sm(III)/Sm(II) couple in LiCl-KCl at 400 – 550 °C. An equivalent circuit that used for modeling porous film was proposed with an additional Warburg element to describe the impedance behavior of U/U(III) system in LiCl-KCl at 450 – 500 °C [11]. An EEC consisting of two parallel RC loops connected in series with each loop having a Warburg element was discussed to describe the impedance behavior of various molten salts at 700 – 800 °C by Cohen et al [12]. Several EEC models were fitted with the EIS data of this work using the Simplex method available with Gamry Echem Analyst (Gamry Instruments, USA, version 6.04) and the EEC model showing a goodness of fitting (χ^2) value smaller than 1×10^{-3} was selected to fit the EIS data. The EIS spectra collected at the OCP conditions could be fitted with an EEC model shown in Table 1. The rationale behind carrying out EIS measurements at OCP is to understand the structural characteristics of the molten salts with and without addition of iodide. The physical and electrical properties of the molten salt systems depend on the structure and interactions of the constituents. The structural arrangements that are present in molten salts can be viewed as intermediates between discrete chemical bonds and periodic crystalline lattices^[iii]. The inter-atomic interactions determine the local ordering of the molten salt. The electrochemical properties are significantly influenced by the structural characteristics of the molten salt. The ion size and type in a molten salt system such as KX-LiX would affect the electrochemical stability. The ordering and structure of the melt could be described based on the entropy. The entropy (ΔS) of the electrolysis of melt can be determined using the relation [13,14]:

$$\Delta S = nF(\partial E/\partial T)_P \quad (36)$$

where, n = number of electrons, $\partial E/\partial T$ = change in electrochemical window with temperature. Low entropy values indicate higher order and enhanced attractive interaction of the species in the molten salt. Generally, an increase in the entropy was observed with increase in the anion size of unary molten salts^[iii]. The electrolysis potential turns out to be more anodic as the

anion size increases due to weaker Coulombic interaction between the anion-cation pairs as well as increased repulsion between the larger anions^[iv]. When two types of cations are present in molten salt with different sizes and different charge densities, an asymmetric polarization of anions is anticipated which may result in the electrostatic stability of the mixture. When two different types of anions such as chloride and iodide are present along with different cations, the asymmetric polarizations of the ions and their effect on the physical and electrochemical properties are not well documented.

The proposed EEC model is similar to that proposed by Yoon et al [15] wherein the Warburg component is replaced with an inductor to represent the adsorption behavior. The resistor R_s represents the electrolyte resistance, R_1 is associated with the charge transfer resistance, and Q_1 is a constant phase element (CPE) which represents the double layer capacitance of the electrode/electrolyte interface. The CPE is given by the relation: $Z = 1/[j\omega)^m Q]$ where $j = \sqrt{-1}$, ω = frequency, and the exponent 'm' represents the surface heterogeneity or continuously distributed time constants for charge transfer when $m < 1$ [16]. A $R_2 \parallel Q_2$ loop with an inductor L_1 in series with R_2 is introduced within the $R_1 \parallel Q_1$ loop to represent the adsorption of ions due to the surface roughness of the working electrode which is similar to that of a porous film model [17]. The R_2 is associated with the charge transfer resistance due to adsorbates similar to the resistance of a coil winding of an inductor. The impedance of an inductor increases with increase in the frequency while the impedance of a capacitor decreases with increase in the frequency.

The solution resistance varied from 0.54 – 1.2 ohm at the investigated conditions. A clear or linear trend could not be established by combining the effect of KI addition and temperature on the solution resistance despite triplicating some of the experiments. The solution resistance increased with increase in the temperature in case of 5 wt% addition while the opposite was noted for other KI concentrations. The charge transfer resistance (R_1) decreased with increase in the temperature for a given concentration of KI, except for 5 wt% KI. It is interesting to note that addition of KI increased the charge transfer resistance in comparison with that of without KI addition. The R_2 , which is associated with the resistance due to inductance, should increase with the increase in the magnitude of L_1 . However, there is no direct correlation between the value of L_1 and R_2 could be observed from the tabulated values, which implied that the adsorbates did not influence the charge transfer resistance following a simple linear

relation. The values of R_2 decreased with increase in temperature for the 0% KI and 2 wt% KI additions, and increased with increase in temperature for the 1 and 5 wt% additions. The Q_1 and Q_2 values of LiCl-KCl without KI addition increased with increase in the temperature. The magnitude of Q_2 was larger than that of Q_1 . It is noted that similar order of R_s , R_1 , Q_1 and Q_2 values were reported by other researchers also [18,19]. Addition of KI lowered the double layer capacitance Q_1 , in general for all the KI concentrations and temperatures than that observed in 0% KI solution. The decrease in capacitance could be attributed to the larger size of I⁻ ions that had lower charge carrier density than the Cl⁻ ions. Similar observation was reported when the cation size increased in the molten salt [20]. An increase in capacitance behavior was observed for the LiCl-KCl melt without KI addition which could be explained by a decrease in the electrostatic interaction between the anions and cations and facilitating formation of the double layered structure [21,22]. On the other hand, addition of iodide increased the randomness in the electrostatic interaction, and therefore no clear trend could be observed on the capacitance behavior as a function of temperature, especially with 1 and 2 wt% KI addition. On the other hand, 5 wt% KI addition decreased the Q_1 values in comparison with those of 0 wt% KI but the capacitance increased with increase in the temperature. A similar observation could be made for the Q_2 values. The magnitude of L1 decreased in general with the addition of KI. Overall, it was observed that addition of KI affected the electrochemical properties negatively by promoting disorder, increasing the charge transfer resistance, and decreasing the capacitance and inductance.

Cyclic Voltammetry in full window: (-2.8 to 1.5 V)

Figure 4.4 shows a CV in full window for LiCl-KCl with no KI at 500 °C run at the scan rate of 100mVps. The figure shows the occurrence of Li reduction peak around -2.7 V and chlorine evolution peak around 1.2 V vs $V_{Ag/AgCl}$ reference electrode. The absence of any other peaks in this region showed the melt free of oxides and other impurities.

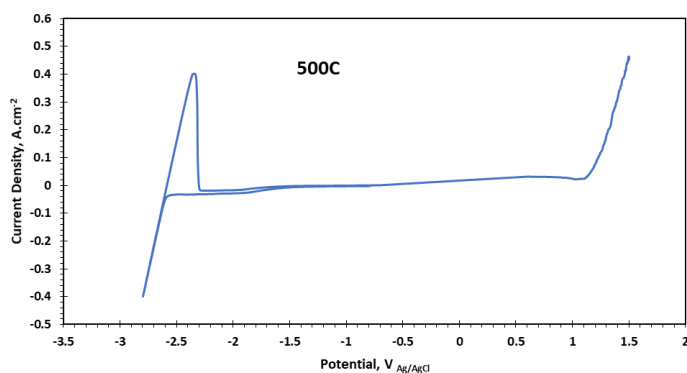


Figure 4.4: Cyclic Voltammetry of LiCl-KCl at 500 °C at scan rate of 100 mV/s
 The rise of current density around 0.6 V could be given to iodine evolution and the trend shows a slight decrease in the current density followed by the rise again which can be attributed to chlorine evolution around 1.2V. There does not seem to be much change in the potential window with the addition of KI in LiCl-KCl. The formal potential for iodine evolution could be easily observed from the figure to be 0.6V vs $V_{Ag/AgCl}$.

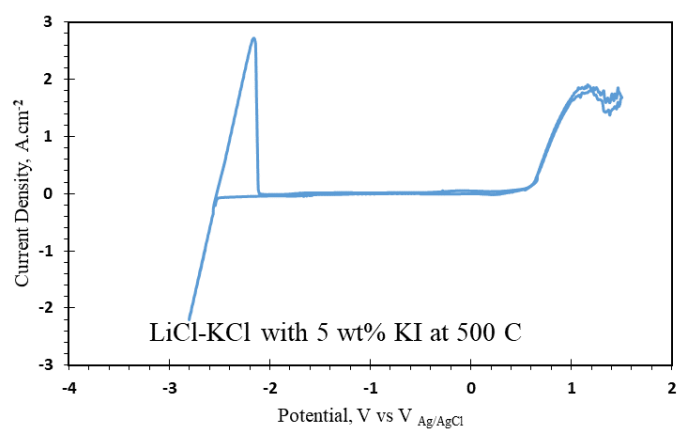


Figure 4.5: Cyclic Voltammetry of LiCl-KCl with 5 wt% KI at 500 °C at scan rate of 100 mV/s

Cyclic Voltammetry in anodic direction: OCP to 0.55 V at 450 C

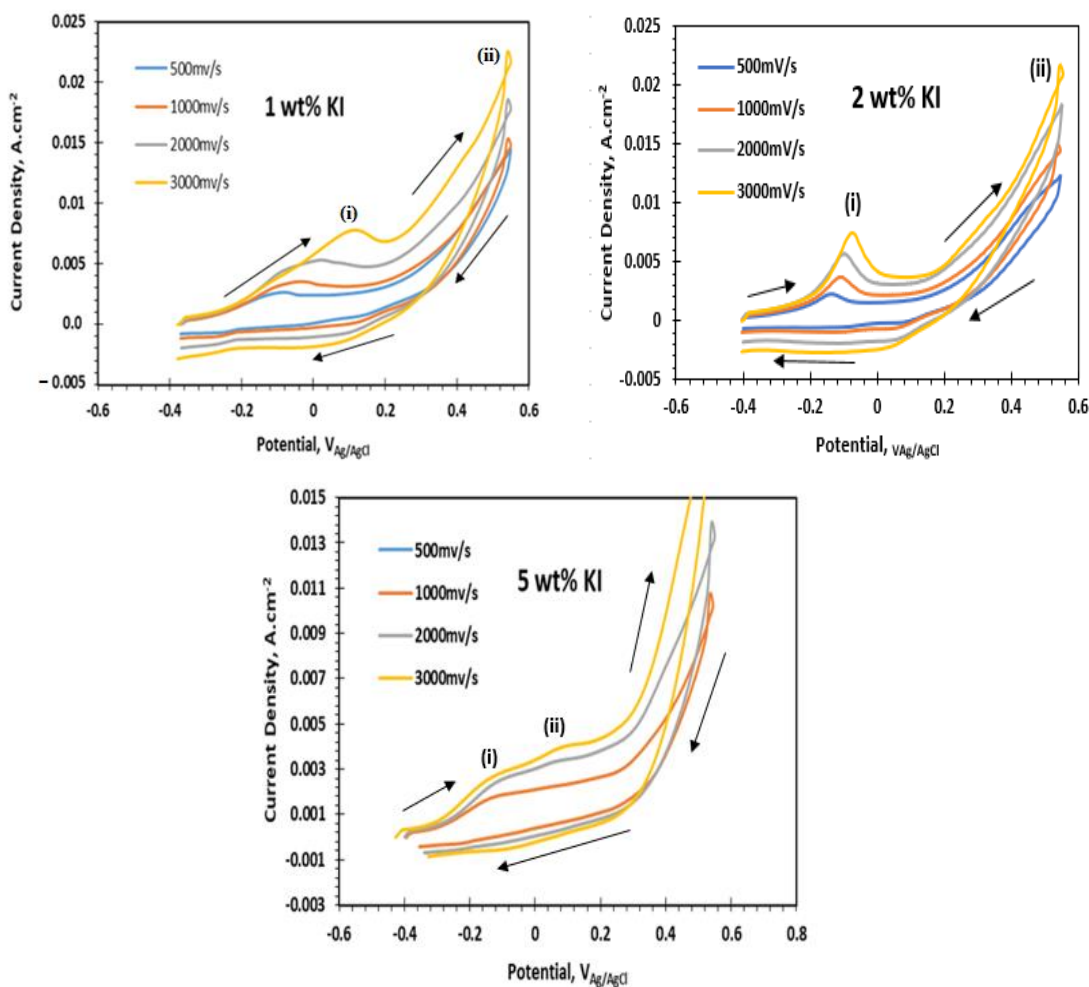


Figure 4.6: Cyclic Voltammetry of 1,2 and 5 wt% KI concentration at 450 °C at scan rates of 500-3000mV/s

Cyclic Voltammetry from OCP to 0.55 V shows a prominent peak for 1 and 2 wt% KI at 450 °C whereas two peaks are seen in case of 5 wt% KI. The potential window is selected in such a way that there is no iodine evolution so that the reversibility of iodide to triiodide and vice versa could be studied closely. According to Hallag, the first peak in case of oxidation of iodide is represented by iodide to triiodide. As oxidation of iodide to triiodide is easier due to less electron transfer and needs less energy [23]. So, the peak (i) in case of 1 wt% Ki at 450 °C is denoted by the following equation:



The presence of crossover point around 0.55V is seen which signifies the formation of an extra layer on the electrode for a very short span of potential which could represent the formation of intermediate anion of dichloroiodide and is given by the following equation:



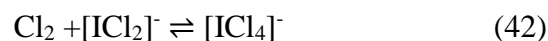
The equation shows that iodide which did not get oxidized into triiodide reacted with the chloride anions adsorped on the surface and formed intermediate anion of dichloromonoiodide. This intermediate anion reacted with the remaining iodide ions to form triiodide during reverse scan. This process is represented by the following equation:



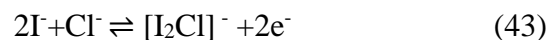
A peak is seen around -0.03V which represents the formation of iodide from the triiodide present on the surface of the electrode and is denoted by the following equation:



The formation of tetrachloroiodide anion is possible when there is presence of high concentration of chloride. The possibility of formation of tetrachloroiodide $[\text{ICl}_4]^-$ is high at high positive potentials as the formal potential of chlorine evolution is 1.2V. This could be represented by the following equations:



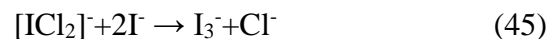
But 5 wt% KI followed slightly different oxidation route compared to 1 and 2 wt% KI at 450 °C. Peak (i) in case of 5 wt% KI represents the oxidation of iodide to triiodide as shown by equation (37). But an additional peak is seen around 0.01 V which could be attributed to formation of interhalide species shown by the following equation:



No crossover point is seen at 0.55V for the high scan rate as the species did not have time to react to form additional interhalide species. Crossover point is clearly seen at lower scan rates. This reaction is represented by the equation below:



No visible peak is seen during the reverse scan which suggests no occurrence of electrochemical reaction. But the occurrence of chemical reaction during the reverse scan is represented by the following reaction:



Cyclic Voltammetry in anodic direction: OCP to 0.55 V at 500 °C

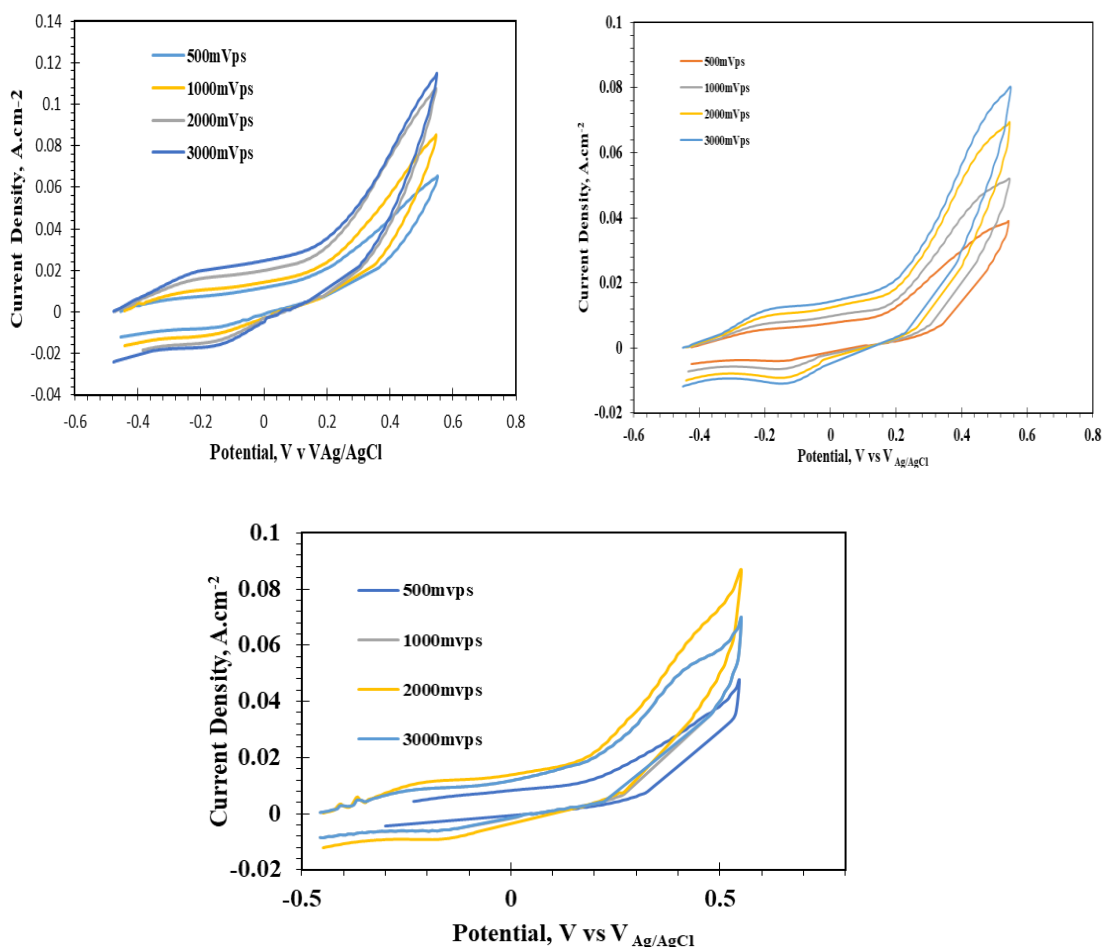


Figure 4.7: Cyclic Voltammetry of 1,2 and 5 wt% KI concentration at 500 °C at scan rates of 500-3000mV/s

CV shows the similar pattern in case of 1,2 and 5 wt% KI at 500 °C. Compared to 1,2 and 5 wt% at 450 °C, a prominent peak is seen in reverse scan direction which represents a electrochemical reaction occurring during reduction process. The first peak observed in 1 wt% KI represents the oxidation of iodide to triiodide given by equation (37). The current density seems to be increasin after 0.2V which represents the formation of interhalide species $[ICl_2]^-$ given by the equation (38). The peak at 0.3V represents the electrochemical reduction reaction in which $[ICl_2]^-$ reduces to iodide and is represented by the following equations:



This pattern of reaction is seen in 2 and 5 wt% KI at 500 °C. The reaction mechanism follows the similar pattern followed by the Room Temperature Ionic Liquid at room temperature explained by Bentley et. al [24].

Cyclic Voltammetry in anodic direction: OCP to 0.55 V at 500 °C

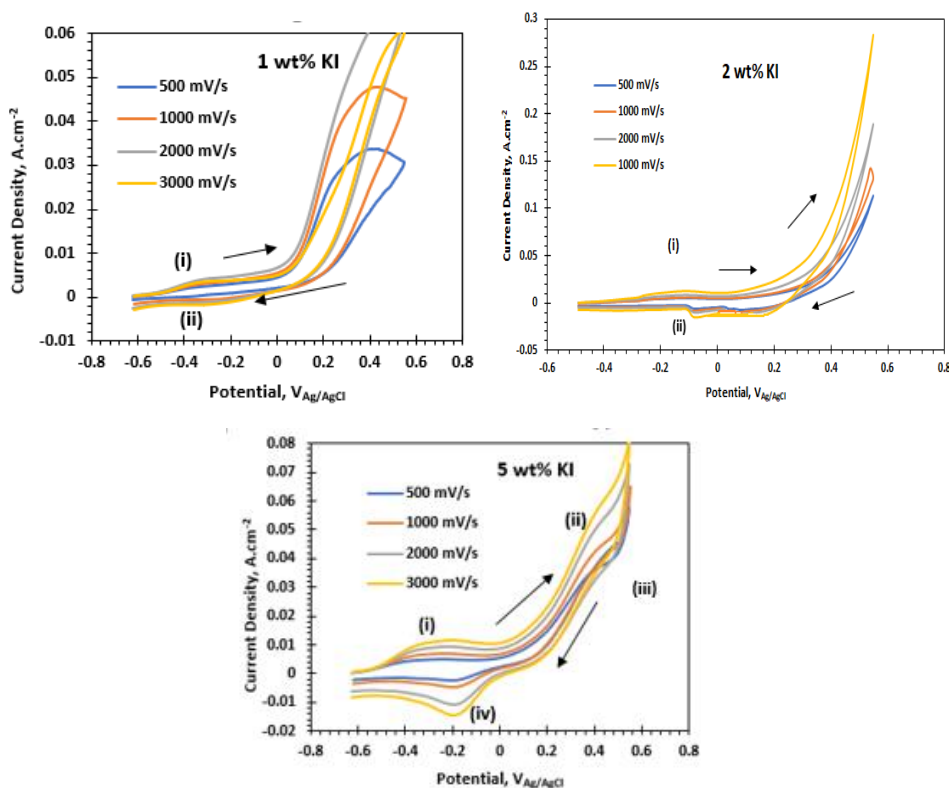
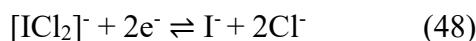


Figure 4.8: Cyclic Voltammetry of 1-5 wt% KI concentration at 550 °C at scan rates of 500,1000,2000 and 3000 mV/s

Figure 4.5 illustrates the CV of LiCl-KCl eutectic with 1,2 and 5 wt% KI at 550 °C. LiCl-KCl with 1 and 2 wt% KI shows two distinct peaks; one is forward and one in reverse scan. Peak (i) represents oxidation of iodide to triiodide followed by the formation of interhalide species represented by equation (38). But LiCl-KCl with 5 wt% KI shows two more peaks with peak (i) showing the oxidation of iodide to triiodide. Peak (ii) represents formation of interhalide species and is given by the equation:



Formation of $[\text{I}_2\text{Cl}]^-$ instead of $[\text{ICl}_2]^-$ could be due to the presence of more iodide ions compared to 1 and 2 wt% KI in LiCl-KCl. This interhalide species gets reduced to $[\text{ICl}_2]^-$ when the CV is scanned in reverse direction. This $[\text{ICl}_2]^-$ gets further reduced to iodide around -0.2 V which is represented by the following equation:



Cyclic Voltammetry in anodic direction: OCP to 1.2 V at 450, 500 and 550 °C

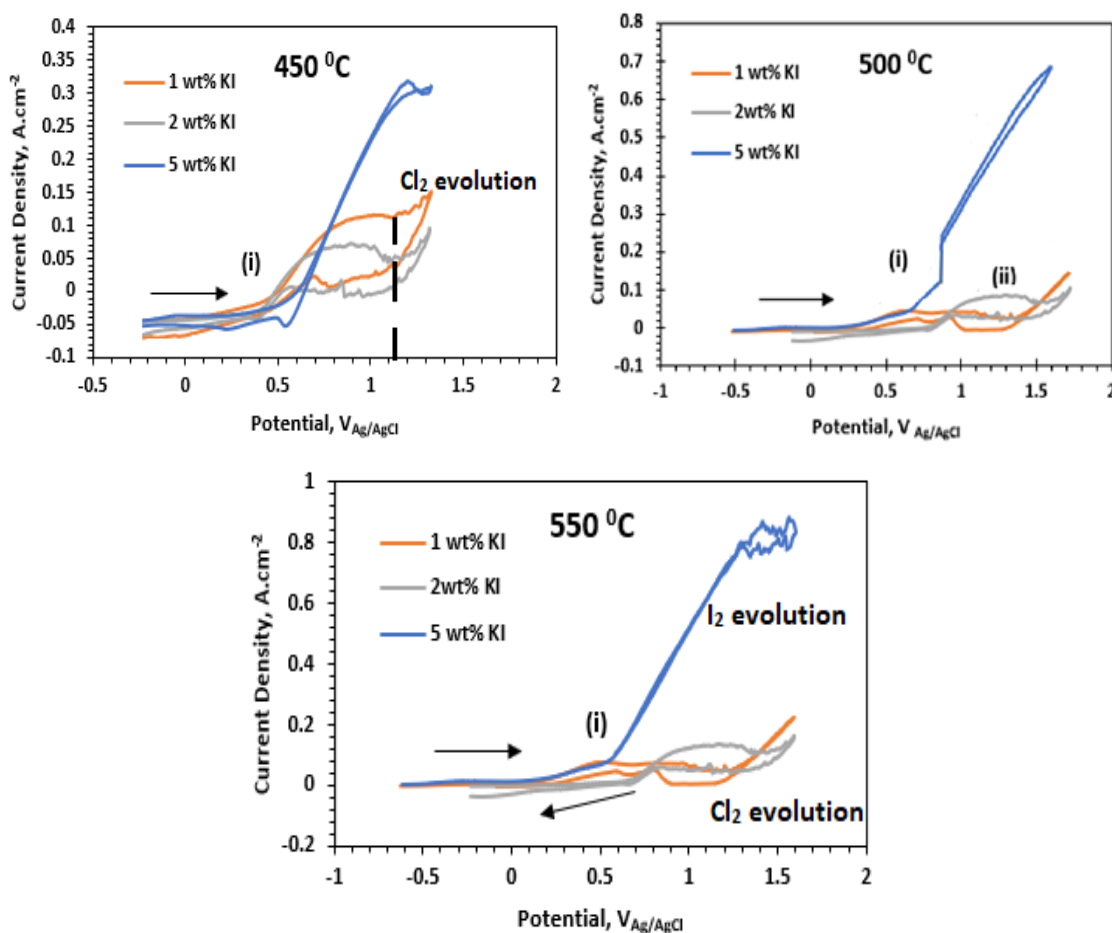


Figure 4.9: Cyclic Voltammetry of 1-5 wt% KI concentration at 550 °C at scan rates of 500,1000,2000 and 3000 mV/s

Figure 4.6 show CV of 1,2 and 5 wt% KI at 450, 500 and 550 °C with clear redox potential for chlorine evolution. The redox potential for chlorine was found to be 1.2 V at 450 °C and around 1.4 V in case of 500 and 550 °C. The take off potential of iodine evolution in case of 450 °C is +0.55 and +0.56 for 1 and 5 wt % KI respectively whereas the redox potential for iodine evolution is 0.64 V at 450 °C. The iodine evolution and chlorine evolution look pretty much similar in case of 500 and 550 °C. Cl₂ evolves at ~ 1.1 V_{Ag/AgCl} in 1 wt% KI solution. 2 wt% KI solution also has Cl₂ potential at ~ 1.1 V_{Ag/AgCl}. The take off potential of iodine evolution in case of 500 and 550 °C is +0.5 V but chlorine evolution is not clearly discerned in 5 wt% KI solution at 450, 500 and 550 °C. Cl₂ evolution takes place around 1.4 volts for 1

wt% and 2 wt% KI at 500 and 550⁰C which is close to redox potential of chlorine evolution potential of 1.4V at 500 and 500⁰C.

Diffusivity Calculation for iodide for LiCl-KCl with 1,2 and 5 wt% KI at 450, 500 and 550 ⁰C

The diffusion coefficient of the iodide species can be obtained from the slope of the line resulting by plotting current density v/s square root of scan rate. In order to figure out the slope, the number of electrons should be known which can be obtained from square wave voltammetry by using the following relationship [24,25].

$$W_{1/2}=3.52 RT/nF \quad (49)$$

Where $W_{1/2}$ is the width of the peak at half height, R is the universal gas constant ($\text{JK}^{-1}\text{mol}^{-1}$), F is the Faraday constant, T is the temperature (K) and n is the number of electrons transferred. Figure 4.7 shows the square wave voltammetry for 5 wt% KI at 500 C ran at 50 Hz frequency from OCP to 1.5 V. Rest of the graph is attached in the appendix for 450 and 550 ⁰C.

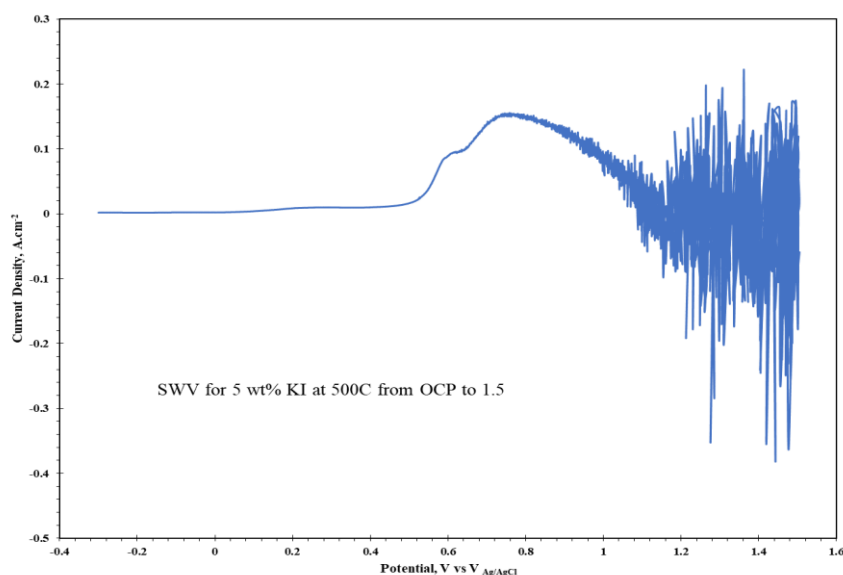


Figure 4.10: SWV for LiCL-KCl-5 wt% KI from OCP to 1.5 V

In many cases, Randles-Sevick equation is used to calculate the diffusion coefficient from the following formula [26,27]:

$$I_p=0.611nFAC_0(nFvD/RT)^{1/2} \quad (50)$$

Where i_p is the peak cathodic current (A), k is the dimesionless parameter obtained from the specific boundary conditions, A is the electrode area (cm^2), C_0 is the bulk concentration of the active species (molcm^{-3}), D is the diffusion coefficient (cm^2s^{-1}) and v is the scan rate (Vs^{-1}).

Since, the CV followed the condition of irreversibility, an alternative method developed by Delahay was used which is given by:

$$I_p = 0.496nFAC(\alpha n_\alpha FvD/RT)^{1/2} \quad (51)$$

Where α is the charge transfer coefficient and n_α is the number of electrons transferred. the value of αn_α can be obtained from the relationship [28-30]:

$$E_p - E_{p/2} = -1.875RT / \alpha n_\alpha F \quad (52)$$

Where E_p is the peak potential and $E_{p/2}$ is the potential when the current is half of the peak current.

The table 3.1 summarizes the values of αn_α obtained at different temperatures:

Table 3.1: Values of αn_α at different temperatures (K)

Temperature (K)	αn_α (1V/s)
723	0.57
773	0.79
823	0.526

Diffusion coefficient is calculated by plugging in the values in Delahay equation. Table II represents the values of diffusion coefficient calculated for 1,2 and 5 wt% KI at 450, 500 and 550 °C.

Table 3.2: Diffusion coefficient of 1,2 and 5 wt% KI at 450, 500 and 550 °C

Concentration	450 °C	500 °C	550 °C
1 wt% KI	9.252E-05 cm ² s ⁻¹	9.0770E-5 cm ² s ⁻¹	6.798E-06 cm ² s ⁻¹
2wt% KI	1.0425E-05 cm ² s ⁻¹	6.457E-05 cm ² s ⁻¹	2.3506E-05 cm ² s ⁻¹
5 wt% KI	1.11E-05 cm ² s ⁻¹	2.048E-05 cm ² s ⁻¹	3.320E-05 cm ² s ⁻¹

Table 3.2 shows the diffusion coefficient for the 1,2 and 5 wt% KI at different temperatures. No consistent trend could be seen in the data set between the concentration and diffusion coefficient. The diffusion coefficient seems to be increasing with the concentration in case of 550 °C.

Activation Energy Calculation

The data from table 3.3, it can be seen that 1wt% KI has the highest activation energy compared to 2 and 5 wt% KI as more energy is required for the charge transfer at lower concentration of KI [28].

Table 3.3: Activation energy for 1, 2 and 5 wt% KI at 450, 500 and 550 °C.

Wt% of KI at 450, 500 and 550 °C	Activation Energy (J/mol)	D ₀ (m ² s ⁻¹)
1	37717.29	4.38E-04
2	29546.29	2.08 E-04
5	31542.48	3.03E-04

Formal potential and stability constant calculation for i⁻, i₃⁻ and i₂

The following equation is used to calculate the formal potential and stability constant for the iodide, triiodide and iodine.

$$E^0(I^-/I_2) - E^0(I^-/I_3^-) = RT/2F \ln(K_{stab}) \quad (53)$$

Where, E^0 is formal potential, K_{stab} is stability constant of the reaction, $R=8.314 \text{ Jmol}^{-1}\text{K}^{-1}$, T is temperature in Kelvin and F is Faraday's constant.

Table 3.4: Formal potential and stability constant calculation for i⁻, i₃⁻ and i₂ at 450 °C

450 °C	i ⁻ /i ₃ ⁻ , V	i ⁻ /i ₂	Ln(K _{stab})	K _{stab}
1	-0.11	0.766	-28.1196	6.13E-13
2	-0.126	0.678	-25.8084	6.19E-12
5	-0.167	0.626	-25.4553	8.81E-12

Table 3.5: Formal potential and stability constant calculation for i⁻, i₃⁻ and i₂ at 550 °C

550 °C	i ⁻ /i ₃ ⁻ , V	i ⁻ /i ₂	Ln(K _{stab})	K _{stab}
1	-0.319	0.72	-29.2998	1.88E-13
2	-0.312	0.663	-27.495	1.15E-12
5	-0.314	0.59	-25.4928	8.48E-12

Weight loss measurement

The concentration of the KI in LiCl-KCl mentioned is based on the initial mixing and pre heating of the sample. Since, the temperature passes the vaporization point of iodine, there is certain loss in the iodide concentration after heating the sample. In addition to this, iodine evolution was clearly seen during the experiment. So, UV-Vis analysis was performed to

measure the weight loss in the sample after heating and experiment. This was done in order to reduce error in diffusivity calculation.

Table 3.6 : Percent weight loss before the experiment and after the experiment

Temperature	1wt% before test (wt%)	1wt% after test (wt%)	2wt% before test (wt%)	2wt% after test (wt%)	5 wt% Before test (wt%)	5 wt % After test (wt%)
450 °C	0.97	4.25	1.96	1.91	4.5	4.25
500 °C	0.96	4.2	1.93	1.88	4.4	4.2
550 °C	0.91	4.16	1.88	1.83	4.3	4.16

Conclusions

Different electrochemical techniques were used to detect the oxidation behavior of iodide as a significant fraction of iodine (78.9mg/g of heavy metal) was reported to be retained in the molten salt as iodide (I⁻). The oxidation of the iodide showed formation of intermediates as expected and the diffusivity increased with the temperature. The study of electrochemical properties of LiCl-KCl with varying concentration of KI showed that accumulation of iodide species could significantly affect the performance of the electro-refiners that are used for electrolytic reduction of actinides. This helped to achieve the objective of this plan to study the electrochemical behavior of iodide in LiCl-KCl at higher temperatures.

References

1. S. M Frank, Summary of Iodine Partitioning in EBR-II Fuel, Internal Report, Idaho National Laboratory, SMF-001-16, Feb 2016
2. P. Masset, Journal of Power Sources 160 (2006) 688–697
3. A.I. Popov, D.H. Geske, J. Am. Chem. Soc., 80 (1958) 5346-5349
4. L-F. Olsson, Inorg. Chem., 24 (1985) 1398-1405
5. K. C. Marsden, and B. Pesic, Journal of The Electrochemical Society, 158 (6) F111-F120 (2011)
6. Kanzaki Y, Takahashi M. J Electroanal Chem Interfacial Electrochem 1975;58:349–56.
7. Pizzini S, Morlotti R. Electrochim Acta 1965;10:1033–41
8. A. Merwin, D. Chidambaram, Met. Mater. Transactions A, 46A (2015) 536-544
9. E. Gileadi, Physical Electrochemistry: Fundamentals, Techniques, and Applications, Wiley-VCH Verlag GmbH & Co. KGaA, (2011) 62
10. S. Vandarkuzhali, Nibedita Gogoi, Suddhasattwa Ghosh, B. Prabhakara Reddy, K. Nagarajan, Electrochimica Acta 59 (2012) 245– 255
11. Y. Dalsun, J. Pormatikul, M. Shaltry, S. Phongikaroon, K. Allahaar, Journal of Radioanalytical and Nuclear Chemistry, 322, pages1031–1037(2019)
12. D. Yoon, S. Phongikaroon, Electrochimica Acta 227 (2017) 170–179
13. S. Yaron, C. Yitzhak and Y. Cohen, ECS Electrochemistry Letters, 4 (1) H1-H4 (2015)
14. J.D. Martin, S.J. Goettler, N. Fosse, L. Iton, Nature, 419 (2002) 381
15. A. J. Bard and L. R. Faulkner, Electrochemical Methods, Fundamentals and Applications, New York., John Wiley & Sons, Inc., (2001).
16. M. Chemla, I. Okada, Electrochimica Acta 35 (1990) 1761
17. I.K. Delimarskii, B.F. Markov, Electrochemistry of Fused Salts, The Sigma Press Publishing, Washington, DC, 1961
18. M. E. Orazem and B. Tribollet, Electrochemical Impedance Spectroscopy, 1st edition, Wiley-Interscience, Hoboken, N.J, 309 (2008).
19. V. Lockett, R. Sedev, J. Ralston, M. Horne, and T. Rodopoulos, J. Phys. Chem. C, 112, 7486 (2008).
20. S. Dokashenko and V. Stepanov, Russ. J. Electrochem., 29, 1129 (1993).

21. E. Hallag, *Journal of the Chilean Chemical Society*, 55(1), (2010)
22. A.S. Basin , A.B. Kaplun, A.B. Meshalkin and N.F. Uvarov, *Russian Journal of Inorganic Chemistry*, 53, 1509-1511(2008)
23. L. Ramaley and M. S. Krasue, *Anal. Chem.*, 41, 1362 (1969).
24. J. Osteryoung and R. A. Osteryoung, *Anal. Chem.*, 57, 101 (1985).
25. P. Delahay, *New Instrumental Methods in Electrochemistry: Theory, Instrumentation, and Application to Analytical and Physical Chemistry*, Interscience, New York, (1954).
26. T. Berzins and P. Delahay, *J. Am. Chem. Soc.*, 75, 555 (1953).
27. H. J. S. Sand, *Philos. Mag.*, 1, 45 (1901).

Chapter 5: Study of Cerium Deposition with the Increase in Concentration of KI in LiCl-KCl Eutectic

The main objective of this task is to determine the effect of iodide species on the reduction process of Ce^{3+} in LiCl-KCl and obtain the electrochemical data like diffusion coefficient, formal potential, number of steps for reduction process and number of electrons exchanged. Cerium ion is used as surrogate for studying the behavior of uranium ion in molten salt due to similar ionic size and electrochemical behavior. Several studies focused on the electrochemical behaviors of CeCl_3 in the molten salt at high temperature that helped in measurement of diffusion coefficient and exchange current densities of CeCl_3 . However, no studies have been reported to the best of our knowledge on how the iodide species affect the diffusion and redox potentials of the Ce^{3+}/Ce . So, in this task, we will be running cyclic voltammetry and EIS of LiCl-KCl with CeCl_3 at different concentration of KI to measure the effect on redox potential and diffusion of cerium species due to iodide.

Introduction

Pyrochemical reprocessing technique is one of the most viable methods to treat used nuclear fuel and recover and recycle actinide elements from used nuclear fuel. This process is considered one of the most promising in present time due to its properties like high thermal and radiation stability which allows a shorter cooling time of fuels, high actinide content and inherent proliferation [1-4]. During pyro-processing, spent fuels are dissolved at anode and uranium is recovered on solid cathode by controlling the voltage applied, so it is important to obtaining the basic electrochemical data of fission products, such as formal potential, diffusion coefficients (D) and redox mechanism, etc. [5]. Many studies on electrochemical behavior of uranium have been carried out in LiCl-KCl in which diffusion coefficients are measured through cyclic voltammetry and chronopotentiometry [6,7]. In other research, CP and chronoamperometry along with linear sweep voltammetry were used to determine the diffusion coefficients of uranium in LiCl-KCl [8,9]. Choi et al. used linear polarization method to measure the exchange current density of uranium [10]. But uranium being a radioactive element has safety issues when used in lab conditions, so cerium is used as a surrogate material to study the behavior of uranium in molten salt. Cerium has similar ionic size of 115pm

compared to 117 pm of U^{3+} and an electrochemical potential that is closer to the uranium than most lanthanides which makes it a suitable candidate to be used as surrogate material [11]. Different studies have been performed regarding the electrochemical behavior of $CeCl_3$ in the recent decade. Du et al. used chronopotentiometry to study the reduction process of Ce (III) in LiCl-KCl melt and proposed the electrochemical reaction as follows:



and the diffusion coefficient is $2.08 \times 10^{-5} \text{ cm}^2/\text{s}$ at 873 K [12]. Similarly, Wang et al. studied the Cerium behavior and indicated that the reduction process of Ce(III) to cerium metal was a single step exchanging three electrons which was controlled by diffusion of cerium(III) [13]. The other studies done by Marsden, Pesic and Iizuka determined various electrochemical properties of Ce(III) like exchange current density, diffusion coefficient and standard potentials at different temperatures [14,15]. Similarly, Castrillejo et al. studied the electrochemical behavior of Ce (III) to be quasi-reversible 3 electron reaction and measured the diffusion coefficient and potential by CV, OCP and Chronopotentiometry [16].

Even though different studies have been done in electrochemical behavior of cerium chloride in LiCl-KCl, not many studies have reported the effect of fission product anions such as iodide in LiCl-KCl and its effect on the electrochemical behavior of Ce (III). Along with accumulation for lanthanide, several radioactive iodine isotopes are also formed as fission products in nuclear fuel and I^{129} is one of the particular concerns. Iodine is retained in the fuel matrix and by containment provided by the fuel cladding. During the dissolution of used fuel in the molten salt, a significant fraction of iodine (78.9mg/g of heavy metal) was reported to be retained in the molten salt as iodide (I^-) (17). During the reduction of used oxide fuels of light water reactors, Iodine gets partition to the salt phase and reprocessing of mixed oxide spent fuels results in elevated concentrations of I in the salt phase [18]. Presence of iodide may affect the reduction behavior of the Ce^{3+} due to interaction with cations and chloride ions. Iodide due to its larger size could affect the diffusivities and shift the redox potentials which eventually affect the reduction of Cerium ions during the processing.

This paper described a study of effect of iodide in the electrochemical reduction of cerium ions in chloride melt at different concentrations. The main aim was to determine the reduction mechanism and obtain the electrochemical data such as the diffusion coefficient and the formal potential, especially, the number of steps for reduction process and the number of

electrons exchanged at each step using methods like cyclic voltammetry, chronopotentiometry, EIS and square wave voltammetry (SWV). This paper also aimed to analyze the morphology of nucleation of cerium on tungsten through SEM observations.

Experimental procedure

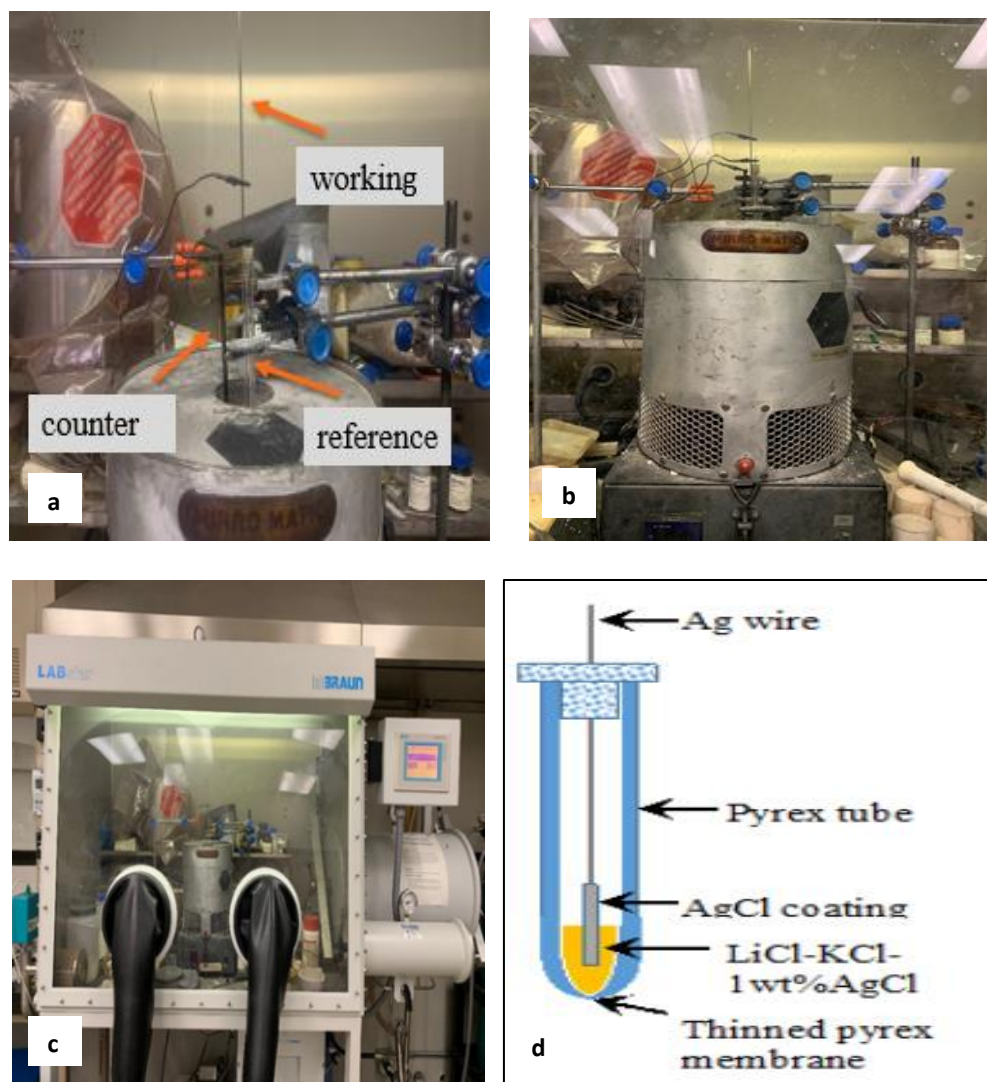
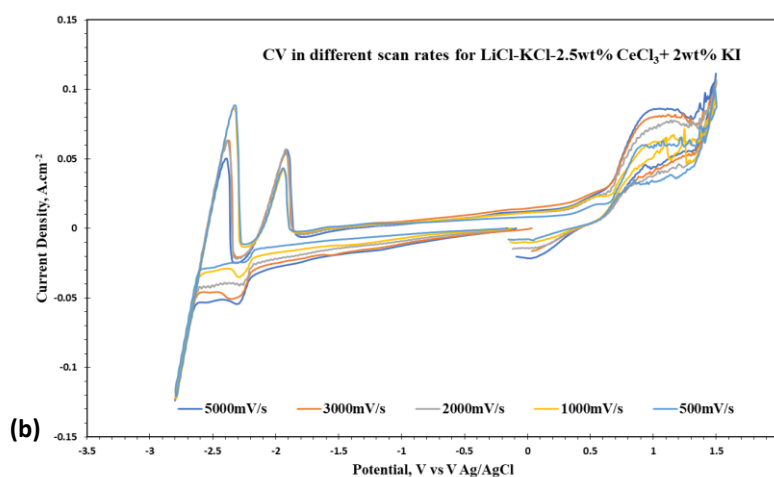
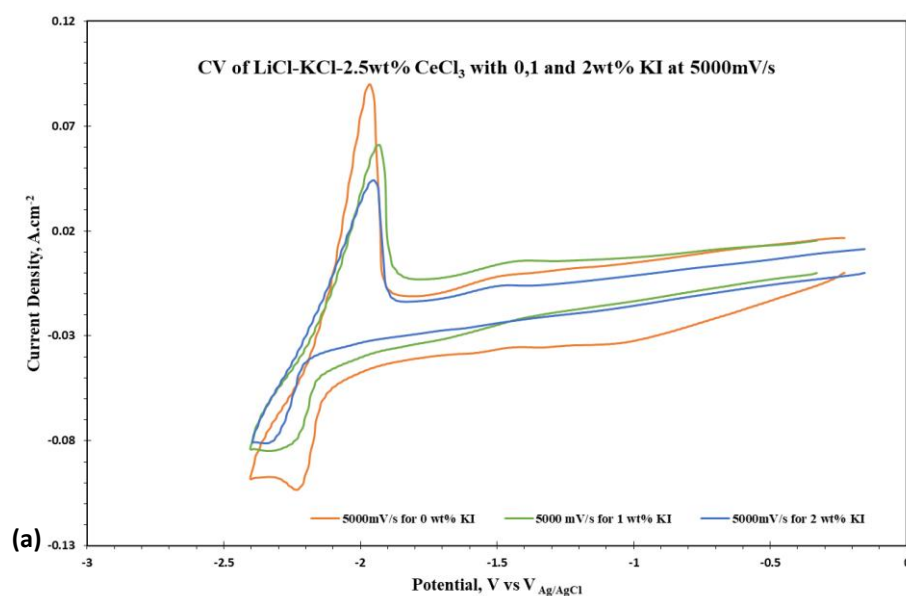


Figure 5.1: (a-c) Experimental setup for the electrochemical measurement and (d) schematic of reference electrode

All the electrochemical experiments were carried out in a glove box (MBraun) controlled with ultra high purity Ar gas at temperature of 450 °C. The oxygen and moisture concentration were monitored and maintained below 2 ppm and electrochemical measurements were performed using Gambry 1000. Three electrode setup was used for the experiments with 2 mm diameter tungsten rod (99.5%, Alfa Aesar) as working electrode and 4 mm diameter

glassy carbon rod as counter electrode. The reference electrode was an in house made AgCl coated Ag wire immersed in LiCl-KCl eutectic containing 1 wt% AgCl. The open circuit potential of the tungsten electrode in the eutectic salt was recorded as a function of time before starting the CV. Square wave voltammetry was conducted between OCP and -2.5 V at a frequency of 30 Hz, pulse size of 25mV, step size of 1mV and pulse time of 0.04 s. 2.5wt% of CeCl_3 (Alfa Aesar, 99.5%) was added in the LiCl-KCl eutectic with varying concentration of KI (Sigma Aldrich). The concentration of KI is varied from 0,1 and 2 wt percent in the eutectic with 2.5 wt% CeCl_3 . The mixture was heated up to 450 °C and the electrochemical measurements were done after the salt was ready as discussed above.

Results and discussion



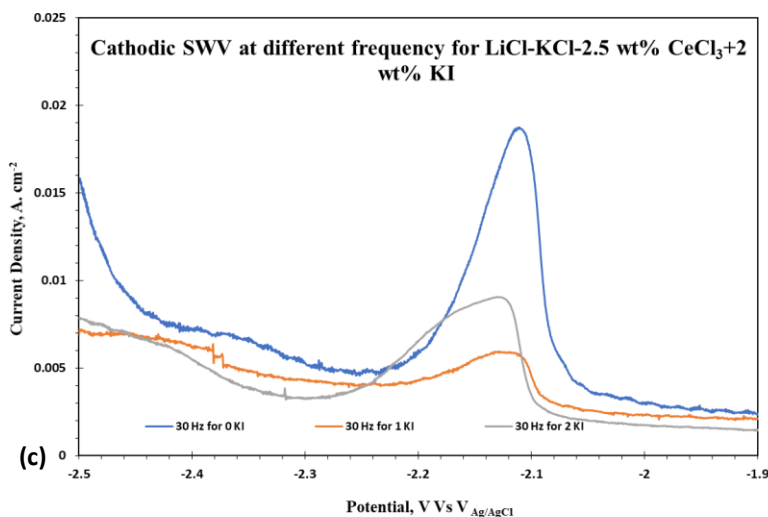


Figure 5.2: (a) CV from OCP to -2.5 with 0,1 and 2 wt% KI at 5000 mV/s (b) CV of LiCl-KCl-2.5 wt% CeCl₃+2 wt% KI at 100-5000 mV/s (d) SWV of LiCl-KCl-2.5 wt% CeCl₃ with 0,1 and 2 wt% KI

Figure 1(a) shows the full CV at 5000 mV/s scan rate in window from OCP to -2.4 V at different additions of KI. The potential below lithium reduction of -2.5 V Vs V_{Ag/AgCl} was selected to get a clear picture of reduction and oxidation of cerium without the participation of lithium ion in the reduction and oxidation processes. For the case with no KI addition, a cathodic peak is observed at about -2.2 V vs V_{Ag/AgCl} and corresponding anodic peak is observed at about -2.05 V vs V_{Ag/AgCl}. These pair of peaks could be attributed to reduction and oxidation of Ce(III), respectively. The reduction peak corresponds to one step three electron reduction reaction of Ce (III) to Ce (0). Yoon et al reported the cyclic voltammetry of LiCl-KCl-CeCl₃ that showed the cerium reduction and oxidation peaks at around -2.2 and -2.09 V which matched with our results for the reduction of Ce in the melt.[20]. The reduction and oxidation potential are almost similar for the electrolyte with 0, 1 and 2 wt.% KI addition. But the reduction current density decreases with the increase in KI concentration from -0.1, -0.09 and -0.08 A.cm⁻² for 0,1 and 2 wt% KI respectively. This could be attributed to the reduction of more cerium ions due to presence of a smaller concentration of iodide anions. The larger iodide anion tends to diffuse quicker than comparatively smaller cerium cation when the concentration of iodide increases due to Chemla effect. This might have led to reduction of less cerium ions in presence of more iodide ions in the salt. The effect of increasing KI in the

LiCl-KCl seems to decrease the reduction of Ce which in turn effects the reduction of uranium in the pyro processing of UNF.

Figure 1(b) depicts the cyclic voltammetry in full window -2.8V to 1.6V for LiCl-KCl-2.5 wt% CeCl₃ with 2 wt% KI to see the overall reaction in the salt. Peak at -2.2 V vs V_{Ag/AgCl} can be attributed to cerium reduction with the respective oxidation at -2.0V vs V_{Ag/AgCl}. Lithium reduction and oxidation peaks are seen to be at -2.7 and -2.5 V vs V_{Ag/AgCl} respectively. In the anodic direction, iodine evolution peak is seen at 0.6 V vs V_{Ag/AgCl} and Chlorine evolution peak is at 1.2 V vs V_{Ag/AgCl}. Since, the pattern with the varying concentration of KI is already shown in figure 1(a), figure 1(b) shows the change in current density with respect to scan rate. As seen in the figure, the current density peak increases with the scan rate which means it is directly proportional to the square root of increasing scan rate. This indicates that this process is controlled by diffusion of cerium (III) towards the surface of tungsten [19].

Figure1(c), indicates the square wave voltammetry which helps delineate the effect of iodide on the Ce reduction behavior. The potential of differential current peak shifted to less negative potentials with the addition of 1 and 2 wt% KI than that of 0% KI addition. This could be because the reaction is quasi-reversible. The number of electrons involved in the cerium reduction process was determined by square wave voltammetry which could be useful in the determination of the calculation of the diffusivity coefficient of cerium ions [20-22].

The difference between peak potential and half peak potential can be used to calculate the number of electrons transferred by the following expression:

$$E_p - E_{p/2} = -0.77 \frac{RT}{nF} \quad (2)$$

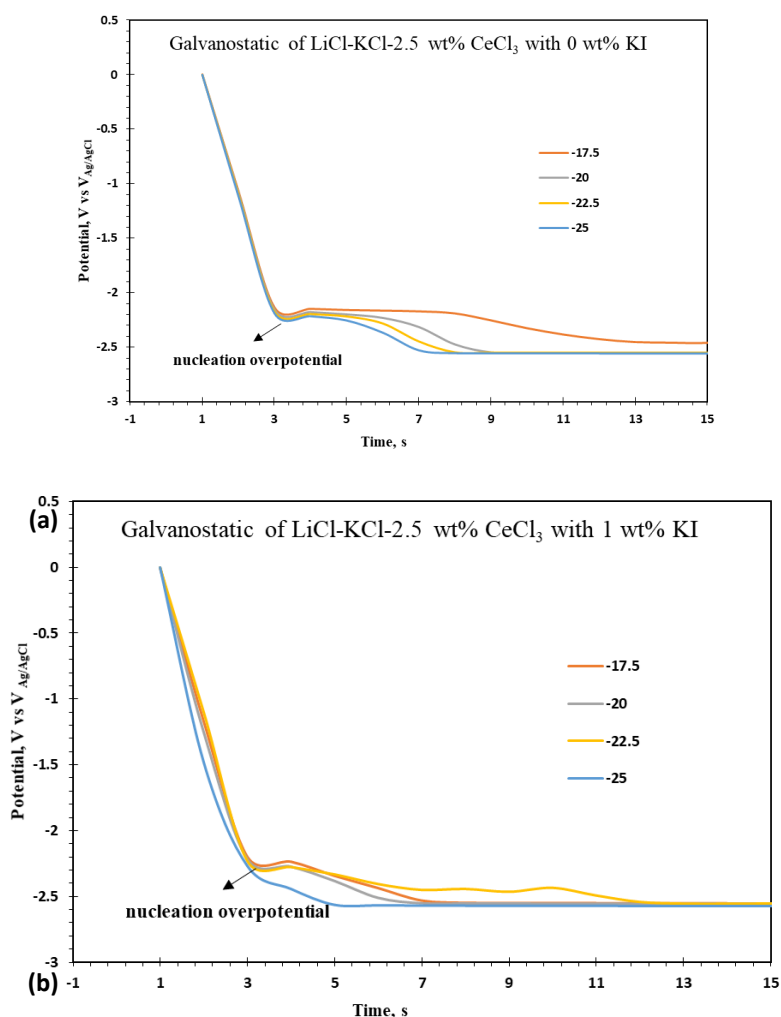
Where E_p is the peak potential, $E_{p/2}$ is the half peak potential, R is the universal gas constant ($J.mol^{-1}K^{-1}$) and T is the absolute temperature (K), F is the Faraday constant ($C.mol^{-1}$) and n is the number of electrons transferred. The calculated number of electrons transferred was ranging from 2.5 to 3.1 agreeing with the expected value for the reduction process of Ce^{3+}/Ce . The diffusivity calculation was done using Sand equation for planar electrode [23]. First, current densities applied are plotted with respect to inverse of time. The resulting slope from the graph is used in equation given below to calculate the diffusion coefficient of the salt.

The equation used is:

$$D = \frac{\pi * slope^2}{nFAC_0} \quad (3)$$

Where, slope is obtained from the graph of current density versus inverse of transition time, A is the electrode area (cm^2), C_0 is the bulk concentration of CeCl_3 ($\text{mol}\cdot\text{cm}^{-3}$), and D is the diffusion coefficient ($\text{cm}^2\cdot\text{s}^{-1}$). Figure 3 (a)-(c) represent chronopotentiometry graph at different current densities for 0,1 and 2 wt% KI respectively in $\text{LiCl-KCl-2.5 wt\% CeCl}_3$. As seen in the figure, different current from -17.5 to -25 mA was applied with an increment of 2.5 mA. The transition time seems to be decreasing with the increase in current density. This transition time is used to calculate slope by plotting with current density. Figure 4 (a)-(c) shows the graph obtained by plotting current density applied with respect to inverse of transition time.

Similarly, morphologies of Ce electrodeposits at different time intervals are depicted in Figures 2- 5 when the deposition was carried out at the shoulder potential of Ce reduction wave (in the range of -2.15 to -2.18 $\text{V}_{\text{Ag}/\text{AgCl}}$).



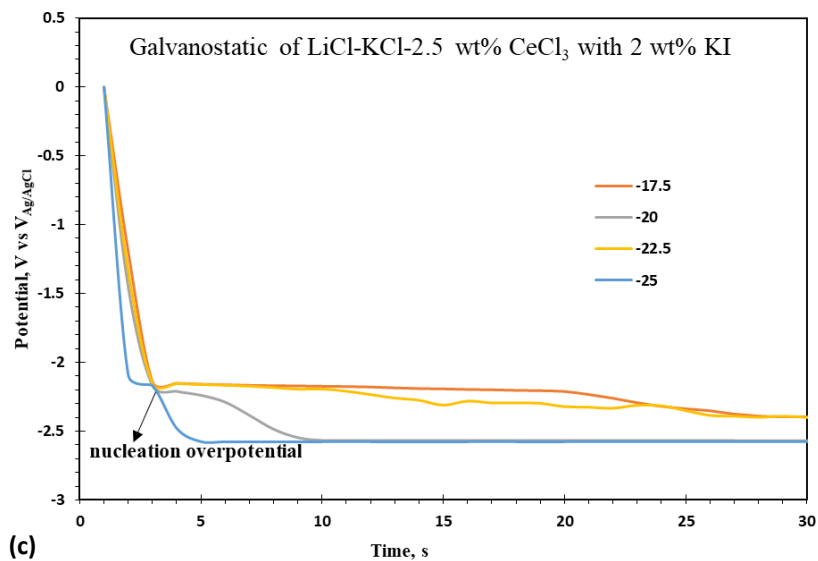
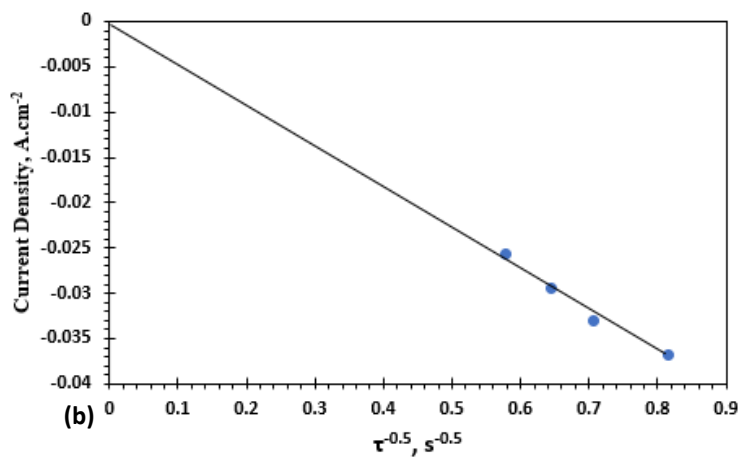
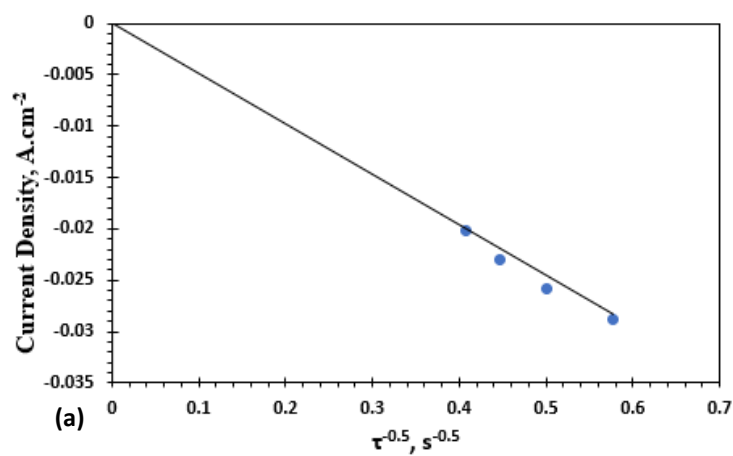


Figure 5.3: Chronopotentiometry at different current densities of -17.5 to -25mA for LiCl-KCl-2.5 wt% Ce with (a) 0 wt% KI (b) 1 wt% KI (c) 2 wt% KI



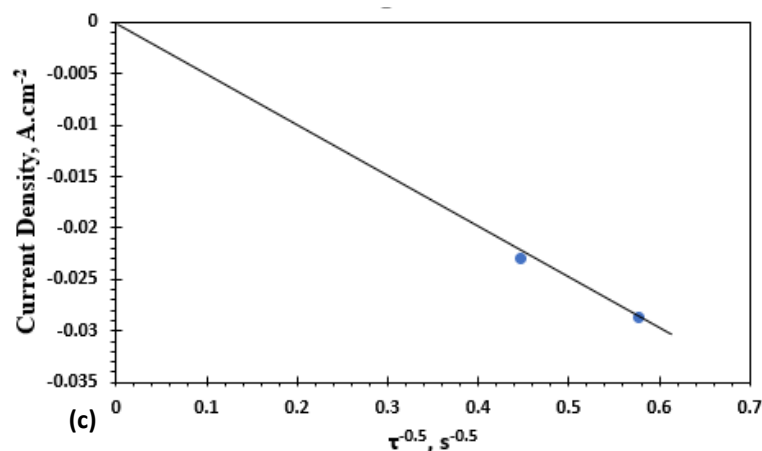


Figure 5.4: Current Density vs inverse of transition time for LiCl-KCl-2.5 wt% Ce with (a) 0 wt% KI (b) 1 wt% KI (c) 2 wt% KI

Table 5.1: Diffusivity Coefficient of Cerium in LiCl-KCl+2.5 wt% CeCl₃ with varying concentration of KI

Concentration of KI in LiCl-KCl-2.5 wt Ce and KI at 450 °C	Diffusivity (10 ⁻⁶ cm ² .s ⁻¹)
LiCl-KCl-2.5 wt% Ce-0wt% KI	2.499
LiCl-KCl-2.5 wt Ce-1 wt% KI	1.5360
LiCl-KCl-2.5 wt Ce-2 wt% KI	1.1041

The diffusivity coefficient seemed to be decreasing from 2.499X10⁻⁶ to 1.1041X10⁻⁶ cm².s⁻¹ with the increase in iodide concentration from 0 to 2 wt% KI. It appears that the larger iodide ions cover the tungsten electrode which in turn affects the diffusivity of the cerium ion in the LiCl-KCl. With the increase of iodide in the solution, the diffusivity of cerium decreased which might have resulted in lower reduction peak for the cerium as represented by the cyclic voltammetry in figure 1(a).

Test for reversibility, irreversibility, and quasi reversibility

The reversibility of the electrode reaction was also determined from the CV obtained in LiCl-KCl-CeCl₃ at different scan rates at 450 °C. The potential difference $\Delta E_p = E_{pa} - E_{pc}$ between two peaks is larger than the value of 2.3 RT/nF which is 55 mV for three electron system. Similarly, the slight increase seen in case of ΔE_p with the constant values of $E_{1/2}$ is also seen. The I_p increased with square root of scan rate and is not proportional to it and E_p^c shifts to

negative direction with increasing scan rate. These reversibility check points towards the quasi-reversibility of the system which is also shown by the square wave voltammetry.

Standard Potential:

Standard CV experiments, the apparent standard potential was calculated from the peak potentials and the formal standard potential is defined as [28]:

$$\frac{E_{Ce^{3+}}^{0*}}{Ce^0} = \frac{E_{Ce^{3+}}^0}{Ce^0} + \frac{RT}{nF} \ln \gamma_{Ce^{3+}} \quad (5)$$

$\frac{E_{Ce^{3+}}^0}{Ce^0}$ is the standard potential and $\gamma_{Ce^{3+}}$ is the activity coefficient.

On assuming the activity of cerium metal as unity, the equation could be written as [29]:

$$E_p = \frac{E_{Ce^{3+}}^{0*}}{Ce^0} + \frac{RT}{nF} \ln (X_{Ce^{3+}}) - 0.854 \frac{RT}{nF} \quad (6)$$

And E_p can be calculated by the equation proposed by Matsuda and Ayabe below [30]:

$$E_p = E_{1/2} - 1.11 \frac{RT}{nF} \quad (7)$$

Here, $E_{1/2}$ is -2.3V which is the cerium reduction potential and n is 3 from the equation above in our experiment.

Based on the extrapolation to infinite dilution of the data of Yang and Hudson [29] at low AgCl concentration in the LiCl-KCl eutectic salts and other references, the potential of the reference electrode used in this work vs Cl_2/Cl^- is given by the expression:

$$E_{Ag/AgCl} (vs Cl_2/Cl^-)/V = -1.0910 - 1.855 \times 10^{-4} T (K) \quad (8)$$

Nucleation characteristics

Investigation of the nature of nucleation of cerium in presence of iodide was also investigated to figure out if it is progressive or instantaneous on a tungsten electrode. The nucleation mechanisms could also be evaluated mathematically by using appropriate models such as those of Scharifker and Hill [31] and visually by scanning electron microscopy studies. One possible nucleation mode is instantaneous, where the nuclei are created at the beginning and further deposition occurs only by growth of these crystals. The second mode is progressive nucleation where additional nuclei continue to grow throughout deposition.

The electrochemical nucleation of cerium was investigated at 450 °C to establish whether nucleation mechanism is progressive or instantaneous on tungsten electrode. Theoretical methods have been well developed to establish the mechanism by analyzing the time and curve shape of the rise to maximum current. Figure 4 (a) illustrates nucleation transients in

30,60 and 120 seconds obtained at potential of -2.3V for cerium without the presence of iodide in LiCl-KCl. The current decreased initially until 0.02 second as the double layer started to charge. The increase in current density is seen after 0.02 secs and reached the highest peak at around 0.035 second as first nuclei generated and grew increasing the active electrode area. Then the current decreased as deposition became limited by the diffusion to the electrode surface.

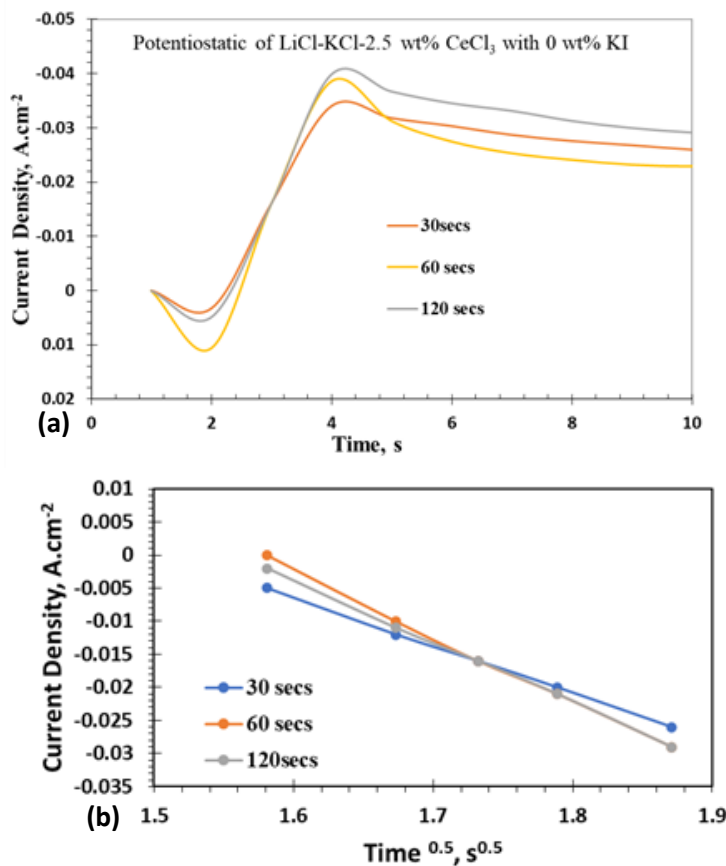


Figure 5.5: (a) Nucleation transients of CeCl₃ in LiCl-KCl with 0 wt% KI at -2.3V potential in 30,60 and 120 secs, (b) Plots of current density versus time^{1/2} from the rising portion of the nucleation transients shown in figure 4(a).

In this case of diffusion control, the rising part of the nucleation curve follows a relationship [33]:

$$i = \alpha t^x \quad (9)$$

where i is the measured current density, α is a function of density of initial nuclei and either the diffusion or kinetic parameters, t is the time, and x is the function of the type of nucleation,

geometry and growth limitation of the nuclei. The plot 4 (b) shows the linear relationship between i and $t^{1/2}$. The work of Allongue and Souteyrand [34] show the value $x=1/2$ corresponds to the instantaneous nucleation mode whose growth is diffusion controlled. Thus, from the transients, it is seen that the nucleation is instantaneous at the potential of -2.3V at the temperature of 450 °C.

The nucleation follows the same pattern when 2 wt% KI is added to LiCl-KCl with Cerium. The figure 5(a) shows the nucleation transients of CeCl_3 in LiCl-KCl with 5 wt% KI addition and 5 (b) shows the plots of linear relationship between current density and time^{1/2}.

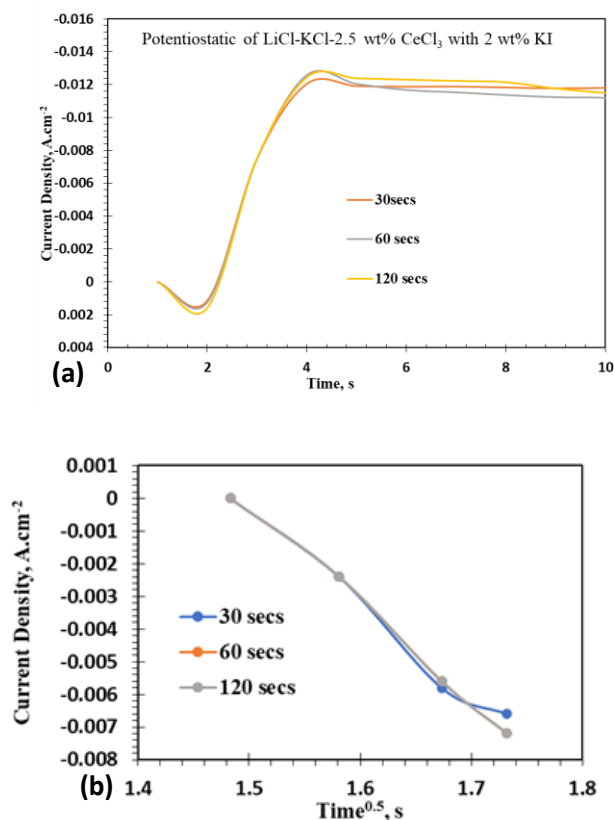


Figure 5.6: (a) Nucleation transients of CeCl_3 in LiCl-KCl with 2 wt% KI at -2.3V potential in 30,60 and 120 secs, b) Plots of current density versus time^{1/2} from the rising portion of the nucleation transients shown in figure 5.6(a).

Figure 5.6 illustrates the two nucleation transients of CeCl_3 with 0, 1 and 2 wt% KI for 60 seconds. As illustrated in figure 4 and 5, both nucleation transients show that the nucleation follows the instantaneous pattern. The nucleation in case of LiCl-KCl+ CeCl_3 with KI appears to have taken a little longer to form. The current density peak when compared between the two melts show that the current density for 0 wt% KI is higher than 1 and 2 wt% KI. Higher

current peak points to more nucleation and it is observed that the instantaneous nucleation rate is lower when 2 wt% KI is added.

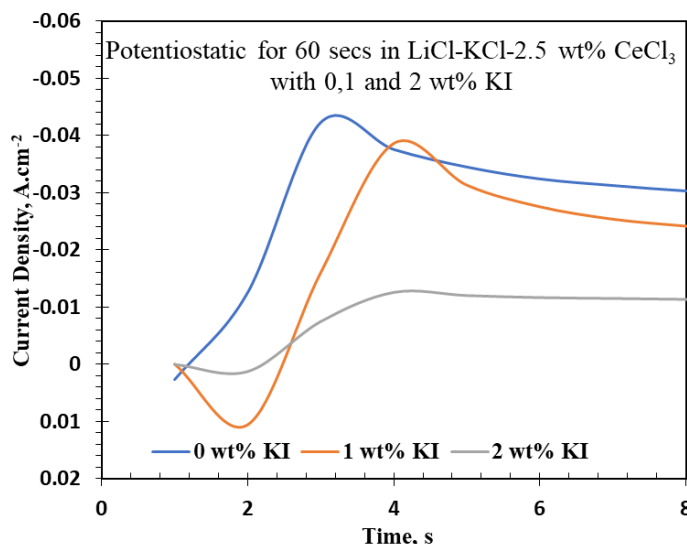


Figure 5.7: Nucleation transients of CeCl_3 in LiCl-KCl with 0, 1 and 2 wt% KI addition

Exchange Current Density of Cerium (III)/Ce(0) Reaction

The exchange current density is a function of kinetic reaction parameters and is linked to reaction reversibility of reduction/oxidation of cerium ions. It indicates the reaction kinetics at the redox (equilibrium) potential. It is also linked to nucleation characteristics and deposit morphology. For these reasons, it was desired to quantify the order of magnitude of exchange current density of the Ce (III)/Ce(0) couple in LiCl-KCl eutectic. Butler-Volmer equation [32,33] described by the following relationship:

$$i = i_c - i_a = i_0 \left\{ \exp\left[\frac{\alpha n F}{RT} (E_{eq} - E)\right] - \exp\left[-\frac{(1-\alpha) n F}{RT} (E_{eq} - E)\right] \right\} \quad (10)$$

where i is net current density, i_c cathodic current density, i_a anodic current density, i_0 the exchange current density, α is the transfer coefficient, n is the number of electrons transferred and E_{eq} is the cell equilibrium potential. In conditions of a relatively large cathodic overpotential, the terms corresponding to the anodic current can be neglected and could be written as:

$$(E_{eq} - E) = \frac{2.3RT}{\alpha n F} \log \frac{i_c}{i_0} \quad (11)$$

which can be further written as:

$$n_c = \alpha + b \log i_c \quad (12)$$

Where n_c is overpotential.

Many techniques could be used to calculate the exchange current density of cerium deposition. Some of the most used techniques are Tafel method, LP method and EIS method. EIS technique is very useful for determining the value of i_0 of transition metals in LiCl-KCl. According to S. Guo et al., the following equation can be used to calculate i_0 from R_{ct} [34]:

$$R_{ct} = \frac{RT}{nFi_0} \quad (13)$$

SEM

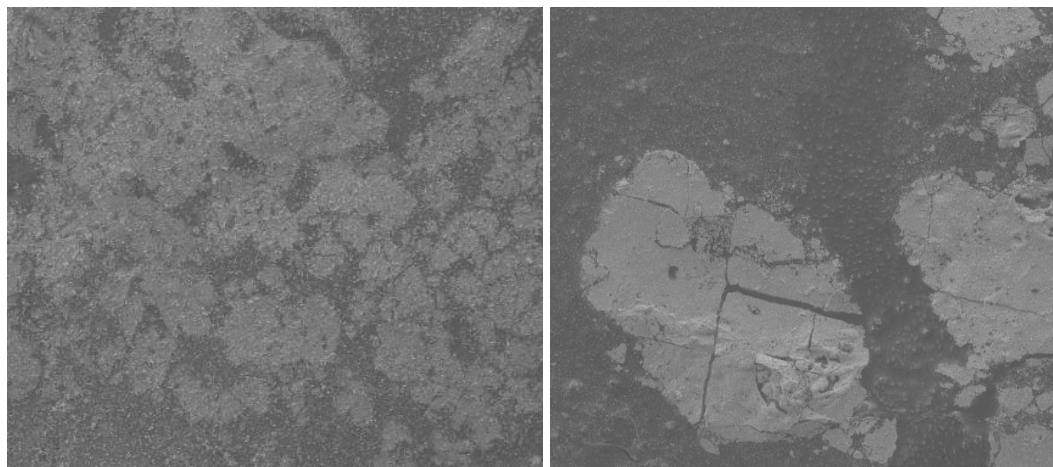


Figure 5.8 (a)-(b): SEM of deposition of Cerium with 0 and 2 wt% KI in LiCl-KCl-2.5 wt% $CeCl_3$ for 120 secs at 100X magnification

The SEM pictures in figure 5.8 (a)-(c) shows the instantaneous increase in the nucleation in all three intervals. As seen from the figure, the development of nucleation was quick and then it started growing which is the characteristics of spontaneous nucleation. This also supported the above mathematical and figurative conclusion of nucleation characteristics being spontaneous rather than progressive.

Conclusion

From the results, it was found that cerium deposition is affected by presence of iodide, and it reduced the rate of cerium deposition. This could be applied to the real world and can be concluded that presence of iodide negatively affects the deposition of uranium so proper treatment of iodide is necessary to improve the efficiency of pyroprocessing. The diffusion rate of cerium seemed decreased with the increase in the percentage of iodide addition in the melt which also shows that the presence of iodide in the melt negatively affects the electrodeposition of the cerium.

References

1. J. P. Ackerman, *Industrial & Engineering Chemistry Research*, 30, 141 (1991).
2. H. P. Nawada and K. Fukuda, *Journal of Physics and Chemistry of Solids*, 66, 647 (2005).
3. P. Soucek, R. Malmbeck, C. Nourry, and J. P. Glatz, *Asian Nuclear Prospects 2010*, 7, 396 (2011).
4. T. Inoue and L. Koch, *Nuclear Engineering and Technology*, 40, 183 (2008).
5. J. Serp, M. Allibert, A. Le Terrier, R. Malmbeck, M. Ougier, J. Rebizant, Gao F X, Wang C S, Liu L S, Guo J H, Chang S W, Chang L, Li R X, Ouyang Y G. Electrode process of La(III) in molten LiCl-KCl. *J. Rare Earths*, 2009, 27(6): 986.
6. P. Masset, D. Bottomley, R. Konings, R. Malmbeck, A. Rodrigues, J. Serp, and J. Glatz, *Journal of The Electrochemical Society*, 152(6), A1109 (2005).
7. P. Masset, R. J. M. Konings, R. Malmbeck, J. Sert, and J. Glatz, *Journal of Nuclear Materials*, 344, 173 (2005).
8. S. A. Kuznetsov, H. Hayashi, K. Minato, and M. Gaune-Escard, *Electrochimica Acta*, 51, 2463 (2006).
9. S. A. Kuznetsov, H. Hayashi, K. Minato, and M. Gaune-Escard, *Journal of The Electrochemical Society*, 152(4), C203 (2005).
10. Choi, B. E. Serrano, S. X. Li, S. Herrmann, and S. Phongikaroon, *Paper 9045 presented at Proceedings of Global 2009*, Paris, France, Sept. 6–11 (2009).
11. K. C. Marsden and B. Pesic, "Evaluation of the Electrochemical Behaviors of CeCl₃ in Molten LiCl-KCl Eutectic Utilizing Metallic Ce as an Anode," *Journal of Electrochemical Society*, 159, F111-F120 (2011).
12. R. D. Shannon, "Revised Effective Ionic Radii and Systematic Studies of Interatomic Distances in Halides and Chalcogenides," *Acta Crystallographica*, A32, 751- 767 (1976).
13. Du S L, Du F Y, Li B S, Lu L Q, Tang D X. Electrochemical behavior of CeCl₃ and SmCl₃ in fused chlorides. *J. Chin. Soc. Rare Earths* (in Chin.), 1986, 12(4)
14. Wang C., Liu Y., He H., Gao F., Liu L., Chang S., Guo J., Chang L., Ouyang Y., *Journal of Rare Earths*, 31,405(2013)

15. K. C. Marsden and B. Pesic, *Journal of The Electrochemical Society*, 159(6), F111 (2011)
16. M. Iizuka, *Journal of Electrochemical Society*, 145, 84 (1998).
17. Castrillejo Y., Bermejo M., Millan R., Martínez A., Barrado E., Caravaca C., Arocas P., *Progress in Molten Salt Chemistry*, Elsevier, New York, 2000
18. Castrillejo Y., Bermejo M. R., Pardo R., Martínez A. M., *J. Electroanal. Chem.*, 2002, 552, 124
19. Castrillejo Y., Bermejo M. R., Barrado E., Martínez A. M., Díaz, Arocas P., *J. Electroanal. Chem.*, 2003, 545, 141
20. Steven M Frank, Summary of iodine partitioning in EBR-II Fuel, Internal Report, Idaho National Laboratory, Report SMF-001-16, (2016)
21. M.F. Simpson, INL Report SMF -001-16, (2016)
22. Hamel C, Chamelot P, Laplace A, Walle E, Dugned O, Taxil P., *Electrochim. Acta*, 2007, 52: 3995.
23. Baur, J.E., *Elsevier*, 2007, 829-848
24. Bard A. J., Faulkner L. R., *Electrochemical Methods: Fundamentals and Applications*, John Wiley & Sons, New York, 2001, 201
25. Osteryoung J., Osteryoung R. A., *Anal. Chem.*, 1985, 57, 101
26. Ramaley L., Krasue M. S., *Anal. Chem.*, 1969, 41, 1362
27. Delahay P., *New Instrumental Methods in Electrochemistry: Theory, Instrumentation, and Application to Analytical and Physical Chemistry*, Interscience, New York, 1954
28. Masset P., Bottomley, D., Konings, R., Malmbeck, R., Rodrigues A., Serp J., Glatz J.P., *J. Electrochemical Society*, 2005, 152
29. Yang L., Hudson R. G., *J. Electrochemical Society*, 1959, 106, 986
30. Matsuda H., Ayabe Y. Z., *Fur Elektrochem.*, 1955, 59, 494
31. Scharifker B., Hills G., *Electrochimica Acta* 28, 1983, 879
32. A. J. Bard and L.R. Faulkner, *Electrochemical Methods: Fundamentals and Application*, 2nd ed., John Wiley & Sons, New York, 2001
33. P. Delahay, *New Instrumental Methods in Electrochemistry: Theory, Instrumentation and Application to Analytical and Physical Chemistry*, Interscience, New York, 1954
34. S. Guo, E. Wu, J. Zhang, *Electrochimica Acta*, 2018, 259, 253-261

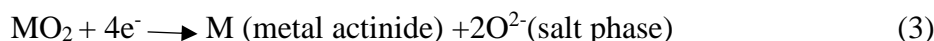
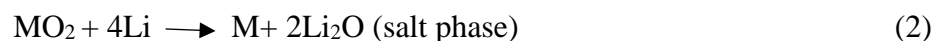
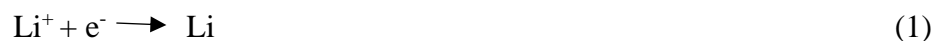
Chapter 6: Study of Electrochemical Behavior of Iodide in LiCl-KCl with 1 and 2 wt % Li₂O at 550 °C

The main objective of this task is to determine stable electrochemical potential window, redox potentials of I⁻ /I₃⁻ and other reaction intermediates of iodide and chloride in LiCl-KCl molten salt in the presence of Li₂O and iodide. Some of the researchers reported that LiCl-KCl-Li₂O has the lower melting point than traditional LiCl-Li₂O and can be used to reduce the uranium dioxide to uranium. The electrochemistry of iodide in high temperature molten salts such as LiCl-KCl eutectic or LiCl + Li₂O is not documented in detail to the best of our knowledge. So, study of electrochemical behavior of iodide in LiCl-KCl with Li₂O is very important.

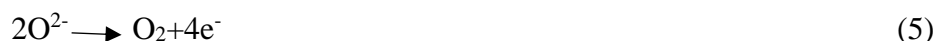
Introduction:

The electrochemical reduction process has been used to reduce the used oxide nuclear fuel to metallic fuel followed by electrorefining in pyro-processing technology [1]. LiCl-Li₂O is used as a molten salt for the reduction process and Li₂O is added in LiCl to speed up the reduction rate and prevent the anodic dissolution of the platinum anode by providing oxide ions to the salt [2]. Two reaction mechanisms are proposed for the electrochemical reduction of oxide fuel. One mechanism is direct electrochemical reduction in which the oxygen ion of the oxide at the cathode is dissolved in molten salt and discharged at anode as oxygen leaving the pure uranium metal at the cathode [3]. The other mechanism is indirect electrochemical reduction of metal oxide to metal by formation of Li at the cathode from the electrolysis of Li₂O. The reactions in each electrode are as follows [4].

Cathodic Reaction:



Anode Reaction:



Li₂O produced by reaction (ii) in molten in LiCl is dissociated into Li⁺ and O²⁻ which further oxidized to give oxygen gas on the anode surface. When the metal oxide is reduced to metal,

it remains at the cathode and the O^{2-} ions produced at cathode are transported through the salt and discharged at the anode to form O_2 gas [5-12].

But recently LiCl-KCl-Li₂O is being considered as potential molten salt for electroreduction process. Dissolution behavior of Li₂O and thermodynamics of the O_2/O^{2-} redox couple in molten LiCl-KCl-Li₂O systems were studied for the application of LiCl-KCl-Li₂O salt to electrochemical reduction processes. The use of LiCl-KCl-Li₂O tends to decrease the operating temperature from 650 to 550 °C. The lower temperature operation has several advantages such as decreased energy cost, lower corrosion, and reduced thermal damage to the vessel and electrode materials. The high reaction temperature causes a dense metal deposition on the electrode which in turn hinders the discharge of oxygen from metal oxide [13]. Mok Hur et al. demonstrated that the electric charge passed through the cell with LiCl-KCl-Li₂O was 200% of the theoretical electric charge necessary for reducing 5 g of metal oxide to metal. The study also showed the additional *in situ* generation of K along with Li metal which helped in the reduction of metal oxide [14]. Kado et al. also observed anodic currents around +2.5 V vs Li⁺/Li and was attributed to the oxidation of oxide ion to form oxygen gas which was confirmed by the gas analyses after the potentiostatic electrolysis represented by the following equation:



The Nernstian equation of the reaction is expressed below using the gas constant R, absolute temperature T, Faraday constant F, pressure of O_2 , P_{O_2} and anion fraction of O^{2-} , $X_{O^{2-}}$:

$$E_{O_2/O^{2-}} = E^{01}_{O_2/O^{2-}} + (RT/2F) \ln(P^{1/2}_{O_2}/X_{O^{2-}}) \quad (7)$$

Where $E^{01}_{O_2/O^{2-}}$ is the standard formal potential of O_2/O^{2-} which is given by the following equation using the standard potential of O_2/O^{2-} , $E^0_{O_2/O^{2-}}$; the fugacity coefficient of O_2 , γ_{O_2} ; and the activity coefficient of the O^{2-} anion, $\gamma_{O^{2-}}$:

$$E^{01}_{O_2/O^{2-}} = E^0_{O_2/O^{2-}} + (RT/2F) (\ln \gamma_{O_2}^{1/2} / \gamma_{O^{2-}}) \quad (8)$$

The standard formal potential of O_2/O^{2-} was determined to be 2.4 V vs Li⁺/Li in LiCl-KCl eutectic melt at 500 °C. Similarly, the formal potential could be calculated by using the following formula:

$$E^{01}_{O_2/O^{2-}} = 2.995(+0.001) - 7.38(+0.14) \times 10^{-4} T/V \text{ vs Li}^+/\text{Li} \quad (9)$$

From the equation, the value of formal potential of O_2/O^{2-} was calculated to be 2.463 V vs Li⁺/Li which is equivalent to 0.0V vs Ag/AgCl electrode[15].

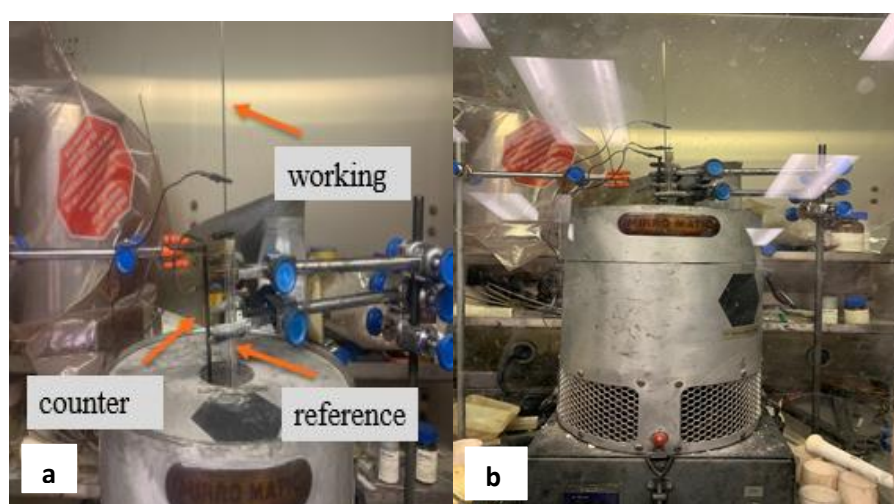
When spent nuclear fuels are processed in an electrolytic reduction cell, salt soluble fission products get accumulated in the salt bath during the electrochemical reduction process and these fission products in the salt affect the reduction rate of metal oxide. These salt soluble fission products accumulate in the LiCl electrolyte and hinder the reduction of actinide oxides and the reduction rate depends on the solubility and the diffusion coefficient of O^{2-} in the molten salt [16,17]. During the reduction of used oxide fuels of light water reactors, iodine gets partitioned to the salt phase and reprocessing of mixed oxide spent fuels results in elevated concentrations of iodine (78.9mg/g of heavy metal) [18].

Iodide reaction in the presence of oxygen: Iodide helps in decomposition of oxygen to oxide and tri-iodide which further gets decomposed to iodine and iodide in molten salt at temperatures greater than $280^{\circ}C$. The evolution of iodine results in lower concentration of iodide in the melt and therefore, iodide may not polarize the electrochemistry in the presence of oxygen [19].



This work focuses on the effect of increasing concentration of iodide in the oxygen reduction which in turn would be helpful to determine the effect of iodide ion in the electrochemical reduction rate of metal oxide to metal.

Experimental Procedure



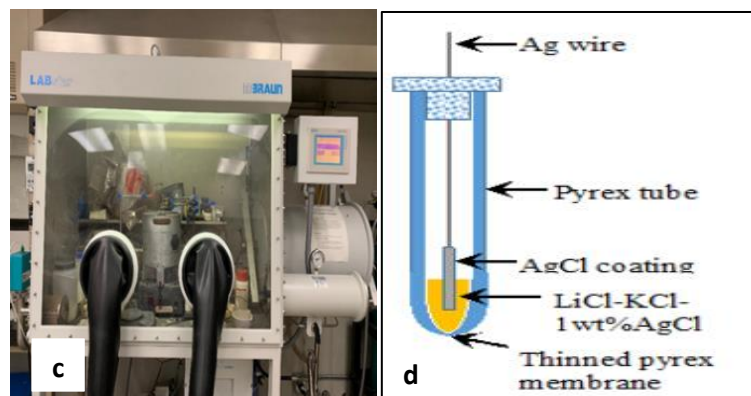


Figure 6. 1(a)-(d): (a)-(c)Experimental setup and (d)Schematic of Ag/AgCl reference electrode

All experiments were carried out in a glove box (MBraun) controlled with ultra high purity Ar gas at temperature of 550 °C. LiCl-KCl-Li₂O melt is made by mixing LiCl-KCl eutectic with varying concentration of KI obtained from Sigma Aldrich. The concentration of KI is varied from 0,1, 5 and 10 wt. percent was added to LiCl-KCl mixture. Lithiumoxide (Li₂O, Alfa Aesar, 99.5%) was added from 1 and 2 wt. percent in LiCl-KCl-KI melt. Conventionally, less than 3 wt % of Li₂O is used so the concentration is kept around 1 and 2 wt%. The solubility of Li₂O in LiCl-KCl eutectic in at temperature of 550 °C is 1.32 mol%.[20]. Tungsten rod (99.5%, Alfa Aesar) with 2 mm diameter was used as working electrode and glassy carbon rod with 4 mm diameter was used as counter electrode. In house made AgCl coated Ag wire immersed in LiCl-KCl containing 1 wt% AgCl was used as reference electrode. The electrochemical experiments were performed by using Gamry 1000. Open circuit potential was run for 15 minutes (900 seconds) followed by electrochemical impedance spectroscopy at OCP and then cyclic voltammetry was run at scan rates of 50, 100, 500, 1000, 3000 and 5000 mV/s in different windows in anodic direction (OCP to 0.6, 0.9 and 2.0V). Square wave voltammetry (SWV) was performed from OCP to 1.6V at frequency of 25 Hz and pulse of 30mV. Electrochemical Impedance Spectroscopy was performed at OCP and different peaks obtained from the CV.

Results and Discussion

OCP

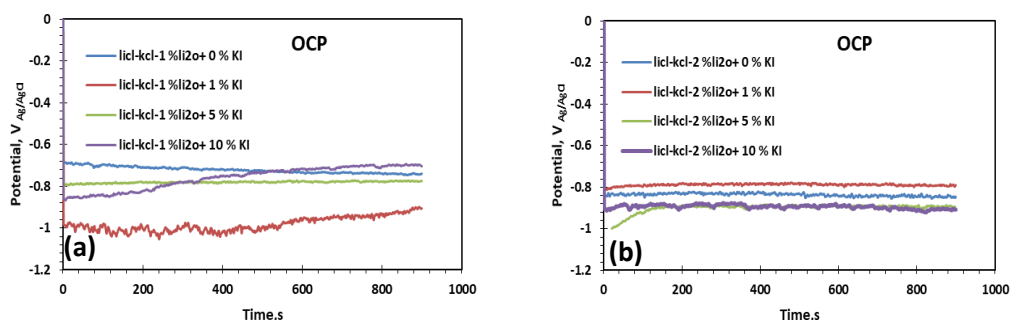


Figure 6.2 (a)-(b): Open Circuit Potential of (a) LiCl-KCl+1% Li₂O and (b) LiCl-KCl+2% Li₂O with varying concentration of iodide

The OCP was recorded for 900 seconds and seem to be stable in case of 1 and 5 wt% KI with 1 wt% Li₂O. But the OCP with 10 wt% KI appeared to be increasing and moving towards more positive than other melts. This could be attributed to increasing oxidizing nature of iodide ion. But the OCP with 10 wt% Ki in 2 wt% Li₂O was more stable and more negative. The OCP observed in the 2% Li₂O molten salt was more stable than that of the 1% Li₂O and more negative. When the OCP values were compared between 1wt% and 2 wt% Li₂O without KI, it could be seen that the OCP for the two percent is shifted towards negative potential from -0.7V to to -0.9 V with the increase in the concentration of Li₂O. This can be attributed to the presence of more oxygren in the melt which makes the metal more corrosive. It could also be attributed to the change in the exchange current density and tafel slopes with increased oxide ions. No particular trend is observed in OCP shift when KI is added to the melt but the OCP range was seen between -0.6 to -1.0 in all the cases.

EIS at OCP

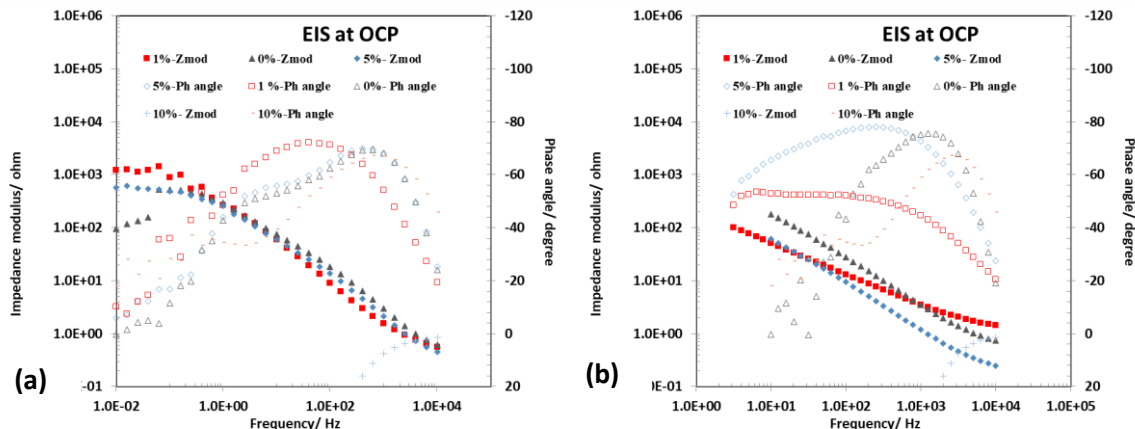


Figure 6.3(a)-(b): EIS at OCP (a) LiCl-KCl+1% Li₂O and (b) LiCl-KCl+2% Li₂O with varying concentration of iodide

Figures 6.3(a) and (b) show EIS results as Bode plots of the LiCl-KCl-1% Li₂O and 2% Li₂O melt with varying concentration of KI. The EIS was carried out at Open Circuit Potential. The impedance data were fitted with Equivalent Electrical Circuits to understand the electrochemical processes occurring at free condition without any polarization.

Cyclic Voltammetry

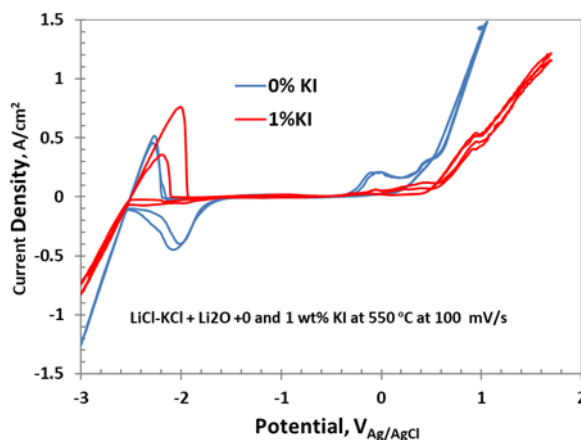


Figure 6.4: Full CV of LiCl-KCl-1 wt% Li₂O with 0 and 1 wt% KI

As seen in the figure 6.4, oxygen evolution peak is seen at 0V and the evolution of oxygen is suppressed in the presence of KI. An additional peak is seen at -2.0 V in case of 0% KI which could possibly represent the reduction of carbonate that formed on the counter electrode and cross diffused to the tungsten working electrode. This process is represented by the following equation:

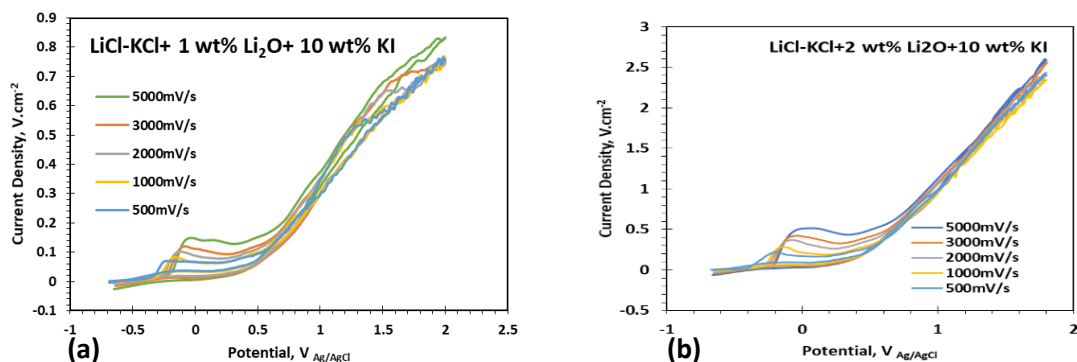
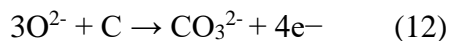


Figure 6.5(a)-(b): Cyclic Voltammetry at scan rate of 500-5000mV/s from OCP to 2.0 of (a) LiCl-KCl+1% Li₂O and (b) LiCl-KCl+2% Li₂O with 10 wt% KI.

Figures 6.5 (a) and (b) show CV of LiCl-KCl+1 and 2wt% Li₂O with 10 wt% KI at different scan rates in anodic direction with potential reaching upto 2.0 volts. A prominent peak around 0.0 volts was seen in both melts which could be attributed to the reaction represented by (16). The shift toward more positive potential with increasing scan rate was observed due to the decrease in the activity of O²⁻ according to Nernst equation. When both melts are compared, the current density for 2 wt% Li₂O is higher compared to 1wt% Li₂O also signifies the dissolution of more O²⁻ ions in the melt. Cyclic voltammetry in smaller window was also run as given in Fig. 6.6 (a) to see a more clear picture of how iodide oxidation of O²⁻ to O₂ and iodide oxidation are related.

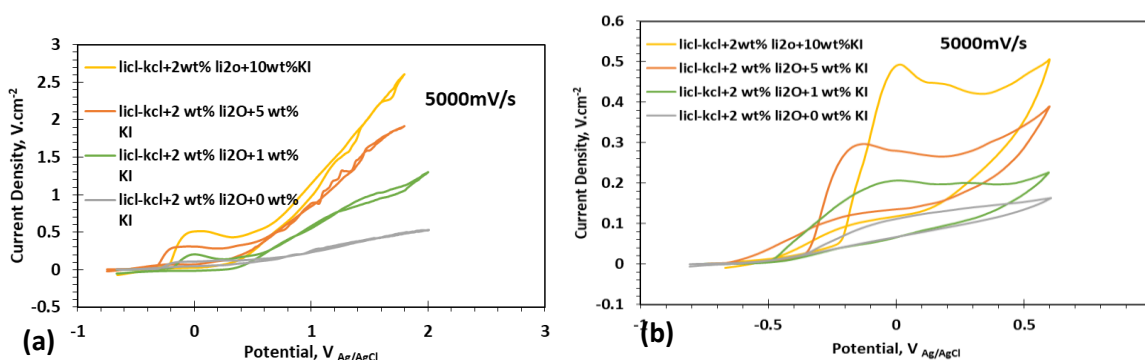
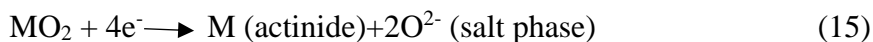


Figure 6.6(a)-(b): Cyclic Voltammetry at scan rate of 5000mV/s in LiCl-KCl+2% Li₂O with varying concentration of KI in the range of (a) OCP to 0.6 and (b) OCP to 2.0V

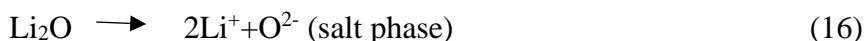
Figure 6.6(b) shows occurrence of two peaks around 0.0V. Only one small peak is seen in case of 0 wt% KI. The occurrence of two peaks in LiCl-KCl+ Li₂O melt with iodide showed

the effect of iodide in reacting with oxygen. The peak could be attributed due to oxidation of iodide to tri-iodide. First peak could be attributed to iodide to triiodide and the second peak could be attributed to the formation of O^{2-} .

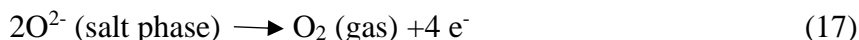
The cathodic reactions in the reduction of spent metal oxide are as follows:



Li_2O produced by reaction 2 in molten $LiCl$ is dissociated into Li^+ and O^{2-} :



The oxygen ions are further oxidized to give oxygen gas on the anode surface as follows:

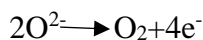


When a negative potential is applied, the actinide metal oxide is reduced to metal and remains at the cathode. The oxygen ion (O^{2-}) produced at the cathode is transported through the salt and discharges at the anode to form O_2 gas. Thus the molten chloride bath containing O^{2-} is used as an electrolyte to speed up the electrochemical reaction.

The anodic reactions that take place during the metal oxide reduction are [21-23]:



Figures 6.6(a) and (b) show the cyclic voltammetry obtained in anodic direction of tungsten electrode at 550 °C in $LiCl-KCl$ melt with 1 and 2 % Li_2O respectively at scan rate of 5000mV/s. No significant current peak was noticed until about 0.0V Vs $Ag/AgCl$. The peak at 0.0V could be attributed to formation of oxygen which is denoted by the anodic reaction:



The second current peak shown around 0.6V is of iodine evolution shown by the following equation:

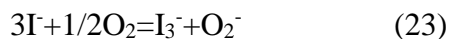


The presence of iodide in the melt helps conversion of oxygen to oxide ions and it also does not hamper in the further process as it gets oxidized into iodine itself and escapes through the solution. This relationship is depicted in the figures 4 (a) and (b) in which the peak attributed

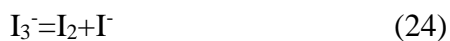
to formation of oxygen gets bigger with the addition of iodide. The figures represent how the diffusion of O^{2-} increases with the iodide concentration which in turn. The peak beyond 1 V shows the gaseous chlorine release according to the reaction [24]:



The reduction process of the metal oxide to metal is affected by two mechanisms: diffusion of Li to the metal oxide and the diffusion of O^{2-} in the bulk electrolyte. According to Sakamura, it was suggested that the diffusion of O^{2-} ions from the inside of the metal oxide to the bulk determined the reduction rate during the electrolysis. In presence of KI, the iodide ion reacts with oxygen from the air to give out O^{2-} in the solution which increases the O^{2-} concentration and the increase in the current density peak showing the decomposition of the oxygen to O^{2-} with the increase in KI concentration of KI in LiCl-KCl- Li_2O melt. This could lead to more O^{2-} in the solution which might cause the decrease in diffusivity of O^{2-} as O_2 from the electrode. Moreover, the presence of bigger iodide anions on the surface might prevent the O^{2-} get oxidized to O_2 . This will lead to the lesser reduction of metal oxide to metal and the efficiency of LiCl-KCl- Li_2O could be decreased due to the presence of iodide in the system. First the iodide anions in molten salt are oxidized by oxygen in air to form triiodide ion (I_3^-) which is given by the following equation:



The triiodide ions formed are changed to iodine molecules which is given by the following equations:



This reaction is accelerated by the increase in temperature. This in turn will lead to the increased diffusion rate of O^{2-} and increased metal oxide reduction [19]. The larger iodide anions get adsorbed on the surface of the electrode surface which would hinder in the diffusion of the comparatively small O^{2-} ion to the solution. Thus, this could possibly lead to the slower diffusion of O^{2-} to O_2 and therefore negatively affect the reduction of metal oxides due to presence of KI.

A closer look of CV in small window from OCP to 0.55V and comparing it with the SWV reveals three prominent peaks. Figure 6.7 (a) shows the close up view of CV at scan rate of

500-5000mV/s with 1wt% KI. This figure is complimented by figure 6.7 (b) which shows the presence of three peaks which are represented by the following equations:



Iodide tends to form triiodide and triiodide also reacts with oxygen and is represented by the following equations:

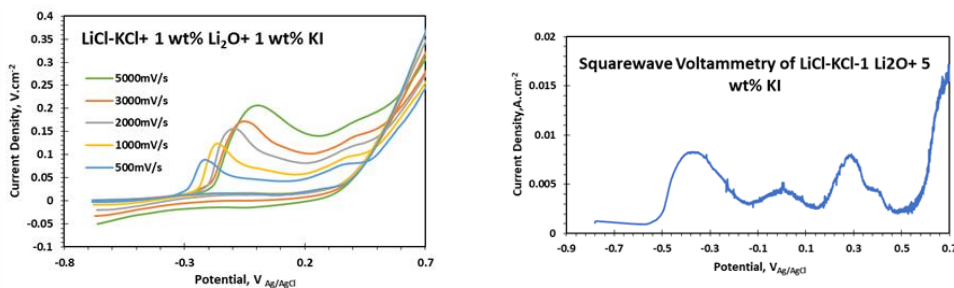


Figure 6.7 (a)-(b): (a) CV at scan rate of 500-5000mV/s from OCP to 2.0 of LiCl-KCl+1 wt% Li₂O with 1 wt% KI (b) SWV of LiCl-KCl +1 wt% Li₂O with 5 wt% KI

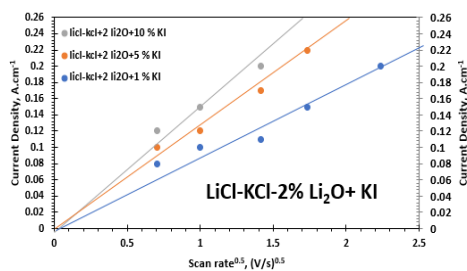


Figure 6.8: Graphical Representation of Peak Current Density Vs Scan Rate^{0.5} LiCl-KCl+2% Li₂O with varying concentration of iodide

Choi et al, showed SWV as a very good tool to monitor the concentration of oxygen ions during the electrochemical reduction of metal oxide. SWV is a pulsed technique, which

provides better sensitivity compared to other analysis technique [26]. Figure 6.7 (b) shows SWV of tungsten wire in LiCl-KCl with 1 % Li₂O with varying concentrations of KI. four clear waves are seen in SWV. But two main waves seen around 0 Volt could be attributed to the reaction given by equation (19) and the peak shown around 0.0V is due to shown reaction (18):

As presented in figure above, the peak current density for the 2 percent Li₂O is seen to be more compared to the 1 percent Li₂O and the current density of in case of oxygen formation increases with the increasing concentration of iodide. The third peak could be attributed to any interhalide formed between iodide and chloride ions. The triiodide formed due to the oxidation of iodide by oxygen is converted into iodide which could be represented by the peak around 0.6-0.7V and the peak around 1.2V could be attributed to the formation of Cl₂.

Square wave voltammetry is used to calculate number of electrons involved in the peak which could be used.

$$n=3.5RT/WF \quad (25)$$

where R=universal gas constant:8.314 J/ mol. K, T= Temperature in Kelvin, W= full width at half peak in volts, F= Faraday constant: 96485 J

The number of electrons could be used to calculate diffusivity coefficient of oxygen ions to oxygen in the LiCl-KCl- Li₂O melt. Figure 6.8 (a)-(b) shows the relationship between peak current density and scan rate for LiCl-KCl-1 and 2% Li₂O with concentration of KI varying 1,5 and 10 wt% KI. The slope calculated from this relationship could be used with the number of electrons calculated from SWV is used to calculate the diffusivity of the melt. The diffusivity of LiCl-KCl-2 % Li₂O with varying concentration of KI is given in Table 6.1:

As seen in Table 6.1, the diffusivity of I⁻ in LiCl-KCl-2% Li₂O increased with increase in the KI additions.

Table 6.1: Diffusivity coefficient of I⁻/I₃⁻ in LiCl-KCl-2% Li₂O with 1,5 and 10 wt% KI

Wt% KI in LiCl-KCl-2% Li ₂ O	Diffusivity coefficient (cm ² .s ⁻¹)
1% KI	1.28 X 10 ⁻⁷
5% KI	1.56X10 ⁻⁶
10% KI	1.28X 10 ⁻⁵

The increase in the diffusivity of iodide from the solution to the electrode surface may adversely affect the diffusion of O²⁻. Thus, the rate of O²⁻ diffusion will be hindered which in

turn affects the reduction of the metal oxide to metal. The presence of iodide in the melt could affect the reduction of metal oxide in a negative way as it affects the diffusion of the O^{2-} in the melt.

Conclusion

The redox potential seen in both cases with 1 and 2 wt% Li_2O showing at 0 V shows the evolution of oxygen in the solution. The diffusion of iodide ions increased with the increase in the KI concentration in 2 wt% Li_2O containing melt. This increase in the diffusivity of iodide may adversely affect the diffusion of the O^{2-} and may hinder the reduction of metal oxide.

References

1. S.M. Jeon, H.S. Shin, S.S. Hong, J.M. Hur, J.B. Do, H.S. Lee, *Electrochim Acta* 55 (2010)1749-1755.
2. E.Y. Choi, J.W. Lee, J.J> Park, J.M> Hur, J.K.Kim, K.Y.Jun, S.M. Jeong, *Chem Eng J.* 514 (2012)207-208
3. Chen GZ, Fray DJ, Farthing TW (2000) *Nature* 407:361–364.
4. J.-M. Hur, C.S. Seo, S.S. Hong, D.S. Kang, S.W. Park, *React. Kinet. Catal. Lett.* 80 (2003) 217.
5. G.Z. Chen, D.J. Fray, T.W. Farthing, *Nature* 407 (2000) 361.
6. Y. Sakamura, M. Kurata, T. Inoue, *J. Electrochem. Soc.* 153 (2006) D31.
7. Y. Sakamura, T. Omori, T. Inoue, *Nucl. Technol.* 162 (2008) 169.
8. J.-H. Hur, S.M. Jeong, H. Lee, *Electrochem. Commun.* 12 (2010) 706.
9. K.V. Gourishankar, L. Redey, M. Williamson, *Light Metals*, 2002, in: W.A. Schneider (Ed.), *The Minerals, Metals, and Materials Society*, 2002, p. 1075.
10. L. Redey, K.L. Gourishankar, US Patent 6540902, April 1, 2003.
11. S.D. Herrmann, S.X. Li, M.F. Simpson, S. Phongikaroon, *Sep. Sci. Technol.* 41 (2006) 1965.
12. Y. Sakamura, M. Kurata, T. Inoue (2006) *J Electrochem Soc* 153(3): D31–D39
13. J. M. Hur, S.S. Hong, H. Lee. *J Radio anal Nuclear Chemistry* (2013) 295:851-854
14. Y. Kado, T. Goto, R. Hagiwara (2008) *J Chem Eng Data* 53:2816–2819
15. Y. Sakamura, *J. Nuclear Materials*, 412 (2011) 177-183
16. G.K. Johnson, R.D. Pierce, D. S.Poa and C.C. McPheeters, *The Minerals, Metals and Materials Society* , (1994) p199
17. S. M Frank, Summary of iodine partitioning in EBR-II Fuel, Internal Report, Idaho National Laboratory, Report SMF-001-16, (2016)
18. S. Fujiwara et al., *J. Power Sources*, 194,1180(2009)
19. Y. Kado, T. Goto and R. Hagiwara, *journal Chemical engineering data*, 2008, 53, 2816-2819.
20. S. M. Jeong, S.-B. Park, S.-S. Hong, C.-S. Seo, and S.-W. Park, *J. Radioanal. Nucl. Chem.*, 268, 349 (2006).
21. J.-H. Hur, S. M. Jeong, and H. Lee, *Electrochem. Commun.*, 12, 706 (2010).

24. Y. Sakamura, T. Omori, and T. Inoue, *Nucl. Technol.*, 162, 169 (2008).
25. V.A. Kovrov, A.R. Mullabaev, V.Yu. Shishkin and Yu. P. Zaikov, *Russian Metallurgy(Metally)* 2018,169-173
26. Sakamura Y. *Journal of Nuclear Materials*. 412 (2011) 177-183.
27. E.Y. Choi, I.Choi, J. Hur, D. Kang, H. Shin and S. Jeong, *Electrochemical and Solid State Letters*, 15,E11-E13(2012)

Chapter 7. Conclusions

The iodide ions in the LiCl-KCl molten salt first oxidized to tri-iodide ions and further oxidized to iodine. The first oxidation peak was observed at around $-0.2 \text{ V}_{\text{Ag}/\text{AgCl}}$. Iodine evolution peak was observed at around $0.6 \text{ V}_{\text{Ag}/\text{AgCl}}$. Without iodide addition, the chlorine evolution peak was observed at around $1.2 \text{ V}_{\text{Ag}/\text{AgCl}}$; however, addition of iodide shifted the chlorine evolution peak to less positive potentials indicating formation of interhalide species such as $[\text{ICl}_2]^-$. The potentials of oxidation peaks shifted to less positive values with increase in the iodide concentration and increase in the temperature.

The diffusion coefficient of 1 wt% iodide in LiCl-KCl molten salt at $450 \text{ }^\circ\text{C}$ was $0.8 \times 10^{-6} \text{ cm}^2/\text{s}$ and increased with increase in the temperature with an activation energy of 37.7 kJ/mol . Increase in the concentration of iodide increased the diffusion coefficient. The activation energy for diffusion decreased with increase in the iodide concentration. The activation energy for diffusion in 5 wt% KI containing LiCl-KCl was 31.5 kJ/mol . The calculated stability constant for the reaction $\text{I}^- + \text{I}_2 \rightarrow \text{I}_3^-$ based on the observed formal potentials was in the order of 10^{-11} at $450 \text{ }^\circ\text{C}$ and 10^{-10} at $550 \text{ }^\circ\text{C}$. The reduction potential of Ce(III)/Ce(0) in LiCl-KCl at $450 \text{ }^\circ\text{C}$ was $-2.1 \text{ V}_{\text{Ag}/\text{AgCl}}$ which shifted to more negative potentials (-2.3 V) upon addition of iodide. The reduction current also decreased with the addition of iodide. The diffusion coefficient of Ce(III) decreased from $2.5 \times 10^{-6} \text{ cm}^2/\text{s}$ to $1.1 \times 10^{-6} \text{ cm}^2/\text{s}$ upon addition of 2 wt% KI. These observations indicated that presence of iodide adversely affected the reduction of Ce(III). The reduction of Ce(III) to Ce(0) occurred in a single step 3-electrons process with and without iodide addition. Chronoamperometry studies indicated the Ce reduction was instantaneous nucleation process without KI addition which changed to progressive upon iodide addition.

The electrochemical reactions of iodide observed in the Li LiCl-KCl molten salt. Oxygen evolution was observed at $0 \text{ V}_{\text{Ag}/\text{AgCl}}$. Multiple oxidation peaks were observed that were attributed to the formation of IO^- , IO_3^- , IO_4^- , and IO_5^{3-} etc. that formed as the reaction products of iodide and oxygen as well as tri-iodide and oxygen. The diffusivity of iodide was about an order of magnitude smaller in the Li_2O containing LiCl-KCl molten salt at $550 \text{ }^\circ\text{C}$ than that observed in the LiCl-KCl eutectic without Li_2O addition due to the reaction between iodide and oxygen. The diffusivity increased with increase in the KI addition. Presence of iodide is considered to adversely affect the reduction process of the used nuclear fuels.

Chapter 8. Future Work

The cyclic voltammetric studies in LiCl+KCl+KI molten salts showed several oxidation peaks associated with tri-iodide, iodine, $[\text{ICl}_2]^-$, $[\text{I}_2\text{Cl}]^-$, and Cl_2 . *In-situ* Spectro-electrochemical, and Raman spectroscopy studies shall be carried out to identify these species. Calculate the formal potentials, stability constants, and diffusion coefficient of the interhalide species based on the spectroscopic studies and electrochemical data. Carry out *in-situ* spectro-electrochemical studies to understand the reaction intermediates of cerium ion reduction in the presence of iodide as a fission product. Design and install a high temperature electrochemical quartz crystal microbalance and carry out electrochemical studies to understand the nucleation of cerium deposition. Devise a better method to clean the molten salt co-deposited on the tungsten electrode surface to understand the nucleation process.

Preliminary studies on differential scanning calorimetry (DSC) using molten salt showed artefacts due to corrosion of crucibles by the molten salt in the liquid and vapor form. Using an inert crucible, carry out DSC of the molten salt with the additions of KI, Li_2O , and CeCl_3 to determine the melting points, heat of fusion, and evaporation rates.